

AD-A078 669

GENERAL ELECTRIC CO CINCINNATI OH AIRCRAFT ENGINE GROUP  
NOVEL CERAMIC TURBINE ROTOR CONCEPT.(U)

F/6 21/5

UNCLASSIFIED

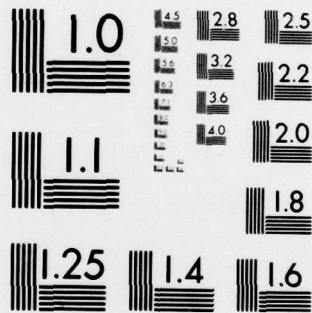
SEP 79 L J STOPPER  
R79AE6527

F33615-78-C-2041  
AFAPL-TR-79-2074

NL

|OF|  
AD  
A078669





MICROCOPY RESOLUTION TEST CHART  
NATIONAL BUREAU OF STANDARDS-1963-A

AFAPL-TR-79-2074

## NOVEL CERAMIC TURBINE ROTOR CONCEPT

### GENERAL ELECTRIC COMPANY

Aircraft Engine Group  
Cincinnati, Ohio 45215

Final Report for Period

22 September 1978 - 22 May 1979

SEPTEMBER 1979

Approved for Public Release; Distribution Unlimited.

REPRODUCED BY  
NATIONAL TECHNICAL  
INFORMATION SERVICE  
U.S. DEPARTMENT OF COMMERCE  
SPRINGFIELD, VA. 22161

Air Force Aero Propulsion Laboratory  
Air Force Wright Aeronautical Laboratories  
Air Force Systems Command  
Wright-Patterson Air Force Base, Ohio 45433

79 12 2

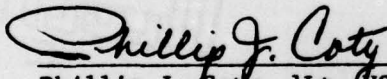
# NOTICE

When Government drawings, specifications, or other data are used for any purpose other than in connection with a definitely related Government procurement operation, the United States Government thereby incurs no responsibility nor any obligation whatsoever; and the fact that the Government may have formulated, furnished, or in any way supplied the said drawings, specifications, or other data, is not to be regarded by implication or otherwise as in any manner licensing the holder or any other person or corporation, or conveying any rights or permission to manufacture, use, or sell any patented invention that may in any way be related thereto.

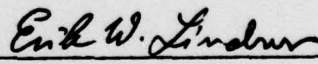
This report has been reviewed by the Information Office (ASD/OIP) and is releasable to the National Technical Information Service (NTIS). At NTIS, it will be available to the general public, including foreign nations.

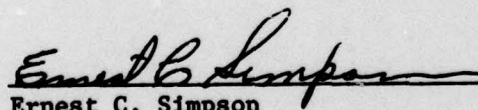
This program was initiated with FY78 Laboratory Director Funds.

This technical report has been reviewed and is approved for publication.

  
Phillip J. Coty, 1Lt, USAF  
Project Engineer

FOR THE COMMANDER

  
Erik W. Lindner  
Technical Area Manager  
Special Engine Technology

  
Ernest C. Simpson  
Director  
Turbine Engine Division

Copies of this report should not be returned unless return is required by security considerations, contractual obligations, or notice on a specific document.



Unclassified

SECURITY CLASSIFICATION OF THIS PAGE (When Data Entered)

19 REPORT DOCUMENTATION PAGE		READ INSTRUCTIONS BEFORE COMPLETING FORM
1. REPORT NUMBER 18 AFAPL TR-79-2074	2. GOVT ACCESSION NO.	3. RECIPIENT'S CATALOG NUMBER
4. TITLE (and Subtitle) Novel Ceramic Turbine Rotor Concept Study		5. TYPE OF REPORT & PERIOD COVERED Final Technical Report 9/22/78 - 5/22/79
7. AUTHOR(s) L.J. Stoffer		6. PERFORMING ORG. REPORT NUMBER R79AEG527
9. PERFORMING ORGANIZATION NAME AND ADDRESS General Electric Company Aircraft Engine Group Cincinnati, Ohio 45215		8. CONTRACT OR GRANT NUMBER(s) F33615-78-C-204
11. CONTROLLING OFFICE NAME AND ADDRESS Air Force Aero Propulsion Laboratory (TBP) Air Force Wright Aeronautical Laboratories Wright-Patterson AFB, Ohio 45433		10. PROGRAM ELEMENT, PROJECT, TASK AREA & WORK UNIT NUMBERS 3066-15-25
14. MONITORING AGENCY NAME & ADDRESS (if different from Controlling Office)		12. REPORT DATE 11 September 1979
		13. NUMBER OF PAGES 84
		15. SECURITY CLASS. (of this report) Unclassified
		15a. DECLASSIFICATION/DOWNGRADING SCHEDULE
16. DISTRIBUTION STATEMENT (of this Report) Approved for Public Release; Distribution Unlimited		
17. DISTRIBUTION STATEMENT (of the abstract entered in Block 20, if different from Report)		
18. SUPPLEMENTARY NOTES This program was initiated with FY78 Laboratory Director Funds. 62203F		
19. KEY WORDS (Continue on reverse side if necessary and identify by block number) Ceramics in Gas Turbine Engines      Compression Structured Ceramic Turbine Turbine      Novel Turbine Design Ceramics      Ceramic Turbine Design Ceramics Application      High Temperature Turbine Design Turbine Design      Compression Structured Design		
20. ABSTRACT (Continue on reverse side if necessary and identify by block number) A novel design concept for a ceramic turbine rotor has been studied in detail for a non-man-rated, limited-life gas turbine engine application. The feature of the design involves keeping the rotating ceramic components in a compression state at all turbine operating conditions. An air-cooled composite material containment hoop is utilized at the outer diameter of ceramic air-cooled fins which support ceramic turbine blades in compression against a radially compliant wheel. → not page		

20. (Concluded)

The design study of this Compression Structured Ceramic Turbine Rotor included detailed material, heat transfer, and 3-D stress analyses. The study effort also looked at the operational limits of the design and a performance and economic analysis comparison to a baseline metal design. Conclusions and recommendations for future development are also presented in this report.

id

## FOREWORD

This final report describes an in-depth study of a Compression Structured Ceramic Turbine. The study was conducted by personnel of the General Electric Company, Aircraft Engine Group, Cincinnati, Ohio, under Contract F33615-78-C-2041, Project 3066-15-25, with the Air Force Aero Propulsion Laboratory, Wright-Patterson Air Force Base, Ohio. Lt. Phillip J. Coty (AFAPL/TBP) was the Air Force Project Engineer.

The work reported herein was performed in a 7-month period starting in September 1978 and ending in May 1979.

The General Electric Program Manager was E.J. Rogala; the Technical Program Manager was R.G. Stabrylla; the Principal Investigator was L.J. Stoffer, the author of this report, who wishes to acknowledge the cooperation and assistance of the following individuals for their contribution to this study.

S. Abujawdeh	- Heat Transfer and Windage Loss Analysis
K. Brown	- 3-Dimensional Finite Element Stress Analysis
Dr. G. Trantina	- Ceramic Material Data
A. Sabatiuk	- Blade Aero Performance Assessment
T. Few	- Design Analysis
J. Monroe	- Design Analysis



## TABLE OF CONTENTS

<u>Section</u>	<u>Page</u>
1.0 INTRODUCTION	1
2.0 COMPONENT DESIGN/MATERIAL/STRESS ANALYSIS	3
2.1 Design Concept	3
2.2 Design Parameters	3
2.3 Component Design	7
2.4 Material/Design Assumptions	9
2.5 Design Evolution	14
2.6 Material	17
2.6.1 Ceramic Components	17
2.6.2 Containment Hoop	17
2.6.3 Disk and Damper Plates	22
2.6.4 Compliant Layers	23
2.7 Heat Transfer and Windage Loss Analysis	24
2.8 Stress and Blade Frequency Analysis	24
2.8.1 Containment Hoop Analysis	24
2.8.2 Ceramic Fin Analysis	34
2.8.3 Ceramic Turbine Blade Analysis	34
2.8.4 Disk and Damper Plate Analysis	37
2.8.5 Blade Frequency	37
3.0 PERFORMANCE ANALYSIS AND OPERATIONAL LIMITS	48
4.0 TASK III - ECONOMIC ANALYSIS AND RECOMMENDED COMPONENT DEVELOPMENT PROGRAM	53
5.0 SUMMARY	55
6.0 CONCLUSIONS	57
7.0 RECOMMENDATIONS	58
APPENDIX A - HEAT TRANSFER AND WINDAGE LOSS ANALYSIS	63
Introduction	63
Model	63
Heat Transfer Calculations	63
Drag Calculations	68
Results	69
Cooling Recommendations	69
APPENDIX B - CONTAINMENT HOOP STRESS CALCULATIONS	83
REFERENCES	85

## LIST OF ILLUSTRATIONS

<u>Figure</u>		<u>Page</u>
1.	CSCT Patent Disclosure.	4
2.	CSCT Model.	5
3.	Conceptual Installation of the CSCT in a Turbofan Engine.	6
4.	CSCT Components, Final Version.	8
5.	Section Diagram of an Installed CSCT.	10
6.	CSCT Fin/Blade Interface.	11
7.	Total Estimated Leakage Through Both Forward (60%) and Aft (40%) Face Seals.	12
8.	CSCT - Single-Piece Blade Concept.	15
9.	CSCT - Separate-Pieces Blade Concept.	16
10.	CJ805 Aft Fan Section with "Blucket."	18
11.	CSCT - With Fan Profiled to do Work.	19
12.	CSCT Evolution Through Four Compliant Disk Concepts.	20
13.	Heat Distribuiton in CSCT Containment Hoop and RBSN Fin Endwall at Seal Level Mach 0.7 - 100% Speed.	25
14.	Windage Loss in Horsepower on CSCT at Sea Level Mach 0.7 - 100% Speed.	26
15.	CSCT Components - Two Approaches to Incorporating the Composite Containment Hoop.	27
16.	Stress Versus Deflection Between Composite Hoop and 360° Ceramic Ring as a Function of Rotor Speed.	29
17.	Stress and Pressure in Containment Hoop and 360° Ceramic Ring as a Function of Rotor Speed.	30
18.	Maximum Hoop Radial Deflection Versus Rotor Speed.	31
19.	Maximum Hoop Tensile Stress Versus Rotor Speed.	32
20.	CSCT Half-Hoop 3-D Finite-Element Stress Model.	33



LIST OF ILLUSTRATIONS (Concluded)

<u>Figure</u>		<u>Page</u>
21.	CSCT 3-D Finite-Element Stress Model.	36
22.	3-D Finite-Element Model of CSCT Blade - View A.	38
23.	3-D Finite-Element Model of CSCT Blade - View B.	39
24.	Levels of 3-D Finite-Element Blade Model.	41
25.	Thermal and Stress Profiles of CSCT Blade at 100% Design - First Iteration.	42
26.	3-D Finite-Element Model of CSCT Half-Disk.	43
27.	3-D Finite-Element Model of CSCT Forward Damper Plate.	44
28.	Average Stresses in the CSCT at 100% Design Speed.	45
29.	Radial Deflection Versus Speed for the Flexible Tangs in Relation to the Hoop and Wheel.	46
30.	Vibrational Analysis Cambell Diagram of the CSCT Blade Compared to a Baseline Metal Blade.	47
31.	Cooling, Leakage, and Drag Penalties - CSCT Versus Baseline.	49
32.	CSCT with Sealed Hoop Compartment.	51
33.	Flow and Horsepower Schematic of CSCT Engine.	59
34.	Hot Test Rig Facility Concept for the CSCT.	61
A-1	Turbine, Fin, and Hoop Assembly with Nodal Volume Sections Shown.	64
A-2	Heat Transfer Coefficients and Boundary Temperature Locations.	66
A-3	Hoop Temperature Distribution Plot for 15-Fin Model (0.25-inch high).	71
A-4	Hoop Temperature Plot for 30-Fin Model (0.20-inch high).	78
A-5	Fin Air Heating Versus Flow for 15-Fin Model (0.25-inch high).	81

# LIST OF TABLES

<u>Table</u>		<u>Page</u>
I.	CSCT Design Assumptions and Some Properties of Ceramic Material at or Near 2400° F.	13
II.	Assumed Properties for Low Density RBSN.	21
III.	CSCT Containment Hoop Load Analysis.	35
IV.	Stress Ranges Encountered in the 11 Levels of the 3-D Finite-Element Model of the CSCT.	40
V.	Potential Aerodynamic Benefits of a CSCT Inverted-Taper Turbine Blade.	50
VI.	CSCT Estimated Costs.	54
VII.	CSCT Component Temperature/Stress Summary.	56
A-1.	Heat Transfer Coefficients and Temperature Boundary Conditions.	67
A-2.	Hoop and Fin Drag Calculations (15 Fins, 0.25-inch high).	70
A-3.	Temperature Distribution Results - 15-Fin (0.25-inch high) Model.	77
A-4.	Temperature Distribution Results - 30-Fin (0.20-inch high) Model.	80

## 1.0 INTRODUCTION

Ceramic materials offer the gas turbine engine designer the attractions of high temperature strength capability and a near-inexhaustible raw materials supply. Recognition of potential payoff for improved engine thrust/reduced fuel consumption and lower production costs has stirred government and industry to investigate ceramic material applications in limited-life, non-man-rated gas turbine engines. In addition to other hot-part engine components, ceramic turbine rotors have been designed and tested. Present-day ceramic blade designs are structured around the conventional design concept that places the blade in a tensile state when the wheel is rotating. Inherently, ceramics have a relatively low tensile strength when compared to metals. The conventional rotor/blade design concept, therefore, incorporates this poor characteristic of ceramics. By contrast, this novel ceramic turbine design concept is structured to utilize the much higher compressive strength characteristic of ceramic materials.

The objective of the Novel Ceramic Turbine Rotor Concept Study was to determine the structural feasibility and performance/cost payoff prospects for a ceramic turbine rotor design in which the ceramic components are maintained in a compressive stress state over the full operating range of the turbine. Again, the advantage of this approach lies in the fact that ceramic material property data have indicated that these materials are significantly stronger in compression than in tension - on the order of three to eight times the tensile strength.

The approach used in this study effort was to:

- Select an advanced technology turbine design and application consistent with the application of brittle turbine materials.
- Perform turbine rotor system studies to identify design features needed to maintain the ceramic components in compression.
- Identify and analyze the thermal and mechanical design details using three-dimensional finite-element analysis techniques.

A baseline engine design with a typical conventional metal turbine was selected for comparison to the novel ceramic turbine. The turbine design conditions established for the study are depicted by a 10-hour life requirement at a turbine rotor inlet temperature of 2400° F at 100% speed. The blade tip velocity is 1807 feet per second.

This turbine inlet temperature level is well within allowing the use of uncooled ceramic blades; metal blades would definitely require cooling. Thus, an engine cycle that would not be penalized with cooling air losses should demonstrate an improved performance over the baseline engine with an air-cooled turbine.



This report covers a detailed structural and heat transfer design analysis of a Compression Structured Ceramic Turbine (CSCT) and compares its projected performance with the selected air-cooled metal baseline turbine. The study performed on this novel turbine involved three tasks:

- Task I - Novel Ceramic Turbine Rotor Design/Materials Selection/Thermal and Stress Analysis
- Task II - Operational Limits and Performance Analysis
- Task III - Economic Analysis and Recommended Component Development Program

Most of the structural analysis of the various components of the CSCT is simply summarized under the respective portions of the text that follows. However, since the heat transfer and windage loss effect is so critical to the evaluation of this particular CSCT in addition to its summary in the main body of the text, a more detailed delineation of this particular analysis is presented in Appendix A.

There are few design possibilities available which could effectively produce a Compression Structured Ceramic Turbine. The design, which is the main subject of this report, is one which adequately fulfills the objective of a compression structured concept utilizing current state-of-the-art materials and processing with structural performance capable of withstanding a severe, life-limited mission environment.

## 2.0 COMPONENT DESIGN/MATERIAL/STRESS ANALYSIS

### 2.1 DESIGN CONCEPT

A patent disclosure concept of a Compression Structured Ceramic Turbine Rotor, illustrated in Figure 1, and a model, pictured in Figure 2, formed the basis for this design study. The concept consists of a ceramic turbine blade, an integral set of ceramic cooling fins, and a composite material containment hoop. A wedge between the ceramic blade root and the torque ring imposes an initial compressive force to the assembly which never relaxes throughout the turbine operating range. The outer fins act to duct cooling air between the hot turbine blades and the containment hoop to maintain hoop temperatures consistent with composite material properties.

The conceptual installation of the Compression Structured Ceramic Turbine in a turbofan engine is illustrated in Figure 3, along with the baseline engine parameters. The air that is ducted through the turbine tip cooling fins is shown exhausted separately.

### 2.2 DESIGN PARAMETERS

The baseline turbine tip speed of 1807 feet per second is 15 to 25% higher than most other dovetail/tensile structured ceramic turbine rotors currently being developed. With the addition of the tip cooling fins and a containment hoop, the tip velocity of the containment hoop at 100% speed is approximately 2340 feet per second.

This study was conducted at the design point conditions of 100% speed at Mach 0.7, sea level, with a 111% rotor speed capability and with the uncooled ceramic turbine rotor inlet temperature ( $T_4$ ) at 2400° F. The design point condition was selected because it represents the most severe operating condition that the turbine would encounter in its relatively short design life of 50 hours. A design safety stress margin of 15% was established for an allowable short-term overspeed condition of 111%.

A list of design concerns for the Compression Structured Ceramic Turbine is summarized below and will be addressed in some detail throughout the discussion that follows:

1. Inertia- and thermal-induced radial mismatch between the disk and tip containment hoop.
2. Hoop integrity versus hoop environment.
3. Hoop and fin drag losses.



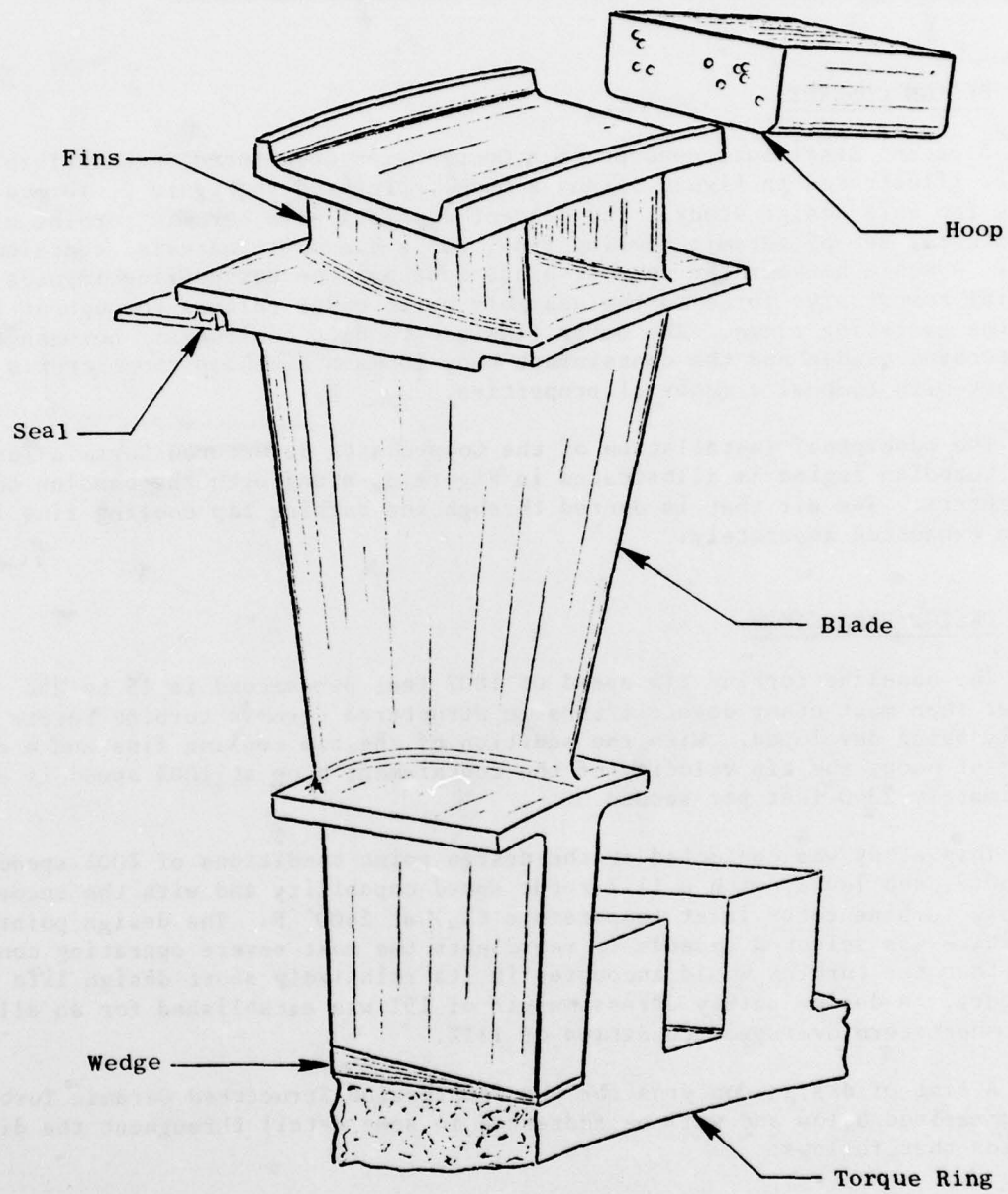
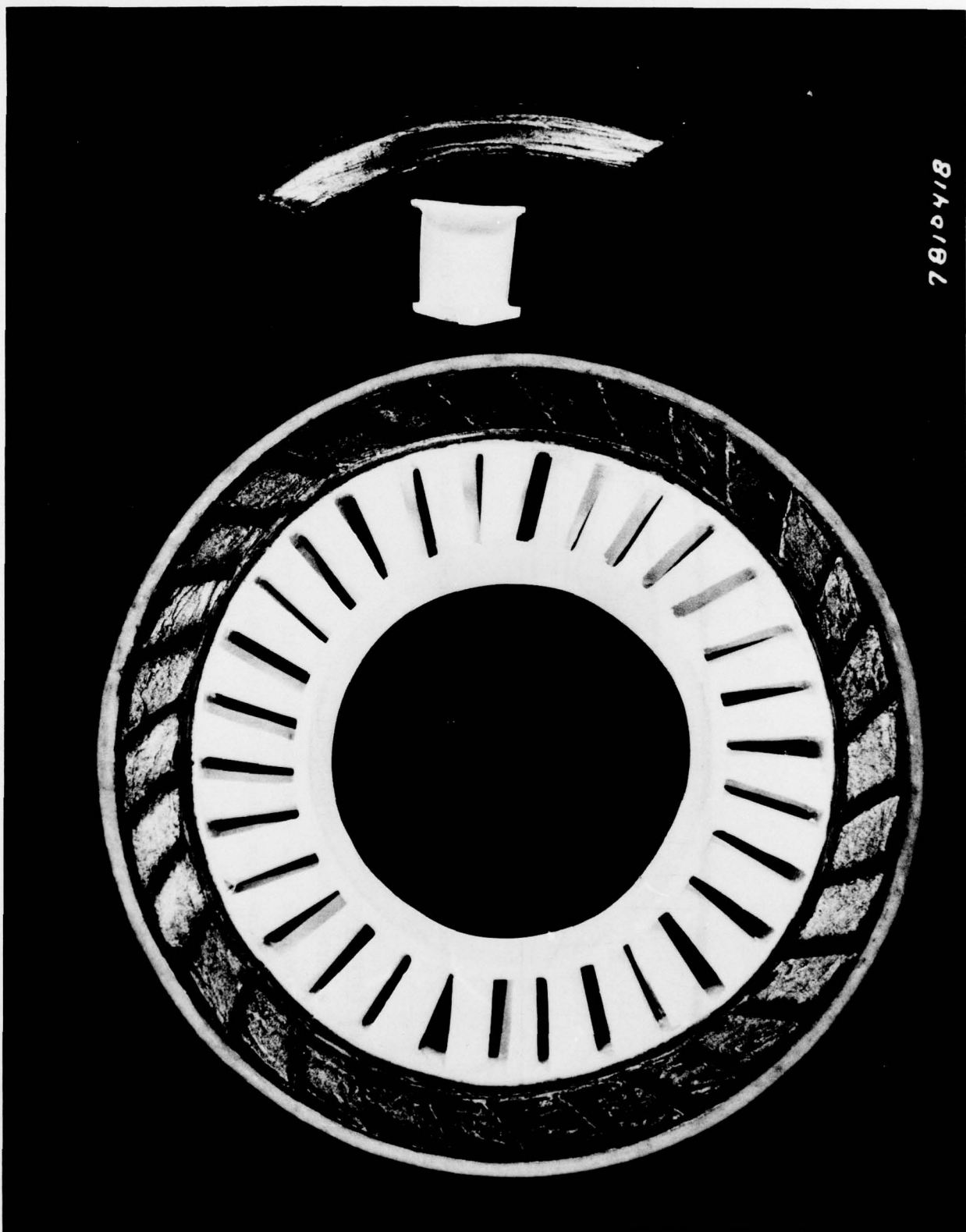
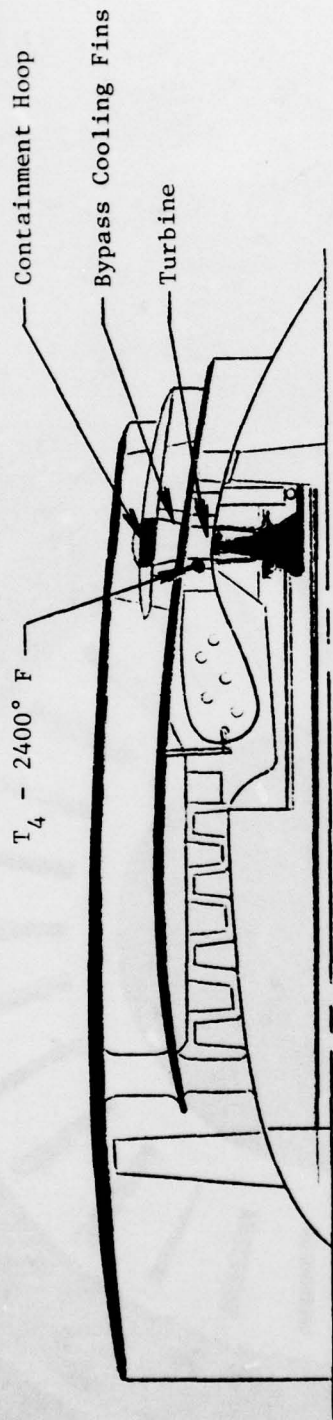


Figure 1. CSCT Patent Disclosure.



7810418



Proposed Initial Application in a Non-Man-Rated Cruise Missile Engine

Parameters

- Turbine Blade Tip Speed at 100% = 1807 ft/sec (Hoop Tip = 2340 ft/sec)
- Turbine Life - 50 hours with 10 hours at 100%; Mach 0.7 at Sea Level
- Turbine Capability - 111% Overspeed - Short Dash

Figure 3. Conceptual Installation of the CSCT in a Turbofan Engine.

4. Rotating seal leakage between the core gas and bypass cooling air duct.
5. Cooling fin work versus aerodynamic cycle match.
6. Compliant interfaces between rotor components.
7. Thrust bearing relationship to seals and engine mount.
8. Lack of material data on compressive strength of ceramics.

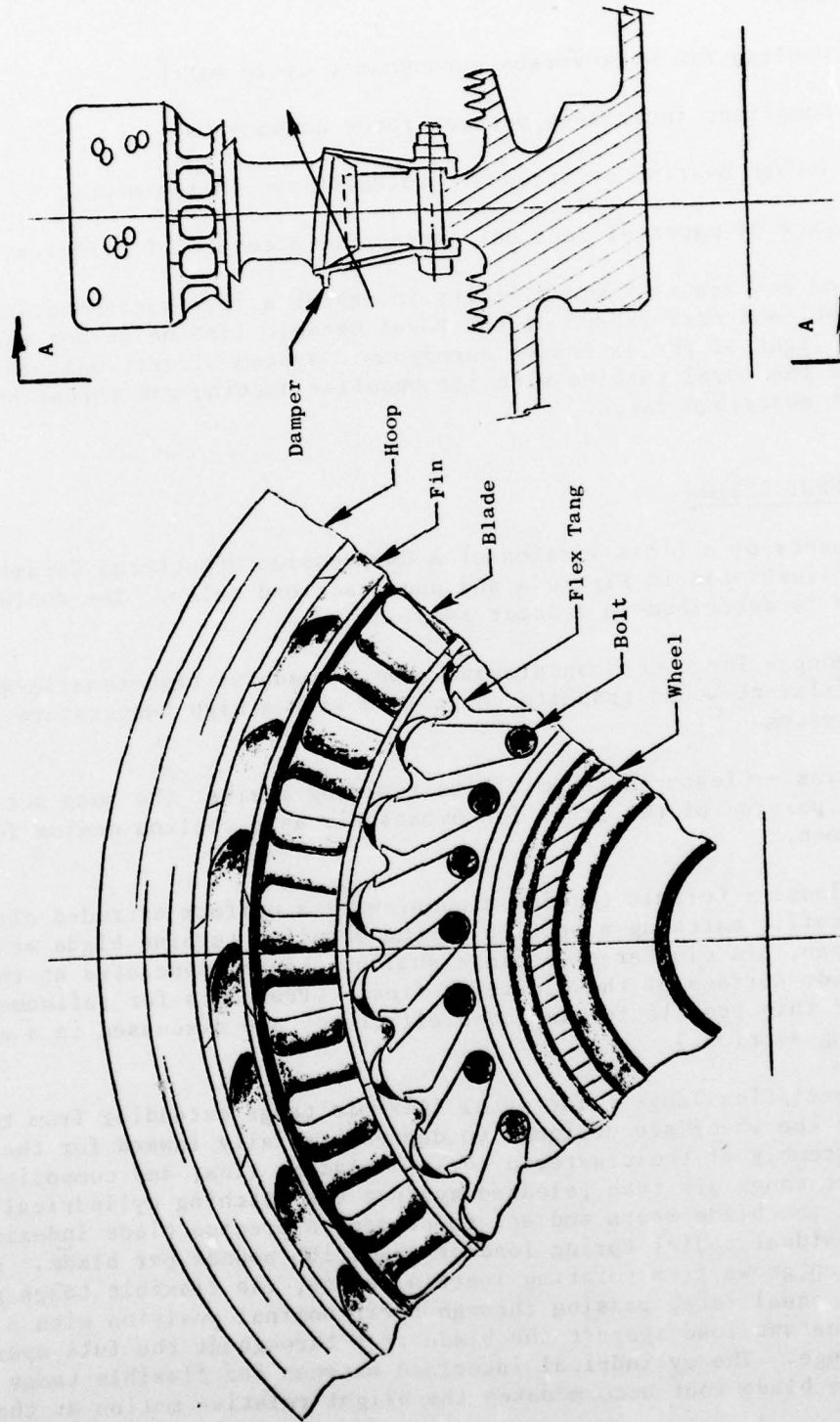
Also of concern is the difficulty in making a fair assessment of the weight, cost, and performance of the Novel Ceramic Turbine versus the baseline turbine in light of the extensive aerodynamic system alterations needed to accommodate the novel turbine with its peculiar ducting and thrust bearing arrangement described later.

### 2.3 COMPONENT DESIGN

Components of a final version of a Compression Structured Ceramic Turbine rotor are illustrated in Figure 4 and are described below. The evolution of this design is described in a later section.

- Hoop - The outer containment hoop is made of high-tensile-strength, filament-wound graphite composited with a high temperature resin system.
- Fins - Clustered ceramic fins residing against the hoop act to duct a portion of the front fan bypass air as a cooling medium for the hoop.
- Blades - Ceramic turbine blades, with a uniform extruded airfoil profile matching a section of the baseline turbine blade at 80% span, are clustered within a shallow channel generated at the inside surface of the clustered fins. (Prospects for refinement of this profile for improved efficiency are discussed in a concluding section.)
- Wheel/Flex Tangs - The metal flexible tangs extending from the rim of the wheel are designed to depress radially inward for the axial assembly of the clustered ceramic blades, fins, and composite hoop. The tangs are then released against the matching cylindrical profile of the blade roots and act to provide a precise blade indexing and residual radial spring load of about 100 pounds per blade. As the hoop grows from rotating inertia forces, the flexible tangs grow at an equal rate, passing through their nominal position with a fairly constant load against the blade root throughout the full operating range. The cylindrical interface between the flexible tangs and the blade root accommodates the slight relative motion at that joint





Section A-A with  
Damper Plate Removed

Figure 4. CSCT Components, Final Version.



while the flexible tangs extract torque and adjust to the difference in growth induced by inertia and thermal gradients between the wheel and the blades.

- Damper Plates - Two damper plates assembled to the wheel fore and aft faces act to locate and contain the blades axially and to inhibit windage losses. The tips of the damper plates reside with some opposing axial force against the platforms of the blades and tend to dampen any vibration that may be induced by the flexible tang system.

A section of the installed Compression Structured Ceramic Turbine is illustrated in Figure 5. A thrust bearing is shown just behind the turbine with its projected path to the engine mounts. As explained later, the location of the thrust bearing is important to the performance of gas path/fan stream sealing. Thrust bearings are usually located at the forward end of the turbine drive shaft, where temperatures can be maintained at cooler levels with less complexity.

In order to draw as close a comparison as possible between the Compression Structured Ceramic Turbine and the baseline turbine, it was established that the cooling fins would do no work on the induced bypass cooling air. The fins would simply knife the air so the net effect of fin/hoop drag could be isolated without the complexity of modifying the baseline engine aero system. The prospect remains to have the cooling fins do some work to offset a portion of the drag losses imposed by the fin/hoop system. Figure 6 illustrates the relative relationship between a zero-work fin angle and six turbine blades. Working fins would extend over fewer blades, the exact number depending on the amount of induced work.

The advantage of incorporating a shrouded turbine blade tip in the Compression Structured Ceramic Turbine is somewhat offset by leakage at the fore and aft seals that separate the turbine gas from the fin cooling air. Figure 7 shows three seal profiles with estimated leakage rates as a function of effective running clearance. Confirmation of the efficiency of such seals will require actual testing. For this study, it was estimated that total leakage at such seals could be restricted to within 1.5% of total core air - a smaller loss in efficiency than the baseline turbine blade would display with a nominal tip clearance of about 8 mils. By locating the drive shaft thrust bearing in proximity to the Compression Structured Ceramic Turbine, thermal migrations that could adversely affect seal clearance could be minimized.

#### 2.4 MATERIAL/DESIGN ASSUMPTIONS

Table I lists a few material assumptions for the main components that were incorporated in this design study. The material proposed for the hoop was a relatively low temperature graphite/epoxy (maximum temperature of 450° F); however, a polyimide material for the hoop presents a strong alternate candidate that could extend maximum temperature capability to over

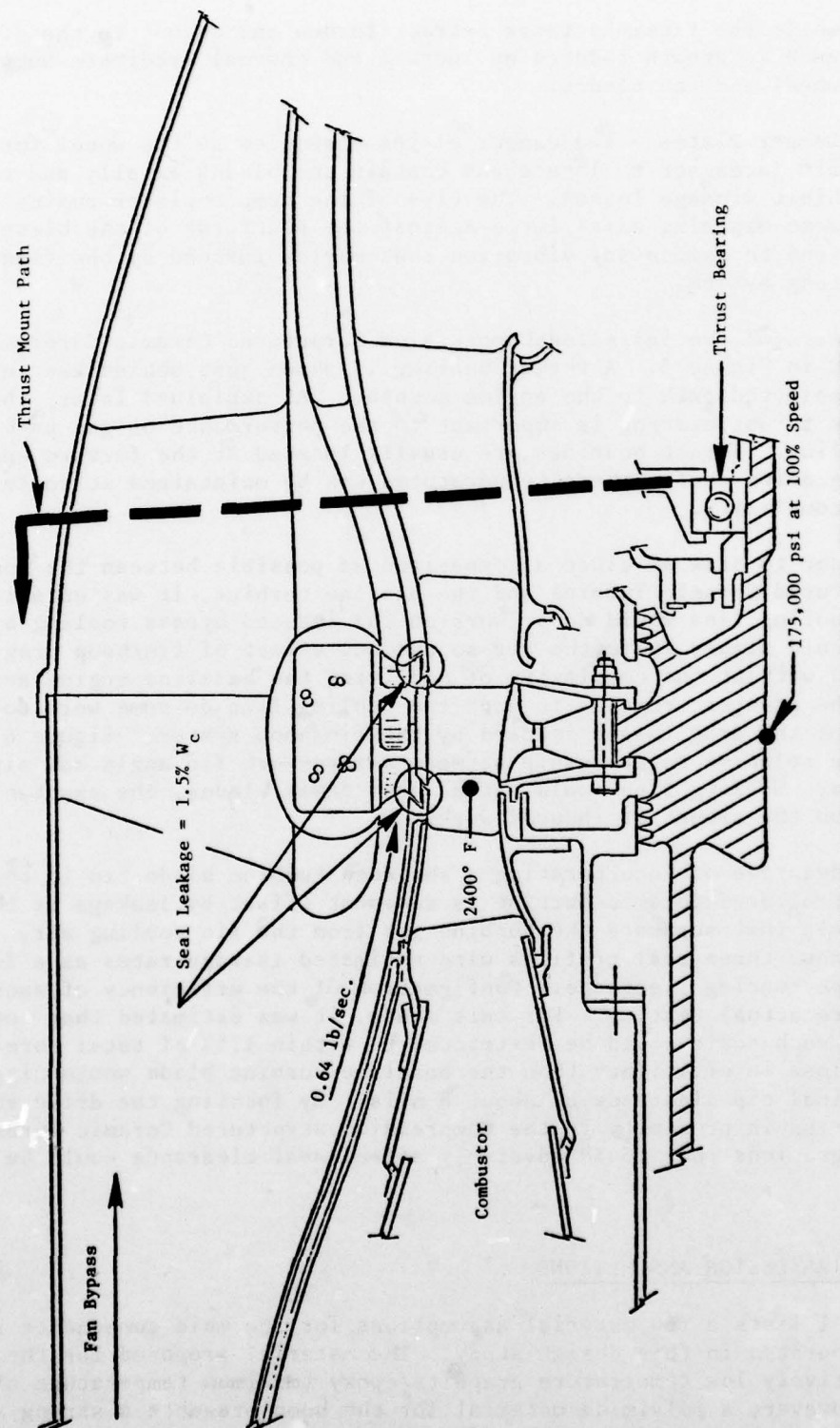


Figure 5. Section Diagram of an Installed CSCT.

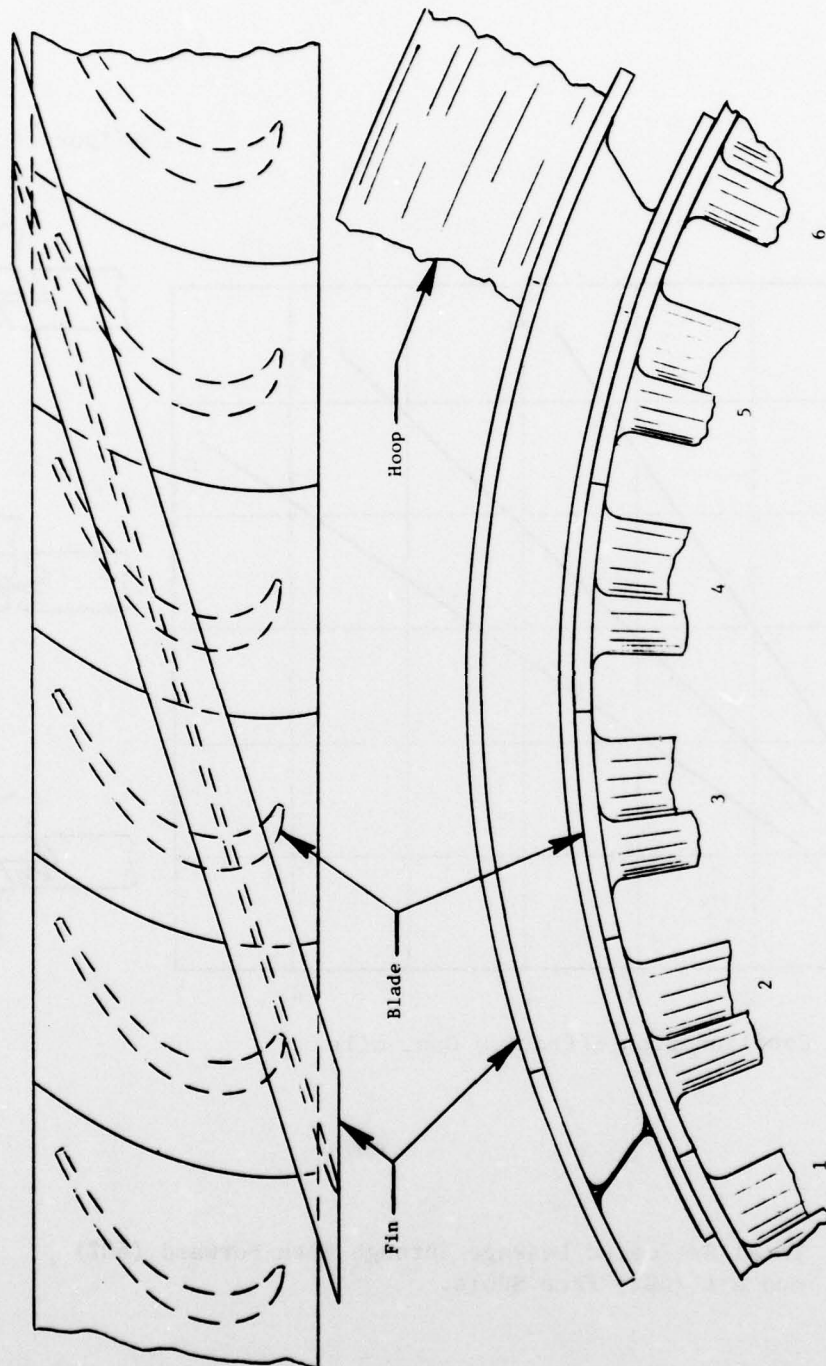


Figure 6. CSCT Fin/Blade Interface.

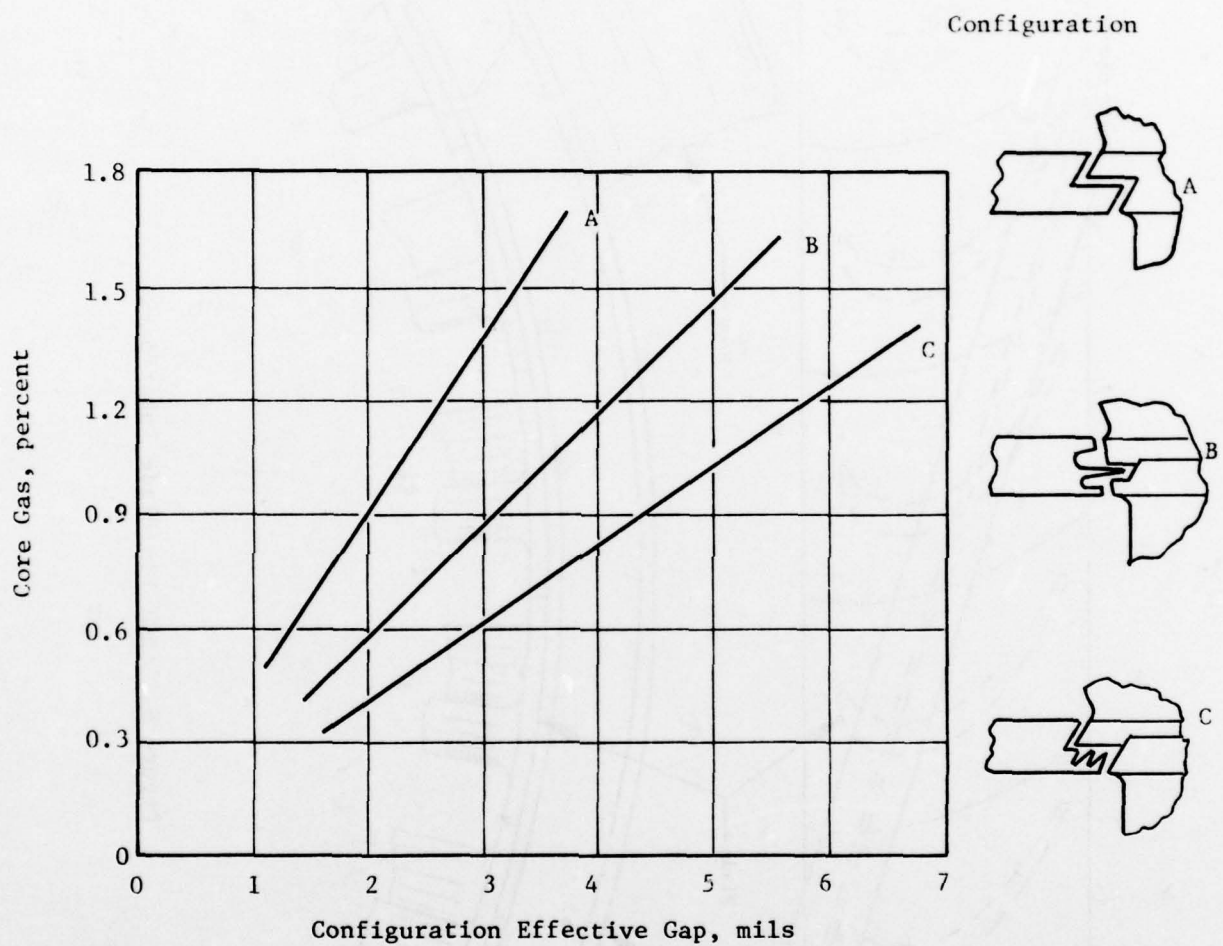


Figure 7. Total Estimated Leakage Through Both Forward (60%) and Aft (40%) Face Seals.



Table I. CSCT Design Assumptions.

	Density, gm/cc	Maximum Temp., ° F	Ultimate Stress, ksi	Allowable Stress, ksi
Hoop (Graphite/Epoxy)	1.55	450	210-Tensile	182-Tensile
Fin (RBSN)	2.3	1700	85-Compressive	74-Compressive
Blade (RBSN)	2.5	2300	110-Compressive	95-Compressive

Some Properties of Ceramic Materials At or Near 2400° F.

	Density (gm/cc)	Tensile (10 <sup>6</sup> psi)	K-Thermal Cond. (Btu-in./ hr-ft <sup>2</sup> -° F)	Coefficient of Thermal Exp. (in./in. 10 <sup>-6</sup> )	Modulus of Elasticity (10 <sup>6</sup> psi)	Poisson's Ratio
RBSN	2.7	53	70	1.63	25	0.18
Sintered S.C.	3.1	70	250	2.7	56	0.14
Silicon/Silicon Carbide (Silcomp <sup>TM</sup> )	2.85	40	178	2.8	42	---

Note: The above values are general averages and are not to be considered as absolute.



600° F. Emerging technology in Graphite Reinforced Glass Matrix may provide containment hoops capable of full strength at operating temperatures close to 1000° F.\* The graphite/epoxy was selected for the study because it is more representative of the current state of the art with sufficient data to support engineering judgments.

The ceramic material proposed for the fins and blades was Reaction Bonded Silicon Nitride (RBSN) with reduced densities for the respective components as stresses and environment would allow. The reasons for selecting RBSN over other possible ceramic materials such as sintered silicon carbide and silcomp were:

- Lower thermal conductivity for less loss of heat to the containment hoop.
- Lower modulus for better stress distribution.
- Lower density for lower induced loads into containment hoop.
- Sufficient strength at required temperature.

Since virtually no compressive strength data were available on any of the ceramic materials considered for this study, it was suggested that a conservative design assumption of no more than three times the published tensile strength be used for a maximum projected compressive strength of the ceramic materials.

Table I also lists comparable values for various properties of the final selection of ceramic materials considered as potential candidates for this application. Values listed reinforce the above reasons for selecting RBSN as the most desirable material for this study.

Although the turbine rotor inlet average temperature for this study is 2400° F, the maximum turbine blade relative temperature is projected to be only 2250° F, due to its rotation; hence the properties of RBSN are adequate.

## 2.5 DESIGN EVOLUTION

An initial concept of a Compression Structured Ceramic Turbine is illustrated in Figures 8 and 9. Figure 8 shows a single-piece ceramic blade/triple fin, while Figure 9 shows the blade as three pieces (forward, middle, and trailing) and the triple fin as a separate piece. It was anticipated that thermal shock and steady-state thermal stresses would be better accommodated with the Figure 9 separate-pieces concept. Moreover, the separate pieces could be made hollow for increased section modulus and/or reduced inertia loads, whereas the single-piece structure in Figure 8 could only be made solid.

---

\*Report NASA CR-158946 (N79-11126)

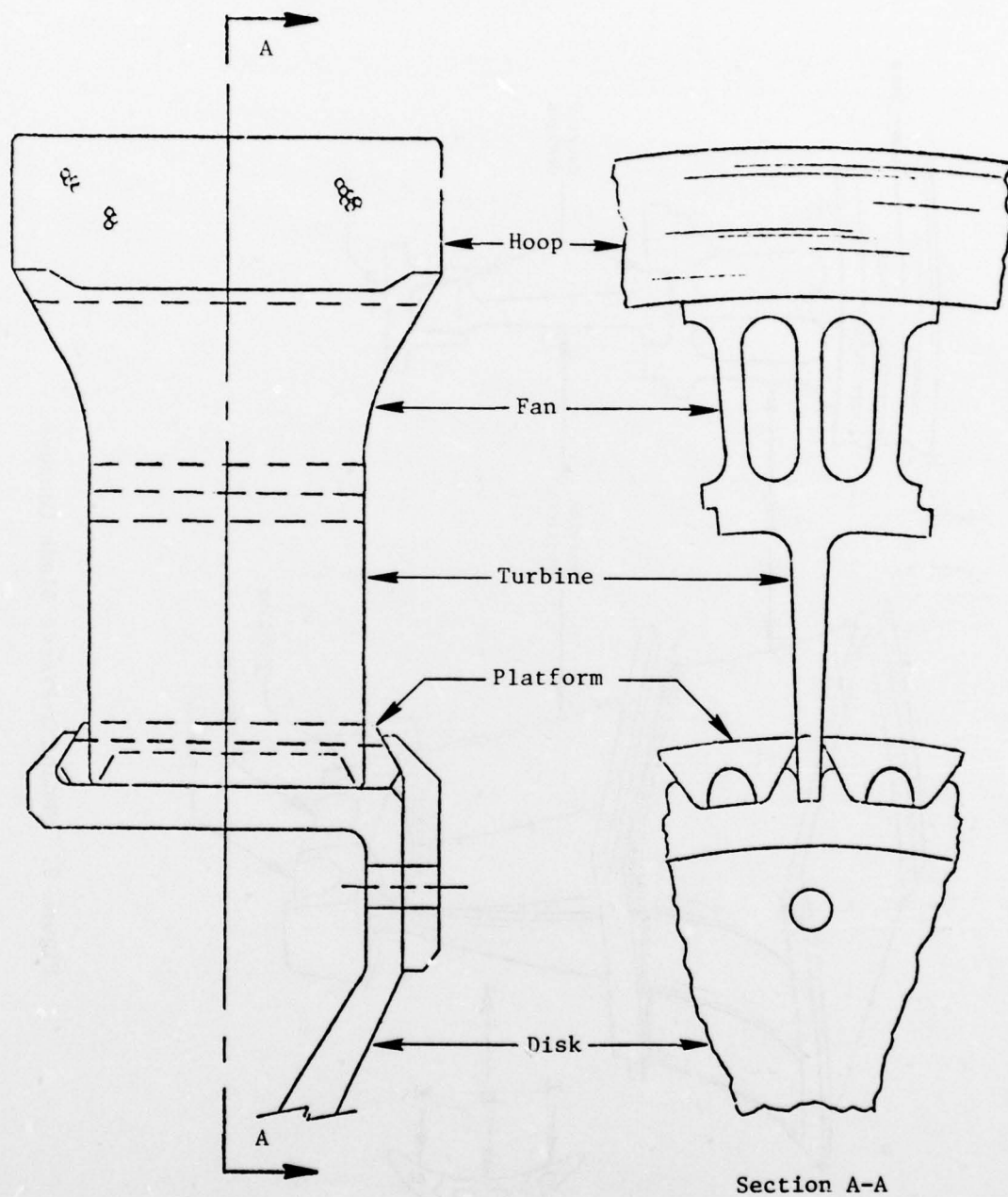


Figure 8. Single-Piece Blade Concept.

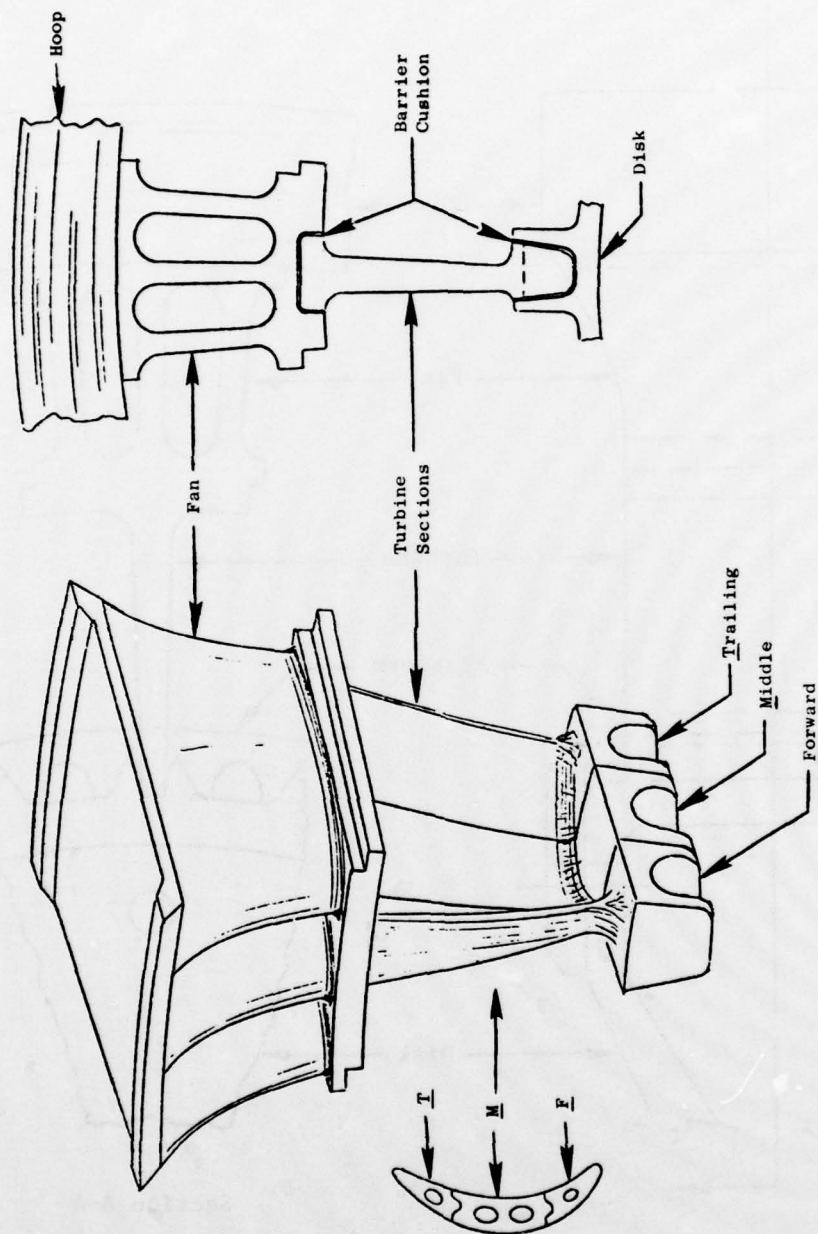


Figure 9. Separate-Pieces Blade Concept.

In the early stages of the design evolution, it was assumed that the tip cooling fins would do work on the bypass air to augment thrust sufficiently to offset the drag penalty imposed by the fin/hoop system. The General Electric CJ805 engine has a similar all-metal turbine/fan structure (shown in Figure 10) with a combined airfoil unit called a "bucket" which has been in service for many years. However, to impose this additional energy extraction upon the baseline turbine - which is already driving a core compressor - would require an entirely new engine aerodynamic turbine system, which is beyond the scope of this study. Figure 11 illustrates an approximation of the relationship between a turbine blade and a fin capable of inducing thrust.

Since the containment hoop will grow at a greater rate than a solid disk would grow, it was necessary to devise some method for a variable radial adjustment between the ceramic blades and the wheel. Figure 12 shows the evolution through four compliant disk concepts, No. 4 being the final design that accommodates the compression feature of the Novel Turbine with the least concern for stress concentrations. Configurations 1 through 3 in Figure 12 tended to impose uneven loading as the rims attempted to roll with radial growth. Concept 4, besides loading evenly, offers precise blade spacing and axial location for better seal control and rotor balance while providing a dampening mechanism to the rotor system with the fore and aft damper plates described earlier.

## 2.6 MATERIAL

### 2.6.1 Ceramic Components

Table II lists properties for two slightly different densities of Reaction Bonded Silicon Nitride (RBSN) compiled for this study by Dr. G. Trantina of the General Electric Company, Corporate Research and Development Center, Schenectady, New York. The 2.3 gram/cm<sup>3</sup> RBSN was selected for the fins, while the 2.5 gram/cm<sup>3</sup> RBSN was selected for the turbine blades.

Unfortunately, there is very little compressive data available on ceramic materials. Density, temperature, and time have an important bearing on ceramic data. Specimen size, specimen loading condition, fabrication, and machining likewise bear directly on test results.

### 2.6.2 Containment Hoop

The graphite fibers and resin systems listed below are considered prime candidates for the proposed containment hoop. Other systems may emerge, such as the Graphite Reinforced Glass Matrix system mentioned in Section 2.4, if the environment should ever require it, but for this particular application, the maximum temperature should not exceed the limits of the resin systems listed below. Unfortunately, no data could be found for the tensile strengths of hoops in the thickness required by this particular CSCT made with any of the listed resin systems at elevated temperatures. However,



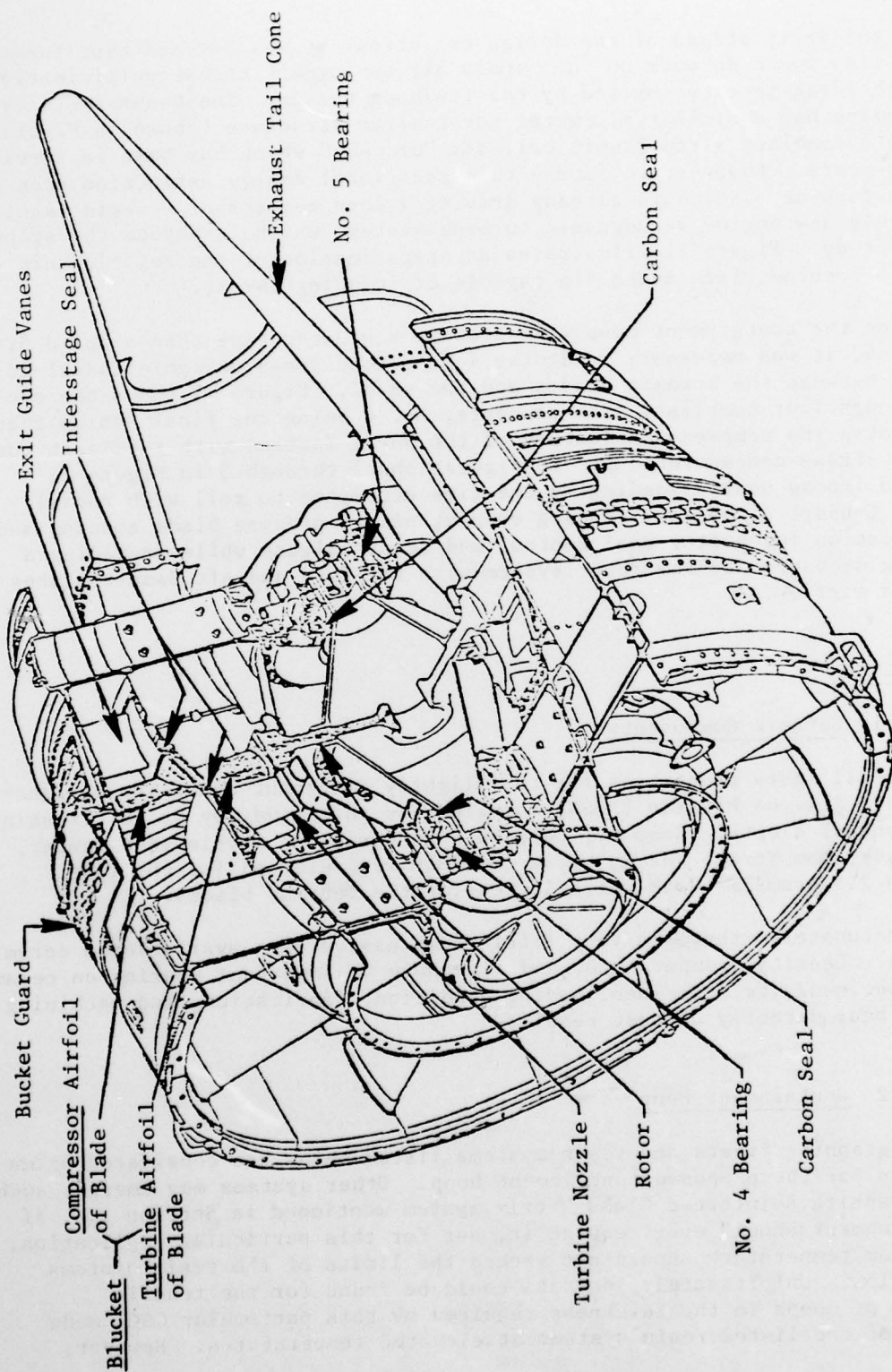


Figure 10. CJ805 Aft Fan Section with "Bucket."

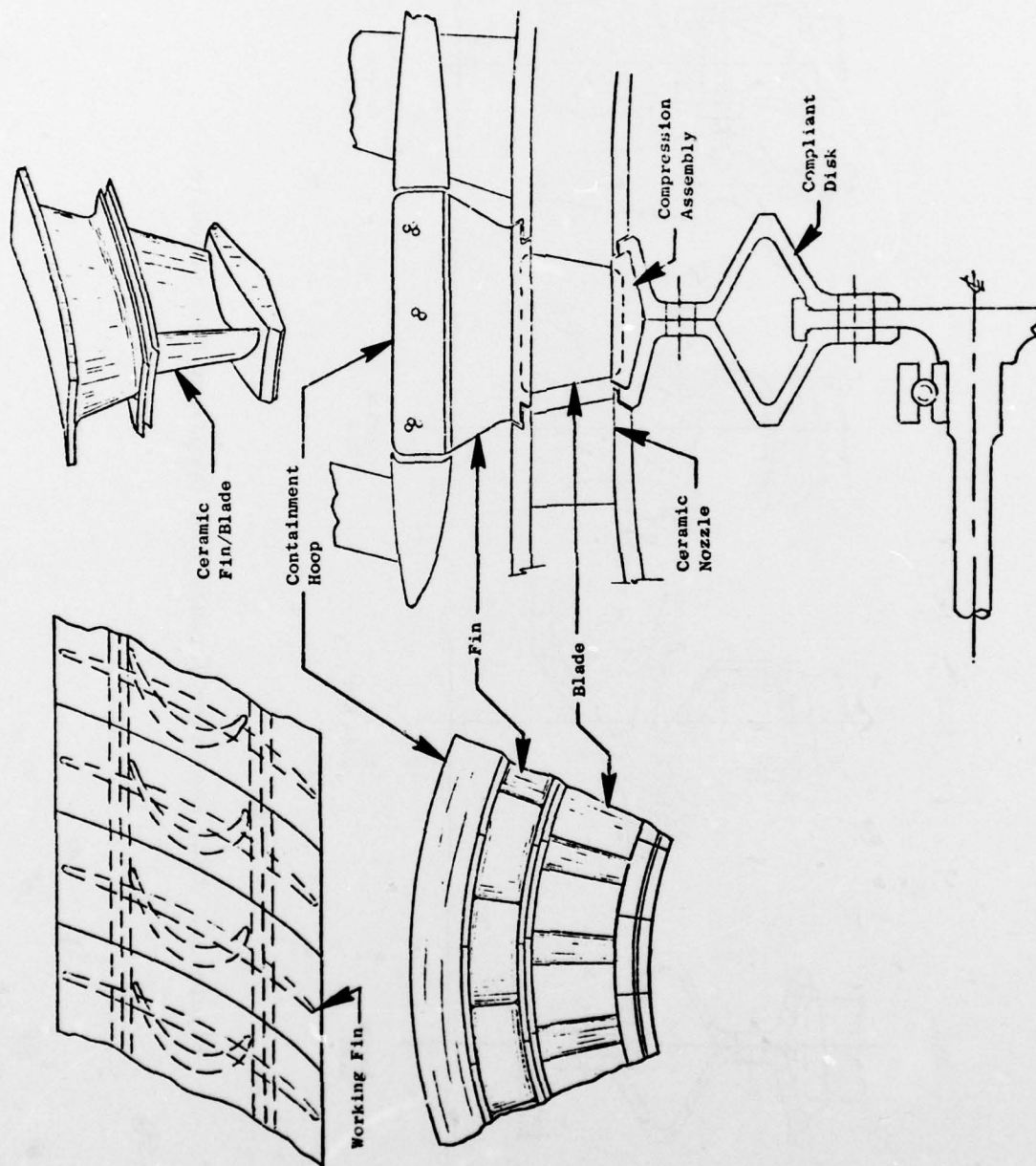


Figure 11. CSCT - With Fin Profiled to do Work.

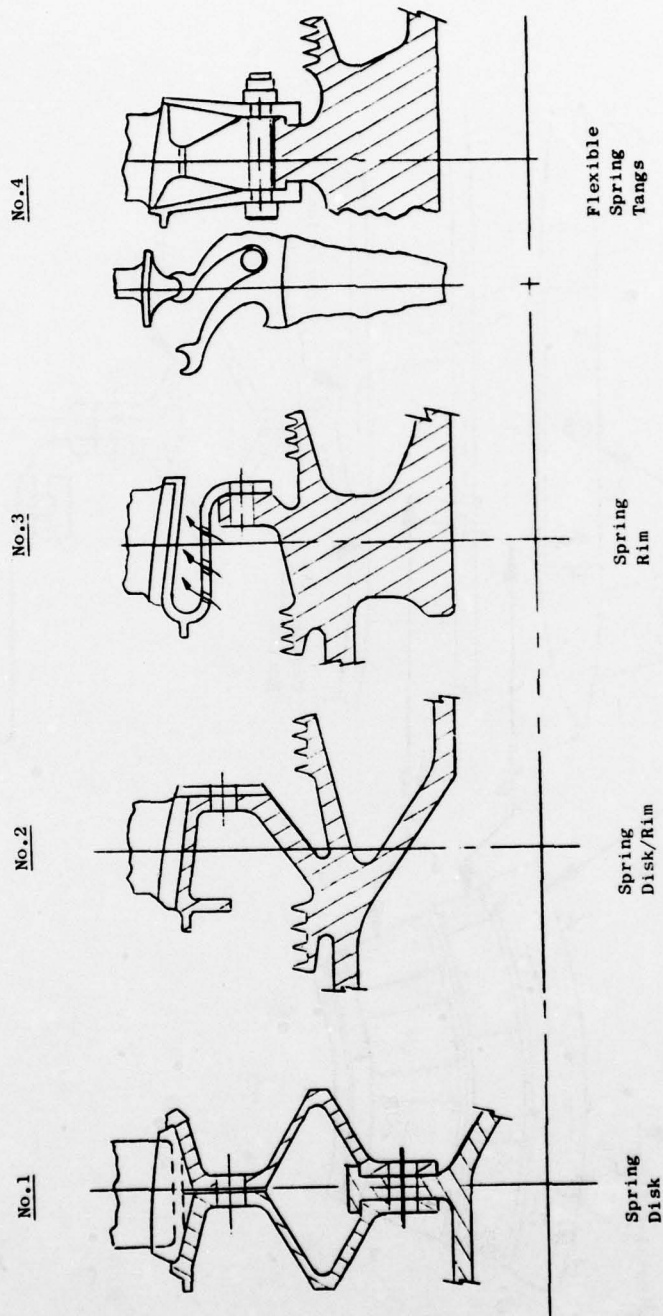


Figure 12. CSCT Evolution Through Four Compliant Disk Concepts.

Table II. Assumed Properties for Low Density RBSN.

Density (gm/cm <sup>3</sup> )*	2.5	2.3
Thermal Conductivity (Btu-in./hr-ft <sup>2</sup> -° F) Room Temperature	125	105
Thermal Conductivity (Btu-in./hr-ft <sup>2</sup> -° F) 2200° F	60	40
3-Point Bend Strength (ksi)	38	30
4-Point Bend Strength (ksi)	32	25
Tensile Strength (ksi)	22	17
Compressive Strength (ksi)	110	85
Weibull Modulus	10	10
Elastic Modulus (10 <sup>6</sup> psi) Room Temperature	26	21
Elastic Modulus (10 <sup>6</sup> psi) 2200° F	28	22
Poisson's Ratio	0.20	0.20
Steady-State Creep Rate at 2460° F	**	**
Thermal Expansion (10 <sup>-6</sup> /° F)	1.7	1.7

Strength at 2200° F may be about 1.7 times room temperature strength.

\*Normal high density RBSN is about 2.7 grams/cm<sup>3</sup>

\*\*Not detectable.



based on experience to date, it is projected that zero or nearly zero oriented filament wound hoops properly processed into the configuration required for this particular application should display ultimate hoop tensile strengths ranging from 230,000 psi to over 250,000 psi to sustain the required loads in any combination of the fiber/resin systems listed below at the related temperatures. A final selection of a containment hoop system would depend on the outcome of a rather extensive development program where a variety of processing parameters including variations in fiber tension, angle, and processing environment could be explored with deliberate iterations, then proof tested in spin tests at elevated temperatures using simulated weight to represent the actual containment loads.

#### Fibers

- A S - for low cost, availability, and experience in usage
- HTS - for resistance to oxidation

<u>Resin</u>	<u>10-Hour Temperature Limit</u>
• Hercules HT	500° F
• Hercules 4397	500° F
• Hercules HR 600	600° F
• PMR 15	500° F
• DuPont NR150B2	650° F

#### 2.6.3 Disk and Damper Plates

- René 95
- Inco 718

Both materials are good candidates but will require about 1.5% expenditure of core cooling air in the rim area due to the 2400° F T<sub>4</sub> condition. Since the rim load is considerably lower than in a conventional turbine, less strategic material, such as A-286, may prove adequate for the life requirement of this particular turbine.

#### 2.6.4 Compliant Layers

In order to inhibit localized high intensity compressive loads between the various components of the Compression Structured Ceramic Turbine, a compliant porous interface between mating ceramic components or mating metal to ceramic components may be desirable.

The compliant porous material crushes at a threshold compressive stress determined by the microstructure. This then redistributes the load over a more extensive bearing surface without degrading the strength of the underlying base structure or damaging the noncompliant mating surface. Some materials that may be considered as good candidates for the various interfaces of the CSCT are listed below:

- Flexible tang to blade root
  - flame-sprayed zirconium
  - platinum foil

Since the compression load at this interface is only about 100 pounds over a total area of about 0.125 in.<sup>2</sup>, and since the temperature in that area is only about 1200° F, a compliant layer (or a layer to inhibit chemical reaction between the metal and ceramic for the 10 hours of anticipated life at that temperature) may not be necessary. Actual future testing will determine its need.

- Blade tip to fin foot
  - porous alumina
  - porous silicon nitride
  - porous RBSN

The porous alumina or porous silicon nitride could be applied chemically to either surface or inserted as a separate thin wafer. The porous RBSN would be achieved chemically as a thin integral layer to one or both contact surfaces.

- Fin tip to containment hoop
  - porous RBSN
  - silicone rubber

A thin porous RBSN layer integral with the fin would be optional, if required. However, the 500° F to 600° F environment may allow a more desirable option of silicone rubber for the 10 hours of anticipated operation at that temperature. The silicone rubber would act as an adhesive to bond the fins to the inner surface of the containment hoop thus assisting in the clustered assembly of blades, fins, and hoop to the depressed flexible tangs from the metal hub as described later.

Final selection of these materials or others would be based on future actual screening tests, but initial selections would probably include only the integral porous RBSN surface treatment between blades and fin and the

silicone rubber between fins and hoop since these treatments would be the most simple and least expensive to accommodate.

## 2.7 HEAT TRANSFER AND WINDAGE LOSS ANALYSIS

A 3-D heat transfer program was used to study the effective fin cooling of the graphite containment hoop of a Compression Structured Ceramic Turbine. Results of two fin configurations are listed in Figure 13 and show adequate cooling of the hoop with a fin airflow rate of 0.64 pound per second. A range of four fin airflow rates versus exit temperature is also listed in Figure 13 for future consideration, if more or less cooling of the containment hoop is desired. Values listed in Figure 13 should be tempered with the fact that seal leakage was assumed to be negligible because there is no way to accurately predict how effectively the seals can perform or how efficiently such leakage can be diverted to minimize mixing before it exits from the fins. Assuming a rather generous total leakage of 1.5% core gas, with a 60/40 forward/aft seal split, and with moderate mixing across the fins, the aft inner hoop temperature could increase from 336° F to 500° F, which is still within conservative high temperature resin limits for the hoop. However, until actual tests are conducted on future hardware, the final selection of hoop resin system should not be confirmed because the difference in cost between an epoxy system and a polyimide system would be significant.

In Figure 14, calculations of windage losses associated with the fin/hoop system are rated in horsepower for seven areas. An evaluation of these drag losses in comparison with the baseline turbine is summarized later in this report in Section 3.0, Operational Limits and Performance Analysis. Details of the heat transfer and windage loss analysis are presented in Appendix A. The prospect that the high energy gas leakage through the face seals could be utilized as an ejector to induce bypass flow and augment thrust has been suggested, but no analysis was made to see if such a cycle would be valid. The aft seal configuration would have to be turned around so its exit vector would be directed rearward like the forward seal in this case. For the same reason that a rocket motor thrust is increased by adding a ring manifold around the rocket nozzle, the hoop/fin system may provide a similar augmentation to the CSCT.

## 2.8 STRESS AND BLADE FREQUENCY ANALYSIS

### 2.8.1 Containment Hoop Analysis

Components of the Compression Structured Ceramic Turbine are illustrated in Figure 15 with two design approaches for incorporating the composite containment hoop. One approach, which would limit radial growth for better seal control, requires pressure-fit assembly between the 360° ceramic ring and the graphite composite hoop. The other approach uses all sectorized ceramic components with no significant prestress to the hoops other than the preload imposed to either version by the hub's flexible steel tangs. By stretching the containment hoop an initial amount, its residual growth at operating speeds



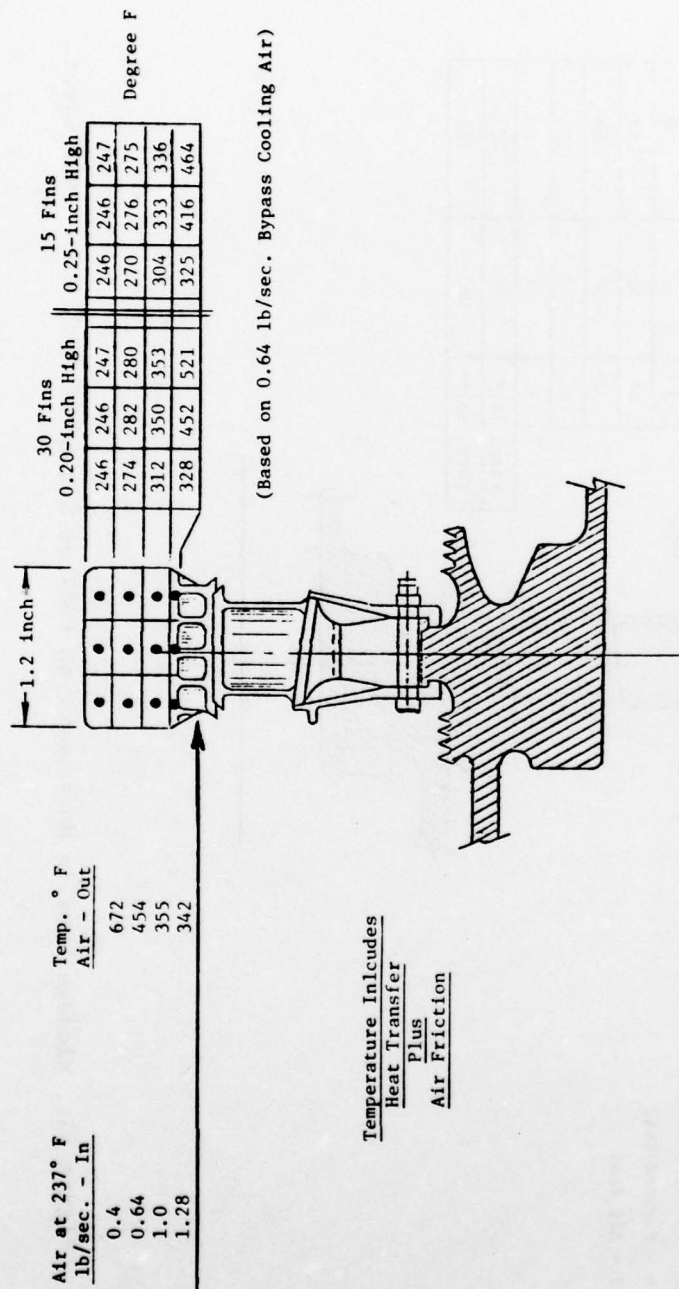


Figure 13. Heat Distribution in CSCT Containment Hoop and RBSN Fin Endwall at Sea Level Mach 0.7, 100% Speed.



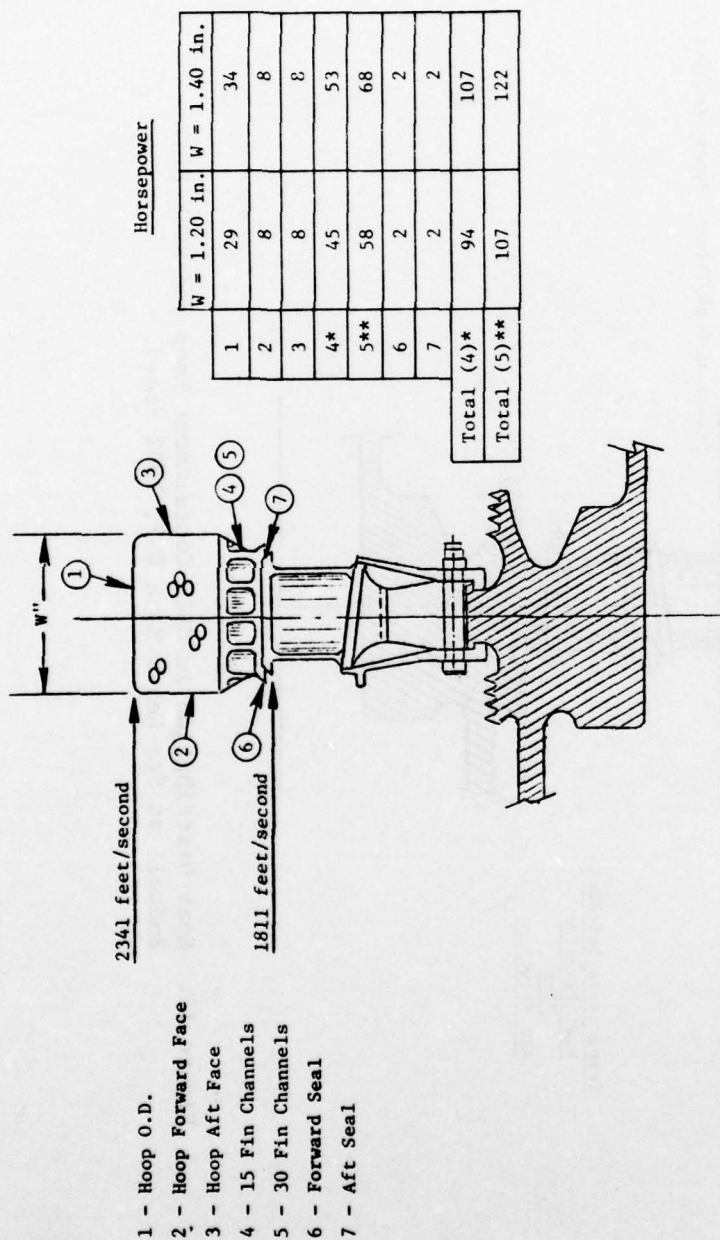


Figure 14. Windage Loss in Horsepower on CSCT at Sea Level Mach 0.7 - 100% Speed.

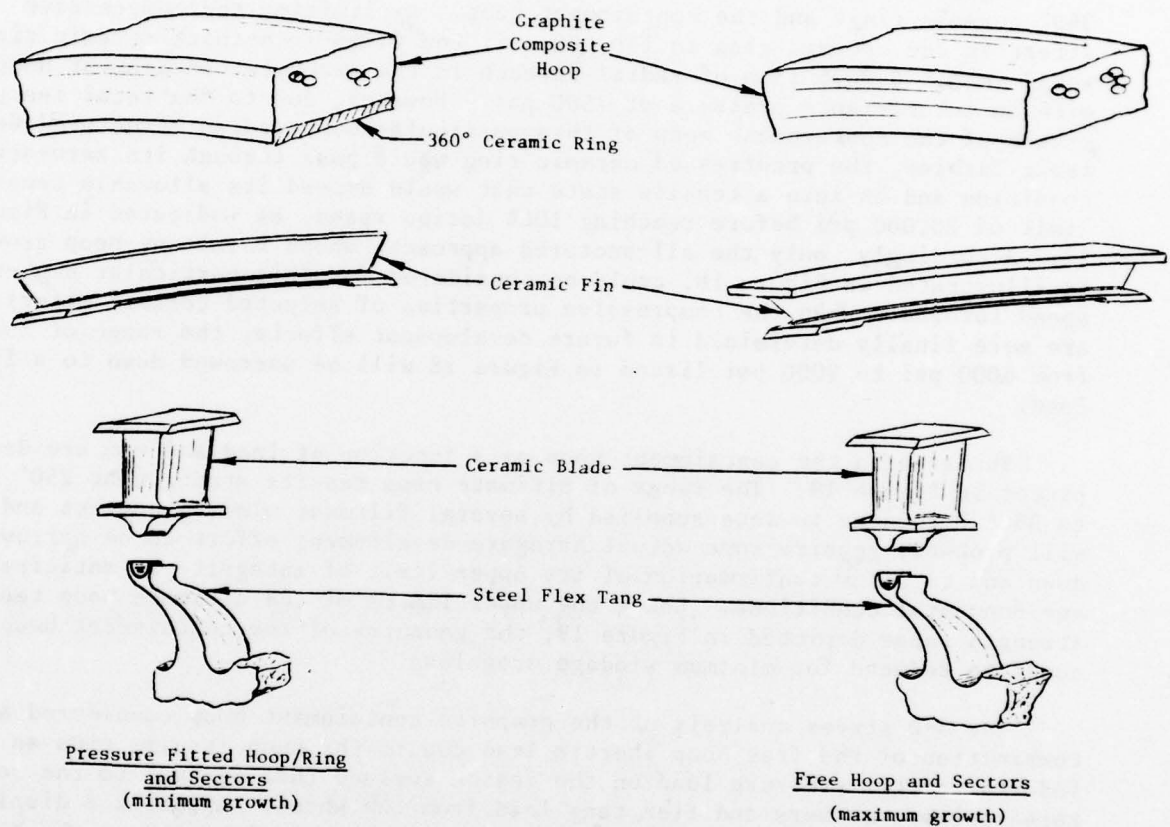


Figure 15. CSCT Components - Two Approaches to Incorporating the Composite Containment Hoop.

would be diminished by the amount of initial stretch. Therefore, the more the hoop can be stretched initially, the less allowance must be made to accommodate face seal clearance over the operating range of the turbine.

Figure 16 shows the relationship of stress versus deflection between two 360° ceramic rings and the containment hoop. By limiting the compressive stress in the ceramic ring to 150,000 psi, the 0.179-inch-thick ceramic ring would impose 0.0095 inch of radial stretch in the graphite containment hoop with an interference pressure of 7500 psi. However, due to the total inertia growth of the containment hoop of this particular Compression Structured Ceramic Turbine, the prestressed ceramic ring would pass through its zero-stress condition and on into a tensile state that would exceed its allowable tensile limit of 20,000 psi before reaching 100% design speed, as indicated in Figure 17. Accordingly, only the all-sectored approach, whose resultant hoop growth is illustrated in Figure 18, could be considered for this particular high-tip-speed turbine. When the compressive properties of selected ceramic materials are more finally determined in future development efforts, the range of loads from 6000 psi to 9000 psi listed in Figure 18 will be narrowed down to a final load.

Stresses in the containment hoop as a function of load and rpm are depicted in Figure 19. The range of ultimate hoop tensile strength at 250° F to 350° F relates to data supplied by several filament winding sources and will probably require some actual hardware development effort to be narrowed down and to allow confirmation of its upper limit of integrity at anticipated environmental conditions. Using the upper limits of the ultimate hoop tensile strength range depicted in Figure 19, the geometry of the containment hoop could be reduced for minimum windage drag loss.

The 3-D stress analysis of the graphite containment hoop considered a combination of the free hoop inertia load due to the hoop itself, plus an induced inertia pressure load on the inside surface that was due to the sectored ceramic members and flex tang load from the wheel. Appendix B displays the approach used to determine total stress in the containment hoop which is factored into the computer analysis. The analysis included input from the steady-state heat transfer analysis described earlier and utilized a time-sharing version of FINITE identified as TSFINE. To increase the accuracy of the 3-D hoop analysis, the hoop was divided into very small elements, then split in half, with axial deflections on one side set to zero, as shown in Figure 20. Out of a computer-allowable maximum of 300 elements, 280 elements were used. Since the exact final weight of the ceramic components cannot be determined until future material data are generated, three internal pressures, including 6000, 7300, and 9000 psi, were used in the analysis. These particular values were selected from hand calculations based on variations in allowable ceramic material density and section thickness. For this particular turbine, refinements in turbine blade or cooling fin geometry should still hold induced load limits to within this range. Hoop thickness was varied from 0.60 to 0.75 inch. While the 0.75-inch-thick hoop displayed about a 2% lower stress than the 0.60-inch-thick hoop, the thicker, lower-stressed hoop was not felt to justify the increased weight and larger radius windage loss associated

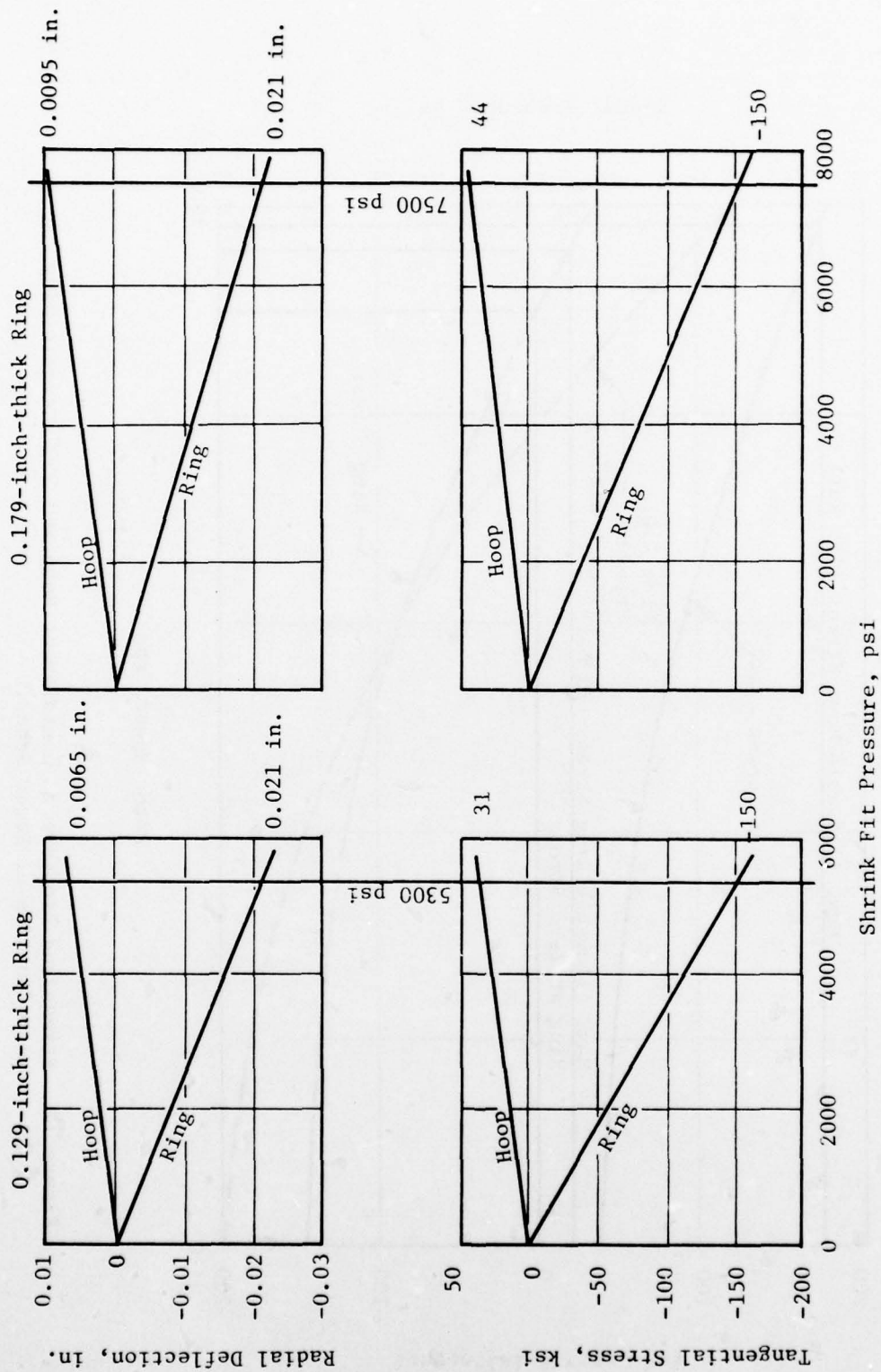


Figure 16. Stress Versus Deflection Between Composite Hoop and 360° Ceramic Ring as a Function of Rotor Speed.



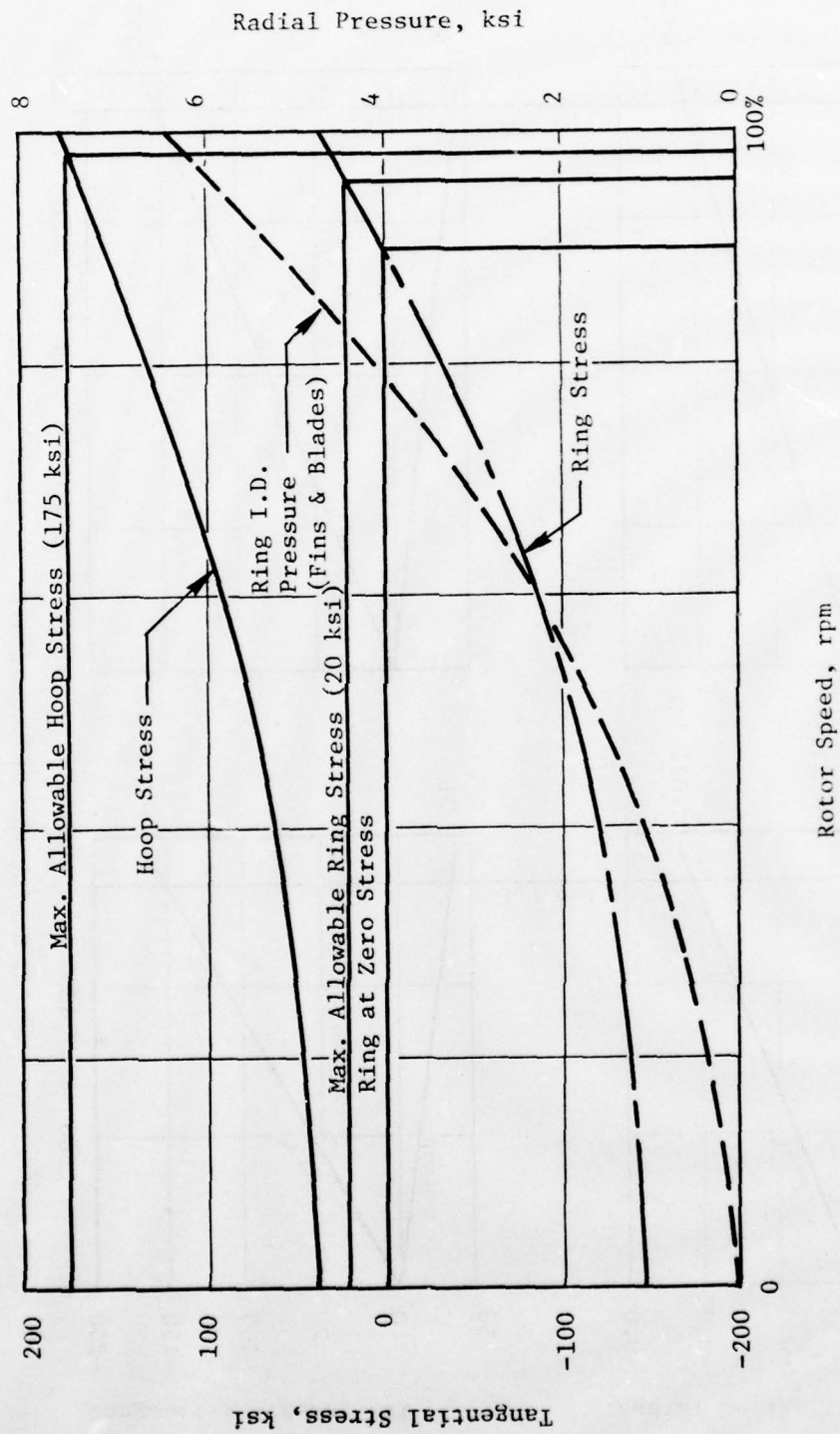


Figure 17. Stress and Pressure in Containment Hoop and 360° Ceramic Ring as a Function of Rotor Speed.

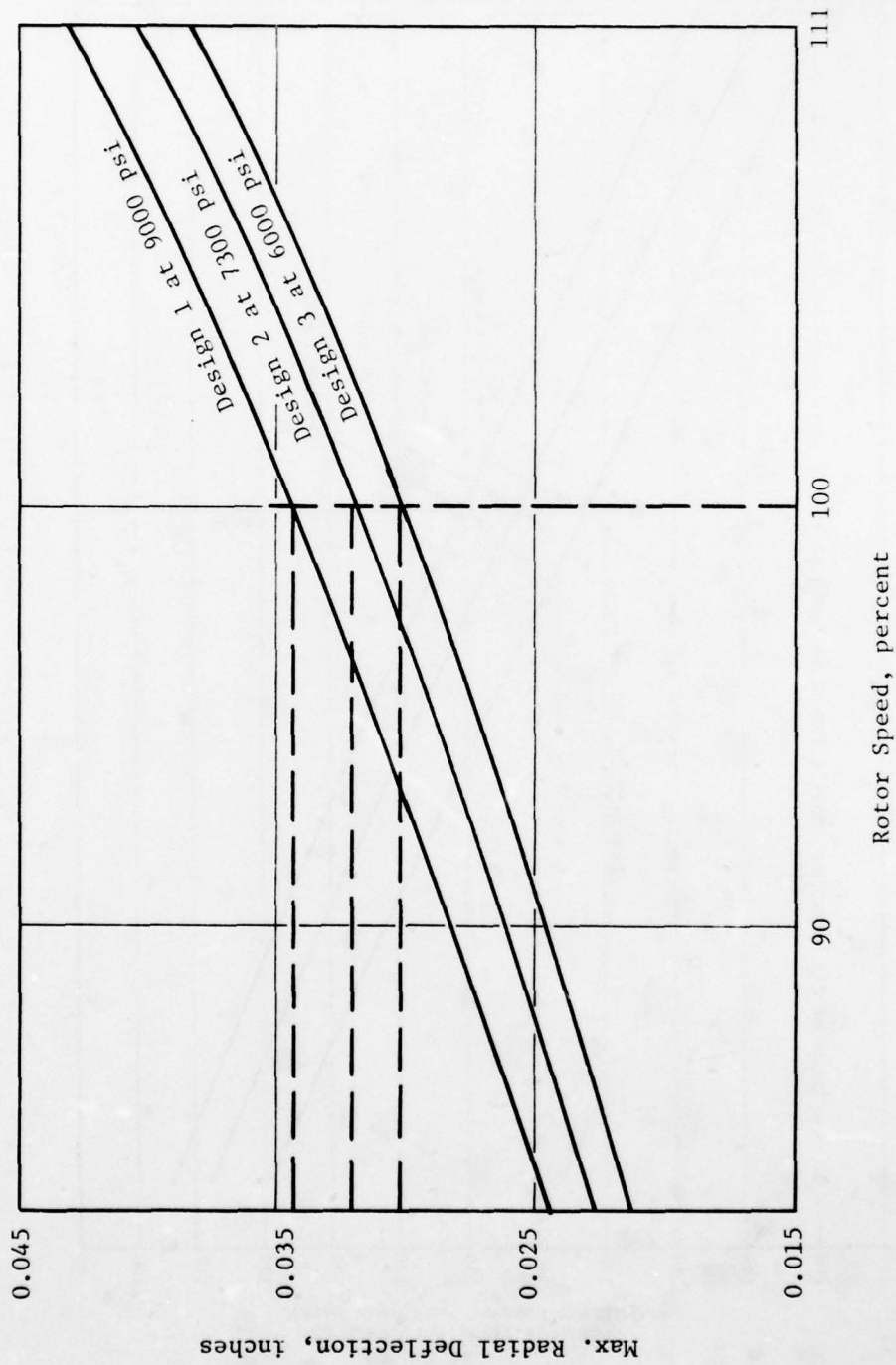


Figure 18. Maximum Hoop Radial Deflection Versus Rotor Speed.

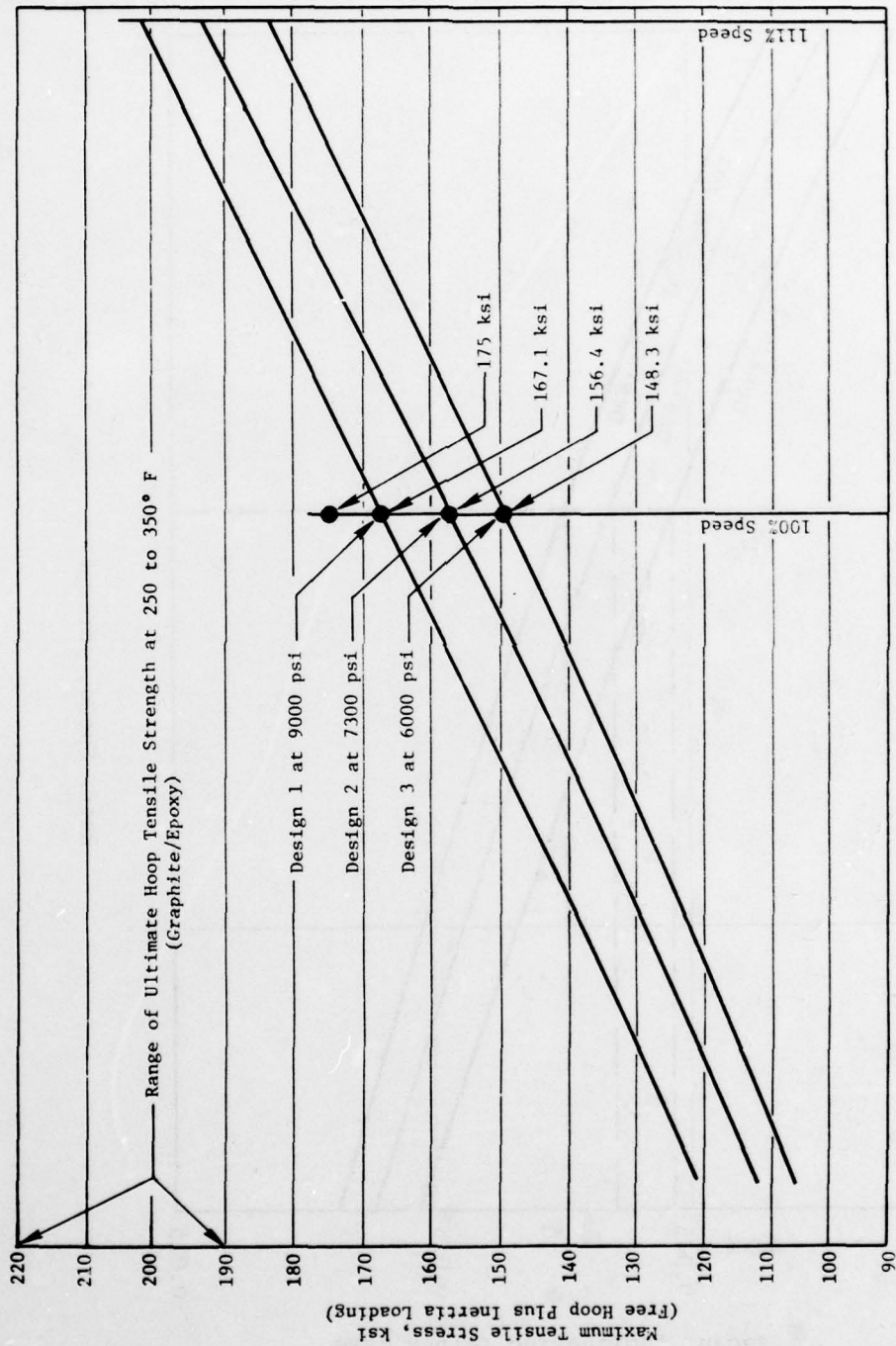


Figure 19. Maximum Hoop Tensile Stress Versus Rotor Speed.

Center

254	256	258	260	262	264	266	268	270	272	274	276	278	280
253	255	257	259	261	263	265	267	269	271	273	275	277	279
226	228	230	232	234	236	238	240	242	244	246	248	250	252
225	227	229	231	233	235	237	239	241	243	245	247	249	251
198	200	202	204	206	208	210	212	214	216	218	220	222	224
197	199	201	203	205	207	209	211	213	215	217	219	221	223
170	172	174	176	178	180	182	184	186	188	190	192	194	196
169	171	173	175	177	179	181	183	185	187	189	191	193	195
142	144	146	148	150	152	154	156	158	160	162	164	166	168
141	143	145	147	149	151	153	155	157	159	161	163	165	167
114	116	118	120	122	124	126	128	130	132	134	136	138	140
113	115	117	119	121	123	125	127	129	131	133	135	137	139
86	88	90	92	94	96	98	100	102	104	106	108	110	112
85	87	89	91	93	95	97	99	101	103	105	107	109	111
58	60	62	64	66	68	70	72	74	76	78	80	82	84
57	59	61	63	65	67	69	71	73	75	77	79	81	83
30	32	34	36	38	40	42	44	46	48	50	52	54	56
29	31	33	35	37	39	41	43	45	47	49	51	53	55
2	4	6	8	10	12	14	16	18	20	22	24	26	28
1	3	5	7	9	11	13	15	17	19	21	23	25	27

Inside Diameter

Figure 20. CSCT Half-Hoop 3-D Finite-Element Stress Model.



with it. Table III lists the loads imposed by the sector ceramic components and summarizes the final hoop stress analysis based on a hoop thickness of 0.60 inch. For the hoop analysis, it was assumed that the pressure loading from the fins into the hoop would be uniform; in reality, however, the load may be more concentrated directly over the fins. It is believed, however, since this is a relatively cool area, that the fin tip platform plus a thin layer of silicone rubber adhesive between the fins and the hoop would distribute the unit loads into the hoop rather efficiently. It is anticipated that point loading would never exceed the 12,000 psi compressive radial stress allowable on the inside diameter of the composite hoop, which is considered the top limit of the fiber matrix system.

Since the fibers in the containment hoop will all be parallel or nearly parallel and will be very densely composited by high tension filament winding, the matrix or binder system will have little influence as a function of hoop temperature. Hoop strength and radial deflection should be uniform at temperatures ranging from 350° to over 600° F.

#### 2.8.2 Ceramic Fin Analysis

A 3-D finite-element fin analysis was conducted. It was determined that the fin airfoil should be slightly canted relative to the parallel sides of the fin foot so that opposite pointed corners of the foot are more evenly supported than if the fin airfoil were straight on the foot centerline. This slightly canted relationship can be observed in Figure 21. Another feature that became obvious relates to the compliant layer between the fin and the containment hoop. If the fin endwall is not strong enough to distribute the load from the fin uniformly into the containment hoop, the endwall would deflect inward while the fin airfoil compresses the compliant layer directly over it. This could result in bending stress in the fin endwall slightly in excess of 50,000 psi. It may be preferable to eliminate any compliant layer between the fin endwall and the containment hoop or at least to keep it to a very minimum thickness of not more than 0.003 inch. More analysis must be done in this component, but before such effort is initiated a determination should be made on whether or not the fins would do work to tend to offset their drag penalty as discussed later, because such determination will affect their geometry significantly thus establishing new boundary conditions for a stress analysis. Regardless of the number of fins or their possible work angle, the total section of all fins carrying the compressive forces induced by inertia loads would average about 50,000 psi compression (as summarized later in Figure 27).

#### 2.8.3 Ceramic Turbine Blade Analysis

The ceramic blade profile was established as a uniform extruded airfoil section taken at an 80% blade span of the baseline turbine. This selection was made as a compromise between the baseline turbine blade and an idealized inverted-taper airfoil, which would be more uniformly stressed in a centrifuged compressive state. However, to invert the taper of a compressively held ceramic blade would require a severe departure from state-of-the-art

Table III. CSCT Containment Hoop Load Analysis.

(At A Blade Tip Speed of 1807 ft/sec - 100% Design)

Sector Component	Density, gr/cc	Inertia Force, lb
Fin Tip	2.3	1478
Fin	2.3	1016
Fin Foot	2.3	889
Blade Tip	2.5	845
Blade	2.5	755
Blade Platform	2.5	756
Blade Shank	2.5	119
Flex Tang		100
Unit Total =		5958 lb

30 Units Exert 178,770 lb

Hoop Internal Area = 26.78 in.

Therefore  $178,770/26.78 = 6676$  psi

Hoop Thickness = 0.6 in.

Hoop Stress from 6676 psi = 43,505 psi

Free Hoop Inertia Stress = 108,387 psi

Total Hoop Stress = 151,892 psi

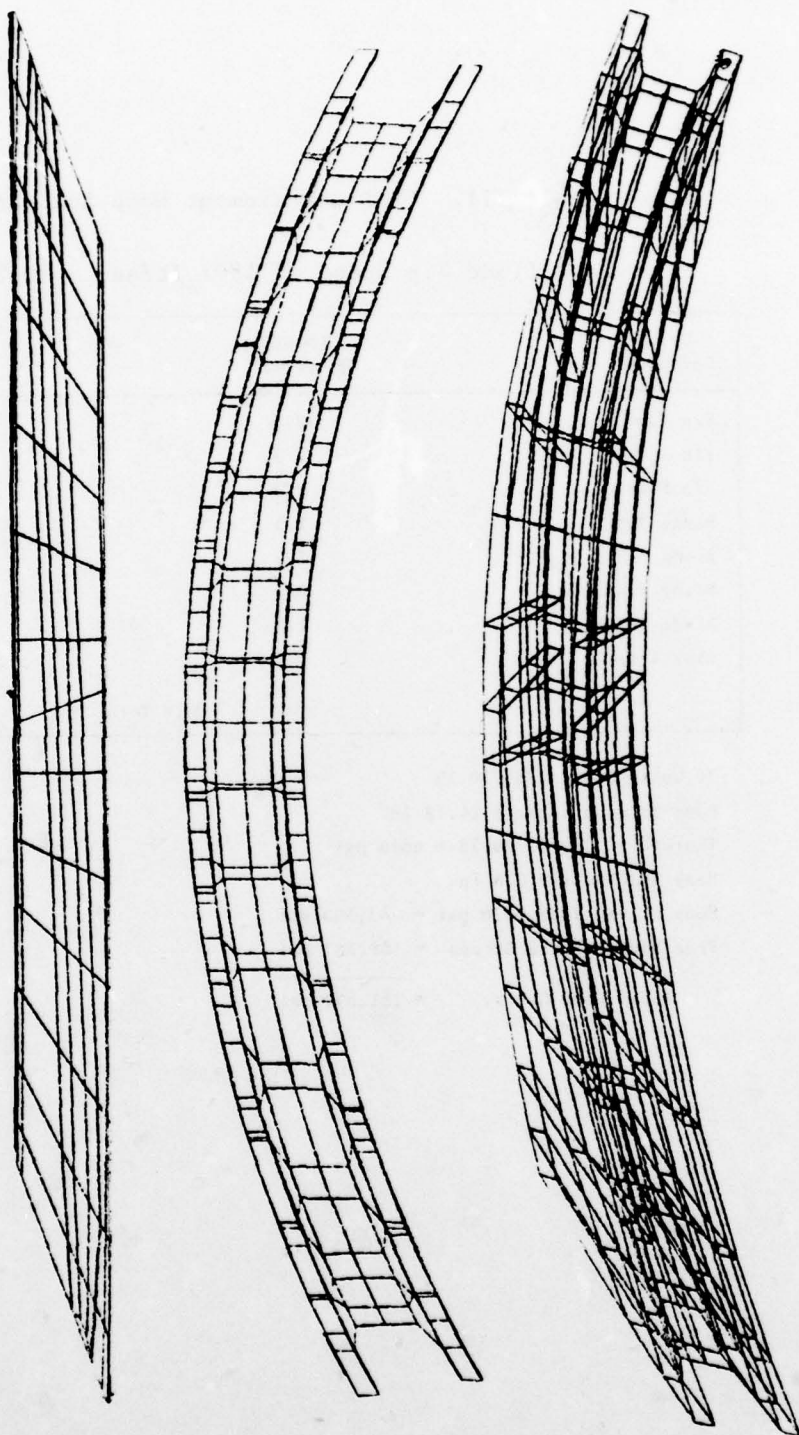


Figure 21. CSCT 3-D Finite-Element Fin Model.



turbine aerodynamics, an undertaking which was beyond the scope of this study. Prospects for utilizing an inverted taper airfoil not only for improved stress distribution within the airfoil but also for higher aero stage efficiency are discussed at the end of this section.

A 3-D finite-element model of the blade is illustrated in Figures 22 and 23. Table IV lists the maximum and minimum stresses within the 11 levels of the blade model. The blade comprises 184 elements and is shown in Figure 24.

Figure 25 shows the first iteration of a plot of thermal and maximum/minimum stress profiles in the blade. The maximum compressive stress of 82,000 psi in the airfoil is conservative, but the bending-induced 20,000 psi tensile in the platform is marginal. Refinements in the platform should reduce the tensile stress in that area by at least one-third.

#### 2.8.4 Disk and Damper Plates Analysis

A 3-D finite-element disk analysis was made with a temperature profile ranging from 800° F at the hub to 1100° F at the rim which is nearly identical to the profile on the baseline turbine. A model of the 3-D finite-element half disk is illustrated in Figure 26. Since the disk is nearly symmetrical, only one-half of its profile was necessary to plot. Likewise, only one damper plate was modeled; it is illustrated in Figure 27.

The disk was profiled to achieve a stress of 175,000 psi at the bore - a stress level which is just under the stress level at that area on the baseline turbine and is the maximum stress in the disk. The two damper plates were sized to be stressed at about 35,000 psi at their point of attachment to the disk. The combined rim load of the damper plates and flexible tangs induced a stress of about 33,000 psi on the rim of the disk just below the radius, where the flexible tangs emerge. The flexible tangs were stressed to 40,000 psi and configured to induce about 100 pounds uniformly against the blade tang from zero rpm to 100% design speed. Figure 28 shows a listing of average stresses at critical areas throughout the Compression Structured Ceramic Turbine. Also listed in Figure 28 are the dynamics of relative growth between the wheel and hoop, a growth accommodated by the flexible tangs from the wheel. Figure 29 illustrates the dynamics of the flexible tangs over the full operating range of the CSCT in relation to the hoop. The tang is shown passing through its nominal position at 57% rotor speed and extending 0.009 inch beyond nominal at 100% speed.

#### 2.8.5 Blade Frequency

A vibrational analysis of the CSCT blade is plotted on a Campbell diagram in Figure 30, together with the frequency range of a normal metal baseline turbine blade. Due to the fixed ends of the CSCT blade, its first flexural frequency is so high that there is no need to display its first torsional or second flexural frequencies, which would be even higher. The prospect of an inverted-taper airfoil would probably affect the frequency, though not significantly.



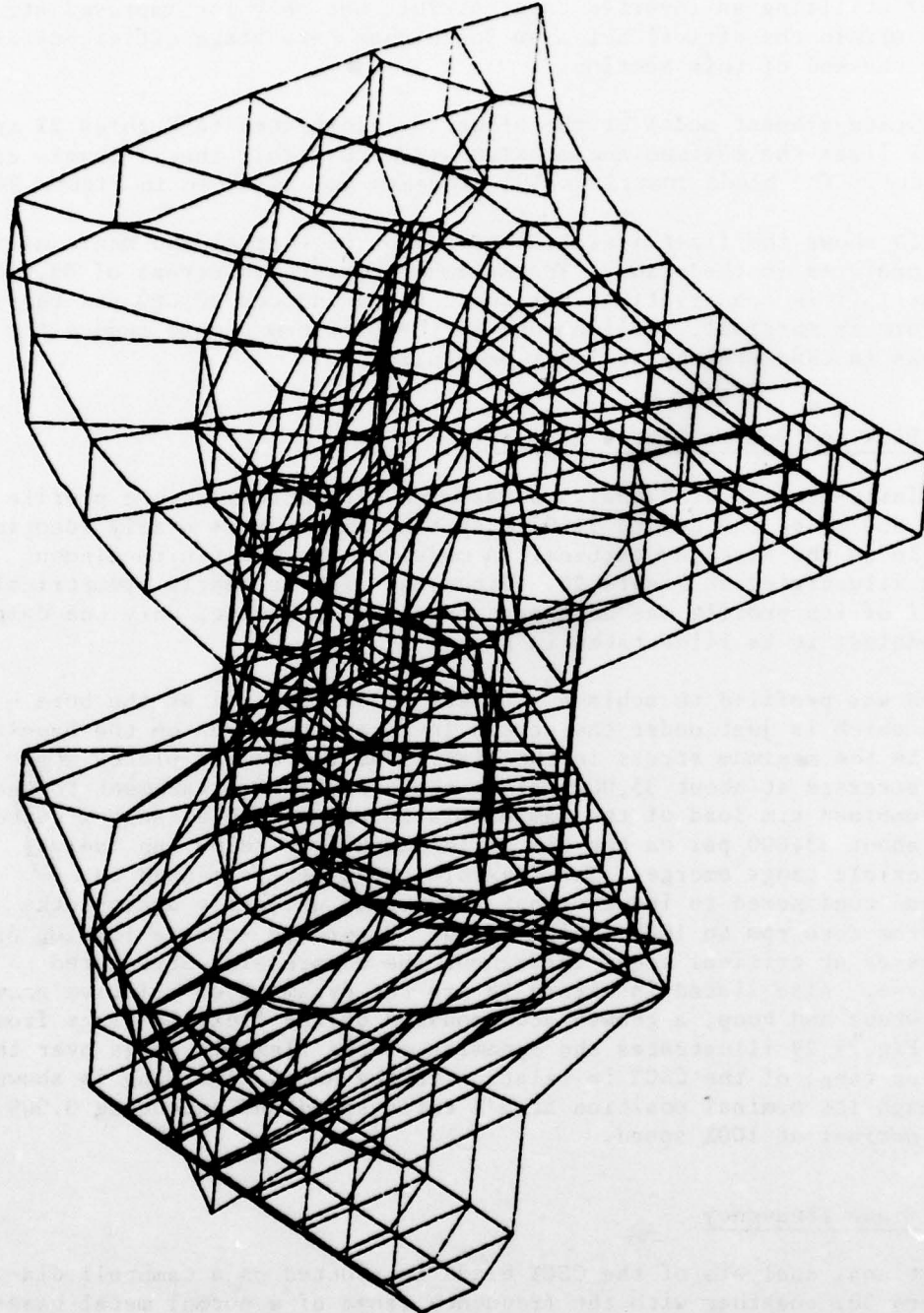


Figure 22. 3-D Finite-Element Model of CSCT Blade - View A.

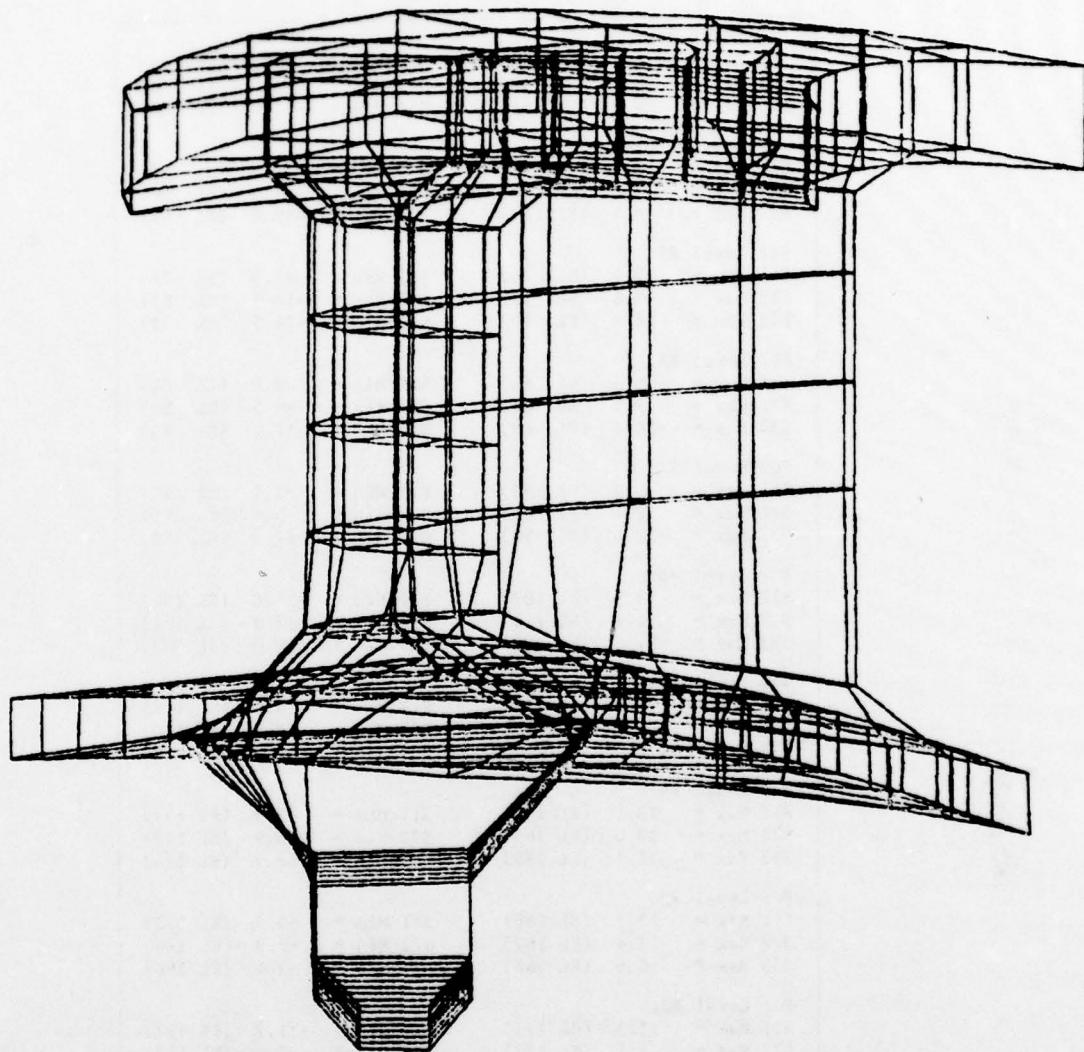


Figure 23. 3-D Finite-Element Model of CSCT Blade - View B.

Table IV. Stress Ranges Encountered in the 11 Levels of the 3-D Finite-Element Model of the CSCT.

For Level R11:			
S11 Max =	6.7* (EL 71)	S11 Min =	-4.7** (EL 69)
S22 Max =	8.1 (EL 40)	S22 Min =	-5.4 (EL 10)
S33 Max =	4.3 (EL 64)	S33 Min =	-21.0 (EL 23)
For Level R10:			
S11 Max =	9.4 (EL 51)	S11 Min =	-20.3 (EL 48)
S22 Max =	5.8 (EL 54)	S22 Min =	-11.4 (EL 50)
S33 Max =	-4.4 (EL 57)	S33 Min =	-52.0 (EL 48)
For Level R9:			
S11 Max =	5.9 (EL 74)	S11 Min =	-23.3 (EL 74)
S22 Max =	-0.6 (EL 72)	S22 Min =	-14.1 (EL 81)
S33 Max =	-28.2 (EL 90)	S33 Min =	-74.5 (EL 73)
For Level R8:			
S11 Max =	6.5 (EL 84)	S11 Min =	-2.8 (EL 84)
S22 Max =	1.3 (EL 82)	S22 Min =	-6.5 (EL 89)
S33 Max =	-24.0 (EL 88)	S33 Min =	-57.1 (EL 83)
For Level R7:			
S11 Max =	4.2 (EL 92)	S11 Min =	-3.1 (EL 92)
S22 Max =	0.4 (EL 92)	S22 Min =	-5.4 (EL 99)
S33 Max =	-22.4 (EL 97)	S33 Min =	-67.3 (EL 92)
For Level R6:			
S11 Max =	3.5 (EL 107)	S11 Min =	-13.8 (EL 102)
S22 Max =	1.1 (EL 111)	S22 Min =	-17.9 (EL 102)
S33 Max =	-24.8 (EL 109)	S33 Min =	-84.0 (EL 102)
For Level R5:			
S11 Max =	4.3 (EL 112)	S11 Min =	-20.5 (EL 113)
S22 Max =	1.1 (EL 121)	S22 Min =	-9.8 (EL 120)
S33 Max =	3.3 (EL 112)	S33 Min =	-47.9 (EL 113)
For Level R4:			
S11 Max =	20.1 (EL 131)	S11 Min =	-9.8 (EL 154)
S22 Max =	19.0 (EL 149)	S22 Min =	-16.9 (EL 149)
S33 Max =	12.1 (EL 160)	S33 Min =	-13.9 (EL 134)
For Level R3:			
S11 Max =	13.7 (EL 166)	S11 Min =	-5.7 (EL 170)
S22 Max =	7.4 (EL 167)	S22 Min =	-2.3 (EL 170)
S33 Max =	-0.6 (EL 168)	S33 Min =	-9.6 (EL 164)
For Level R2:			
S11 Max =	5.3 (EL 171)	S11 Min =	-11.7 (EL 171)
S22 Max =	0.1 (EL 177)	S22 Min =	-3.4 (EL 177)
S33 Max =	-1.3 (EL 175)	S33 Min =	-10.8 (EL 171)
For Level R1:			
S11 Max =	7.6 (EL 178)	S11 Min =	-7.6 (EL 178)
S22 Max =	1.2 (EL 184)	S22 Min =	-6.7 (EL 181)
S33 Max =	-1.3 (EL 184)	S33 Min =	-6.1 (EL 184)

\*6.7 = 6700 psi tension

\*\* -4.7 = 4700 psi compression

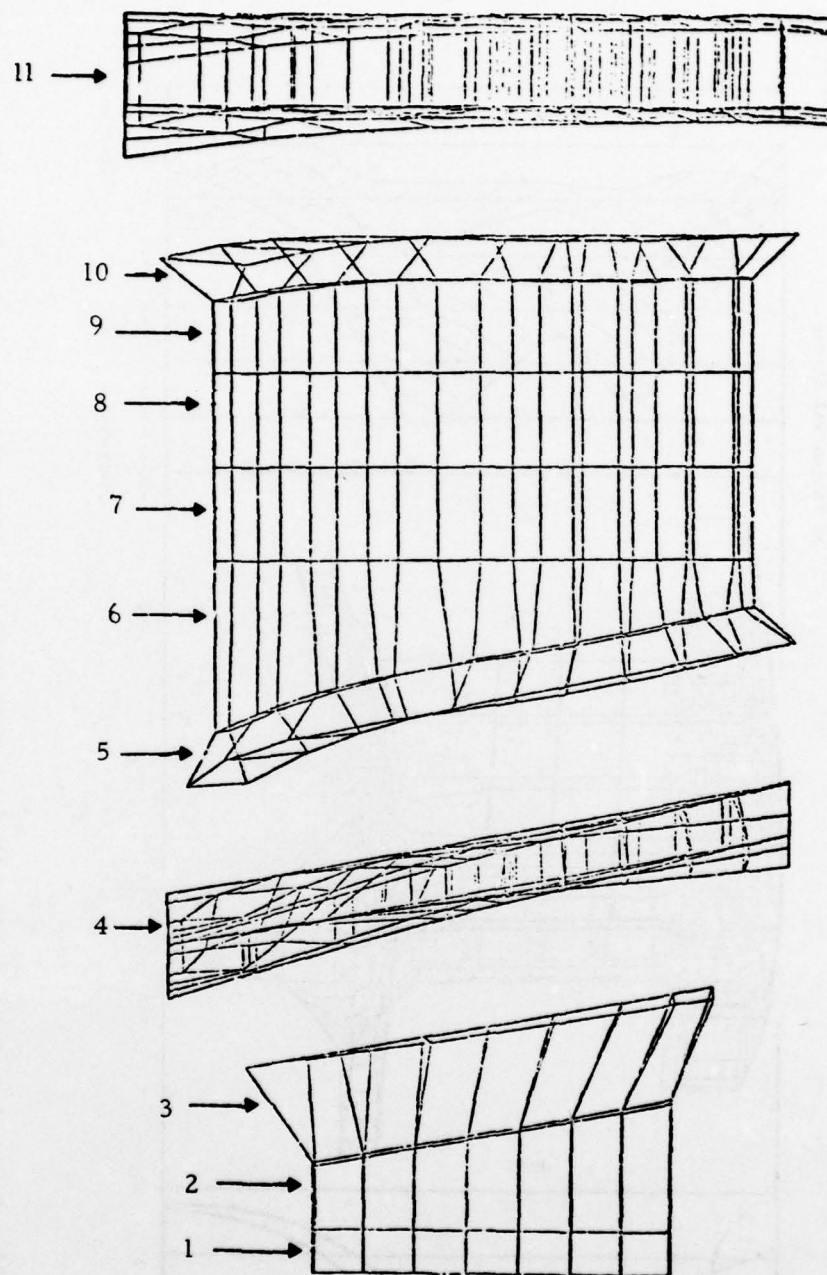


Figure 24. Levels of 3-D Finite-Element Blade Model.



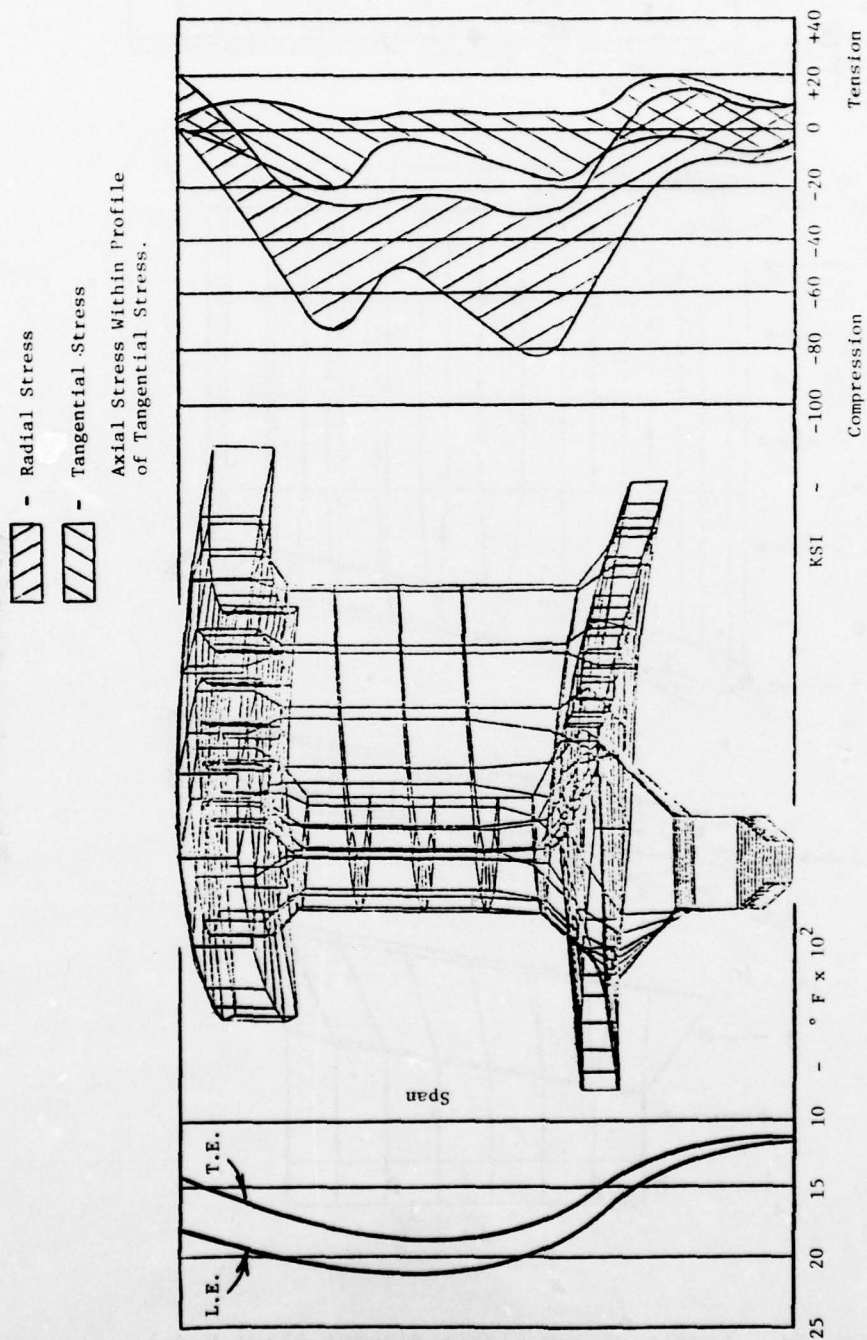


Figure 25. Thermal and Stress Profiles of CSCT Blade at 100% Design - First Iteration.

Center

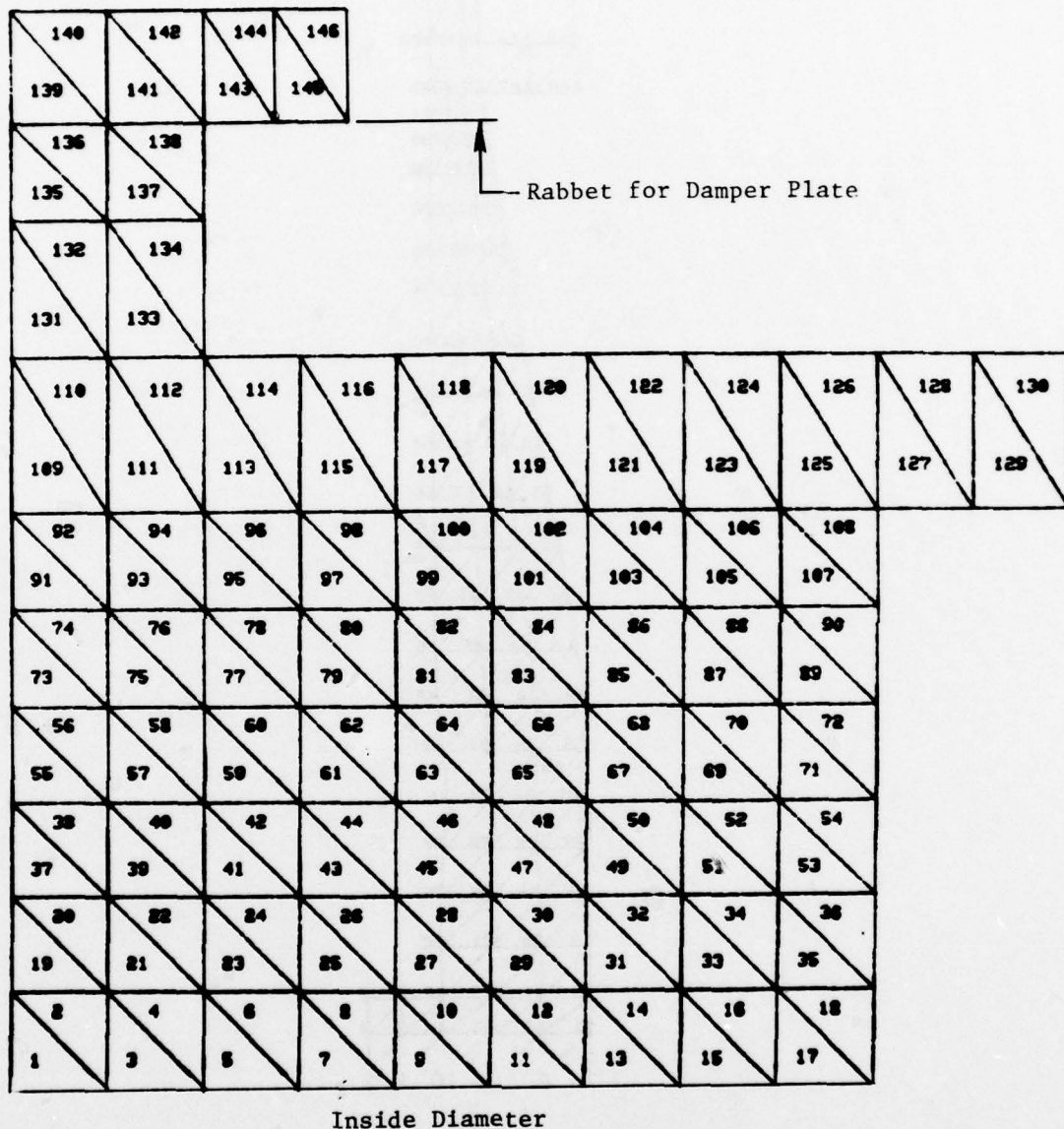
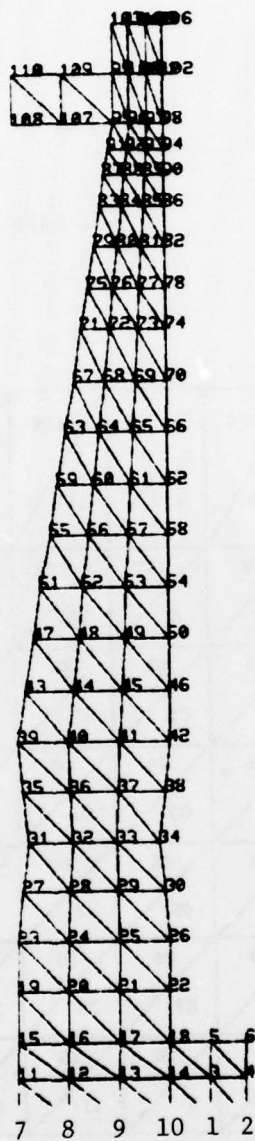


Figure 26. 3-D Finite-Element Model of CSCT Half-Disk.



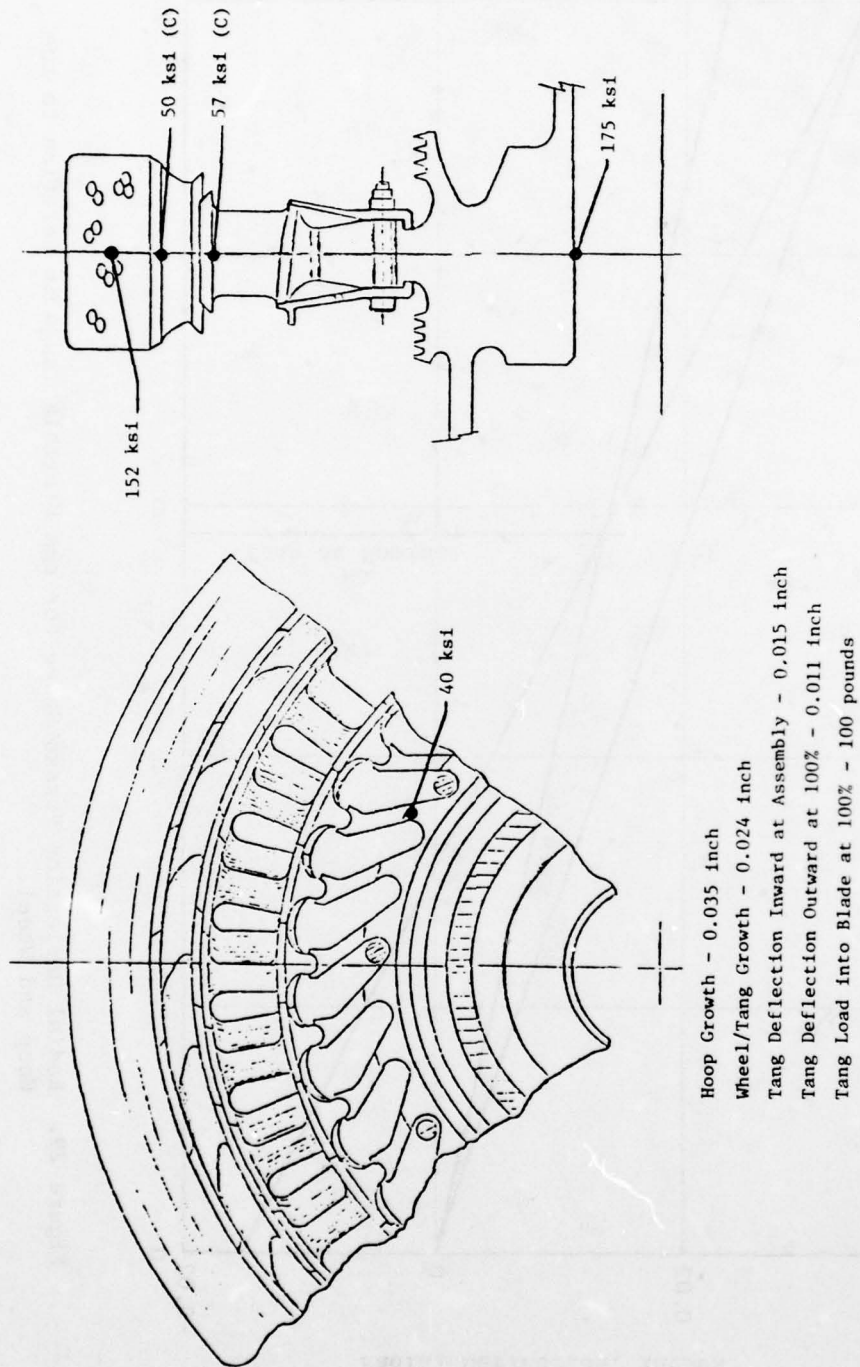


Figure 28. Average Stresses in the CSCT at 100% Design Speed.



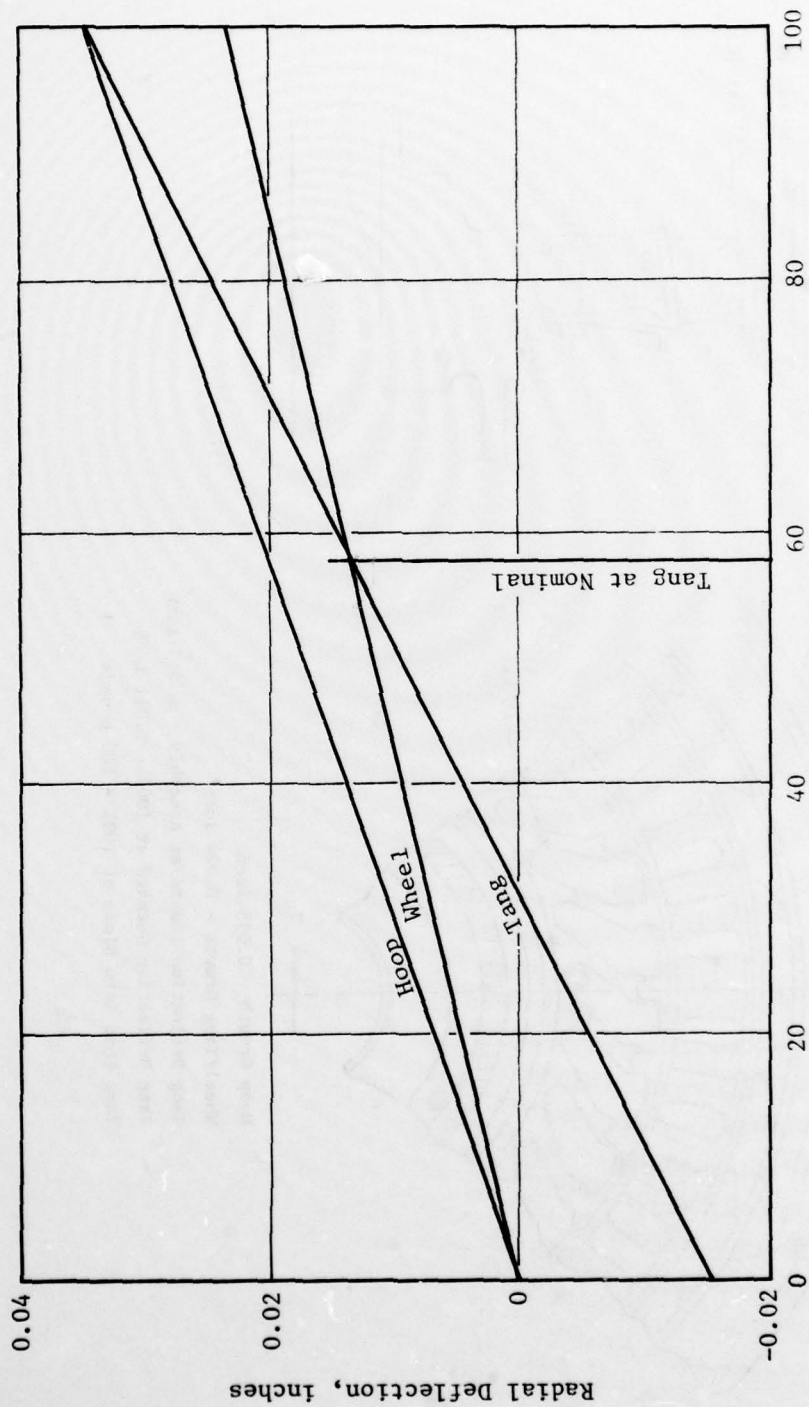


Figure 29. Radial Deflection Versus Speed for the Flexible Tangs in Relation to the Hoop and Wheel.

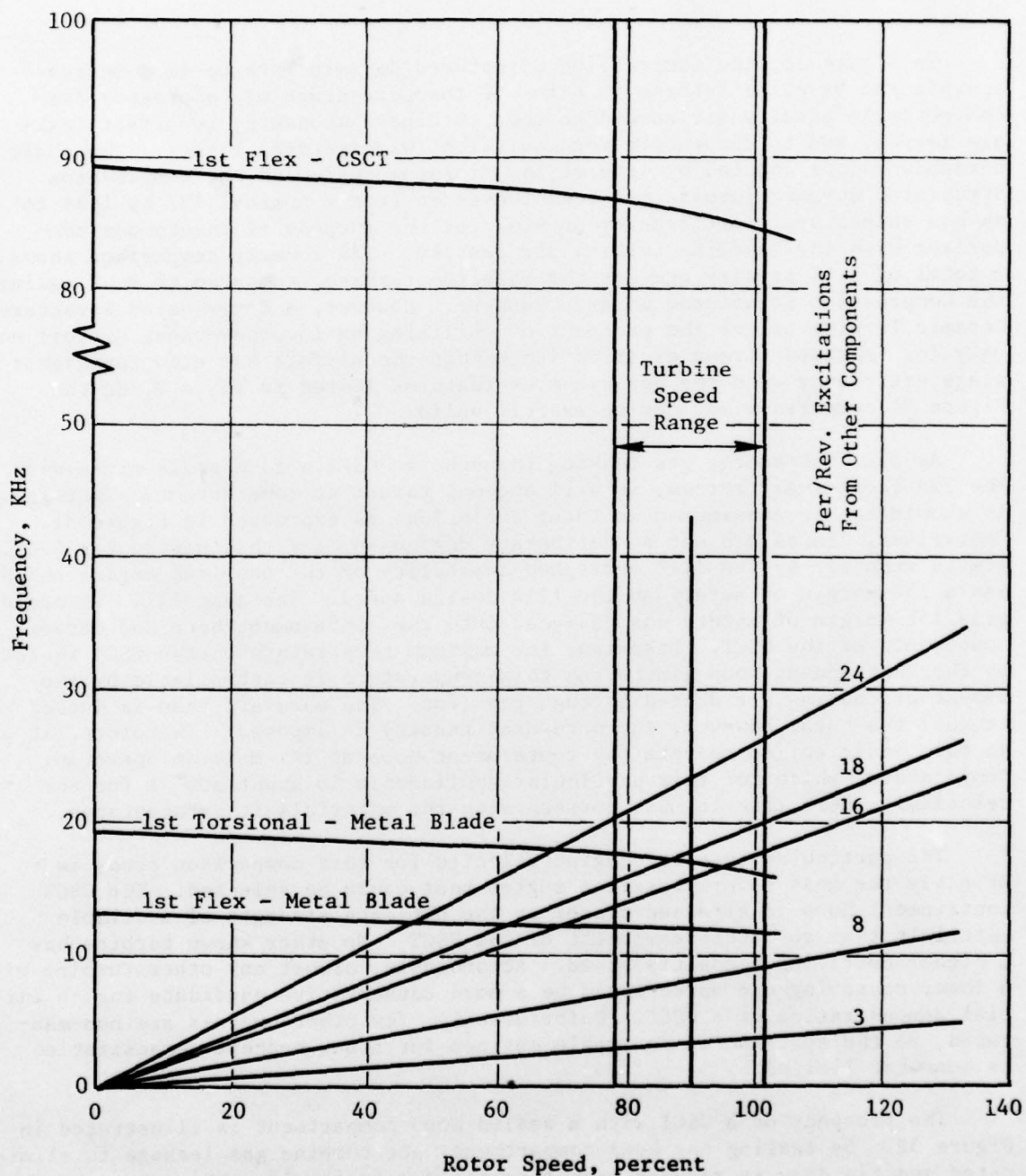


Figure 30. Vibrational Analysis Campbell Diagram of the CSCT Blade Compared to a Baseline Metal Blade

### 3.0 PERFORMANCE ANALYSIS AND OPERATIONAL LIMITS

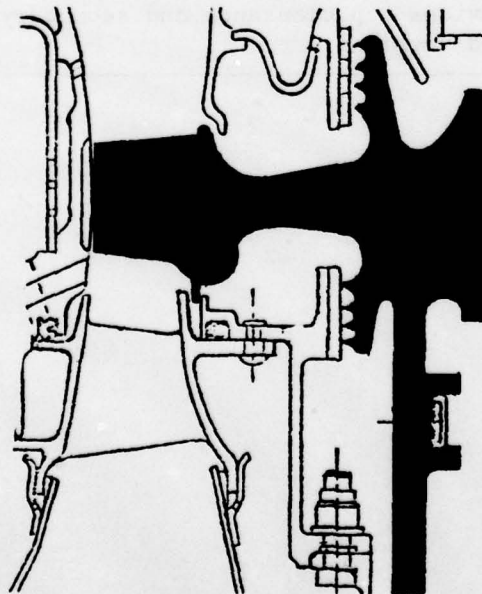
In Figure 31, the Compression Structured Ceramic Turbine is compared against the baseline turbine in terms of the percentage of compressor discharge cycle penalty air needed to cool turbine components, to offset leakage losses, and to compensate for equivalent windage/drag losses. The shaft horsepower loss induced by drag of the fin/hoop system on the Compression Structured Ceramic Turbine has been converted from a nominal 107 hp loss to an equivalent cycle air penalty of 6.4% for the purpose of one-to-one comparison with the baseline turbine air penalty. The summary comparison shows a total of 5.1% penalty against the baseline turbine, compared to 9.4% against the Compression Structured Ceramic Turbine. However, a Compression Structured Ceramic Turbine offers the prospect of utilizing an inverted-taper airfoil not only for improved stress distribution within the airfoil but also for higher stage efficiency with the aerodynamics features listed in Table V, so the Figure 31 comparison may not be exactly valid.

As the high-energy gas leaking through the CSCT's face seals mixes with the fin cooling-air stream, it will augment thrust to some extent. Therefore, it should not be considered as total cycle loss as expressed in Figure 31. Operational limits are set by deliberate design so, for this particular CSCT, limits were set by the 111% overspeed capability of the baseline engine which has a 15% margin of safety at the 111% design speed. The same 111% overspeed plus 15% margin of safety was designed into the containment hoop and ceramic components of the CSCT. Likewise, the maximum temperature on the CSCT is set by the containment hoop limits and this temperature is controllable by the amount of cooling air ducted through the fins. The more air that is ducted to cool the hoop, however, the more drag penalty is imposed. Therefore, it is more efficient to operate the containment hoop at its maximum operating temperature, which for this particular application is about 600° F for the relatively short life it must perform with the materials it incorporates.

The particular baseline engine selected for this comparison study is probably the most severe baseline engine that could be selected. The CSCT containment hoop is stressed closer to the ultimate strength of available materials than any other component of the CSCT. No other known turbine has a higher operating blade tip speed. Accordingly, almost any other turbine with a lower operating tip speed would be a more conservative candidate for an initial demonstration of a CSCT. Unfortunately, few other engines are non-man-rated, so the spectrum of desirable engines for a new concept demonstration is somewhat limited.

The prospect of a CSCT with a sealed hoop compartment is illustrated in Figure 32. By sealing the hoop compartment, hot turbine gas leakage is eliminated and tip drag is reduced significantly due to its lower tip speed, lack of fins, and lower relative Mach number in a 1500 to 1800° F environment. This concept is illustrated from U.S. Patent No. 3,857,650 by R. Cerrato, Turin, Italy, 1974. Unfortunately, no evidence could be found that the carbon

Baseline

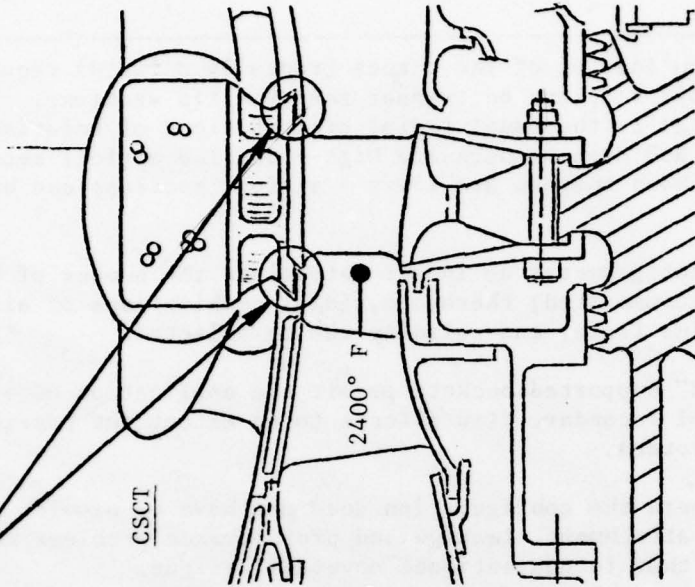


% Core Air

2.5	Blade Cooling
1.1	Tip Clearance
1.5	Disk/Dovetails
0	Tip Face Seals
0	Hoop/Fin Drag
5.1	Total

Seal Leakage = 1.5%  $W_c$

CSCT



0	Blade Cooling
0	Tip Clearance
1.5	Disk/Dovetails
1.5	Tip Face Seals
6.4	Hoop/Fin Drag
9.4	Total

(Equivalent to H.P.)\*

\*This value may be reduced by the considerations listed in Table V.

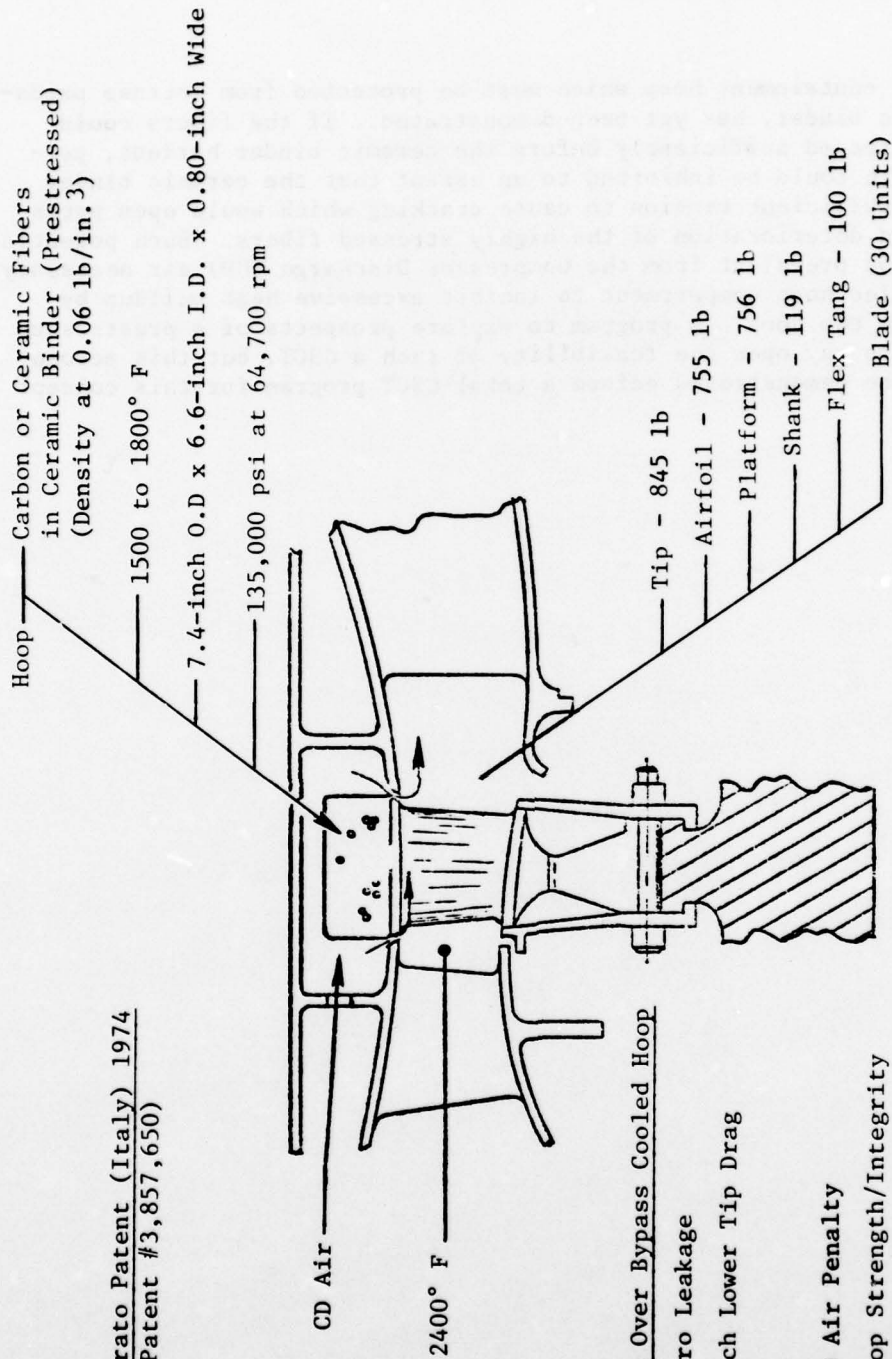
Figure 31. Cooling, Leakage, and Drag Penalties - CSCT Versus Baseline.



Table V. Potential Aerodynamic Benefits of a CSCT Inverted-Taper Turbine Blade.

1. The compression loading of the blades (radially outward) requires that hub airfoil sections be thinner than the tip sections. This is perfectly suited to the usual radial distributions of relative entry Mach number. Hub Mach numbers are high - desired airfoil sections are thin; tip Mach numbers are lower - airfoil sections can be thicker.
2. Blade attachment geometry no longer determines the number of blades that can be accommodated; therefore, ideal combinations of airfoil section, annulus flare, and solidity can be selected.
3. The "fixed end" supported buckets permit the application of blade lean to control secondary flow effects to an extent not possible in conventional rotors.
4. At the hub, where the configuration does not have to provide for a "radial pull" attachment, leakage and protuberance problems should be less acute than in conventional dovetail designs.
5. The thinner trailing edges should be an advantage, since no cooling-air passages and holes need to be accommodated.
6. A shrouded rotor provides tip clearance and secondary flow advantages over unshrouded versions.

Refer R. Cerrato Patent (Italy) 1974  
(U.S. Patent #3,857,650)



Advantages Over Bypass Cooled Hoop

- Zero Leakage
- Much Lower Tip Drag

Unknown

- CD Air Penalty
- Hoop Strength/Integrity

Figure 32. CSCT with Sealed Hoop Compartment.

or ceramic fiber containment hoop which must be protected from intense oxidation by a ceramic binder, has yet been demonstrated. If the fibers could somehow be prestressed sufficiently before the ceramic binder hardens, perhaps radial growth could be inhibited to an extent that the ceramic binder would never see sufficient tension to cause cracking which would open paths for oxidation and deterioration of the highly stressed fibers. Such potential oxidation would be prevalent from the Compressor Discharge (CD) air necessary to purge the sealed hoop compartment to inhibit excessive heat buildup by air friction from the hoop. A program to explore prospects of a prestressed fiber/ceramic hoop may open the feasibility of such a CSCT, but this accomplishment should be demonstrated before a total CSCT program for this concept is undertaken.

#### 4.0 TASK III - ECONOMIC ANALYSIS AND RECOMMENDED COMPONENT DEVELOPMENT PROGRAM.

The severe alterations to the aerodynamic cycle that would invalidate a CSCT/baseline weight comparison would likewise invalidate a cost comparison for the total engine system. For this study, a direct comparison of the turbine rotor is made to indicate the payoff prospect. Table VI shows a cost breakdown on the CSCT for the 250th unit and compares it with a projected cost of a baseline air-cooled turbine 250th unit as extrapolated from a 2100° F air-cooled turbine.



Table VI. CSCT Estimated Costs.

Tooling Plus Initial Hardware		250th Unit
12 to 18 Hoops	\$25,000	\$150
180 Fins (6 sets)	50,000	750/Set
180 Blades (6 sets)	56,000	750/Set
1 Wheel	12,000	3,600
Baseline - 250th Bladed Turbine Wheel/Shroud		\$10,000*
CSCT - 250th Bladed Turbine Wheel		5,250

(CSCT Ducting and Mounting Costs not Considered)

\*Cost estimate for a 2400° F blade extrapolated from a 2100° F blade.

## 5.0 PROGRAM SUMMARY

The goal of this program was to explore the feasibility of a novel Compression Structured Ceramic Turbine and compare its projected performance with the equivalent performance of a baseline engine of equal size and operation. Sufficient detailed analysis of each component of the novel CSCT was conducted to confirm that its total structural integrity would have a high probability of survival for the life mission for which it was intended. Table VII lists a few of the peak temperatures and stresses encountered in the analysis of the various components of the CSCT. Future refinements could reduce some of the peak stresses by as much as 30%. The list of design concerns described in Section 2.2, Design Parameters, has been addressed in detail. Some of the design concerns were eradicated with positive solutions while others will require some development effort to accurately assess the magnitude of the problem and to evaluate possible solutions. None of the design concerns appears to be an absolute barrier to a functionable CSCT.

The final comparison of performance with the baseline engine shows a significant penalty of performance over the baseline engine due to drag of the fin/hoop system. However, the prospects of utilizing the fins to offset this loss by augmenting thrust and the possibility that inverted taper turbine blade airfoils may increase stage efficiency significantly remain to be explored before a final overall assessment of this particular CSCT can be made.

Table VII. CSCT Component Temperature/Stress Summary.

Component	Material	Temp (C)	Peak Stress (ksi)	Average Stress (ksi)
Disk	René 95	950	180-T	175-T
Flex Tangs	René 95	1100	45-T	40-T
Blade Root	RBSN (2.5)	1200	10-T 10-C	5-T 5-C
Blade Platform	RBSN (2.5)	1500	20-T 82-C	20-T 40-C
Blade	RBSN (2.5)	2250	72-C	57-C
Blade Endwall	RBSN (2.5)	1800	20-T 20-C	5-T 10-C
Fin Root	RBSN (2.3)	1700	25-C	20-C
Fin	RBSN (2.3)	900	70-C	50-C
Fin Endwall	RBSN (2.3)	600	30-C	25-C
Hoop	Graphite/Pl	600	160-T	152-T

C = Compression

T = Tension

## 6.0 CONCLUSIONS

- A Compression Structured Ceramic Turbine looks structurally feasible.
- The operational limits of a CSCT would probably depend more on the reliability of the containment hoop than on the ceramic components.
- The structural analysis of this particular CSCT indicates that its design goals can be achieved with a 15% margin of safety at 111% rotor speed.
- A new engine aerodynamic cycle with effective working fins to offset windage loss, a reduced tip speed to reduce hoop/fin drag and to enhance aeromechanics for the prospect of doing work with the fins, and the possibility of utilizing the high energy leakage gas to augment thrust must be evaluated before real payoff of a CSCT can be determined.
- The prospect of improved turbine efficiency from the potential benefits of inverted taper airfoils listed in Table V should be evaluated and included with a future CSCT payoff study.
- A weight and cost analysis comparing the CSCT with the baseline turbine is not meaningful due to the severe alterations to aeromechanics required by the comparison.
- The survivability of a CSCT over a Tensile Structured Ceramic Turbine may be at least equal to the ratio of the ceramic material's compressive strength to its tensile strength or 300% to 800% greater. Such speculation must be confirmed by future testing.



## 7.0 RECOMMENDATIONS

In order to exploit any potential payoff that may be inherent in a Compression Structured Ceramic Turbine, the following three-phase program is recommended.

### 1. Phase I - New Engine Study

#### Task 1

Conduct an in-depth study of the prospects for improved turbine performance utilizing an idealized inverted-taper airfoil. (See Table V.)

#### Task 2

Conduct an in-depth study for the prospects for doing work with the tip cooling fins to offset fin/hoop drag losses. Size the turbine aerodynamic features to accommodate both fin work and core compressor work; include estimated leakage losses and account for any potential leakage gas mixing recovery to augment thrust.

#### Task 3

Conduct a new engine design study applicable to incorporating the unique features of a Compression Structured Ceramic Turbine. The study would include:

- Selecting an application for the new engine
- Defining an engine cycle such as the one illustrated in Figure 33
- Preliminary mechanical design of the new engine
- Detail mechanical design of the CSCT for a hot-test demonstration

### 2. Phase II - Optimization of CSCT Components

#### Task 1 - Demonstrate Reliable Limit of Containment Hoop Integrity

- Select candidate materials projected on proposed engine cycle environment (epoxy or polyimide/graphite).
- Design, fabricate, spin test, and iterate several dozen hoops, using deadweights to simulate CSCT loads. Optimize hoop thickness, width, and fiber pattern, varying the fabrication techniques.

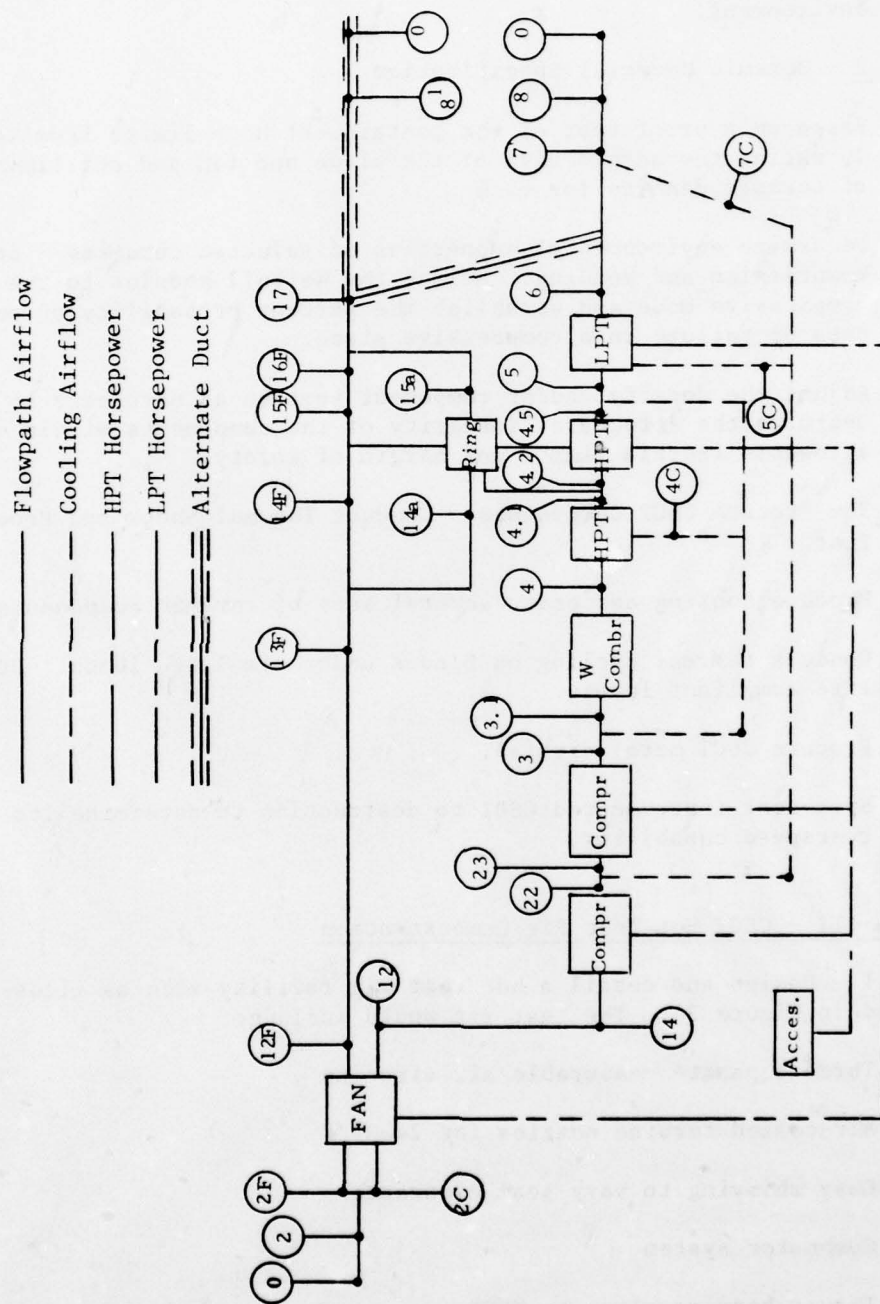


Figure 33. Flow and Horsepower Schematic of CSCT Engine.

- Monitor stresses, temperature, and windage loss in a partial vacuum during spin test. Project the windage lost to engine environment.

#### Task 2 - Ceramic Material Specification

- Based on a proof test of the containment hoop limits from Task 1, refine the aero design of the blade and fin and set limits of ceramic density for each.
- Determine environmental properties of selected ceramics - in compression and bending. Relate the Weibull modulus to the compressive mode and establish the percent probability of success or failure in a compressive state.
- Adjust the density and/or component section as necessary to optimize the structural integrity of the components within allowable inertia limits and margin of safety.

#### Task 3 - Procure CSCT Components - Conduct Thermal Shock and Proof-Spin Test.

- Procure tooling and order several sets of ceramic components.
- Conduct thermal cycling on blades under simulated loads. Utilize compliant layers.
- Procure CSCT metal disk(s).
- Spin-test instrumented CSCT to destruction to determine its overspeed capability.

### 3. Phase III - CSCT Hot Test Rig Demonstration

Task 1 - Design and detail a hot test rig facility such as illustrated in Figure 34. The test rig would include:

- Three separate measurable air circuits
- Air-cooled turbine nozzles for 2400° F
- Easy shimming to vary seal clearance
- Combustor system
- Thrust bearing close to CSCT
- Water brake or equivalent measurable torque extraction
- Instrumentation slipring and controls

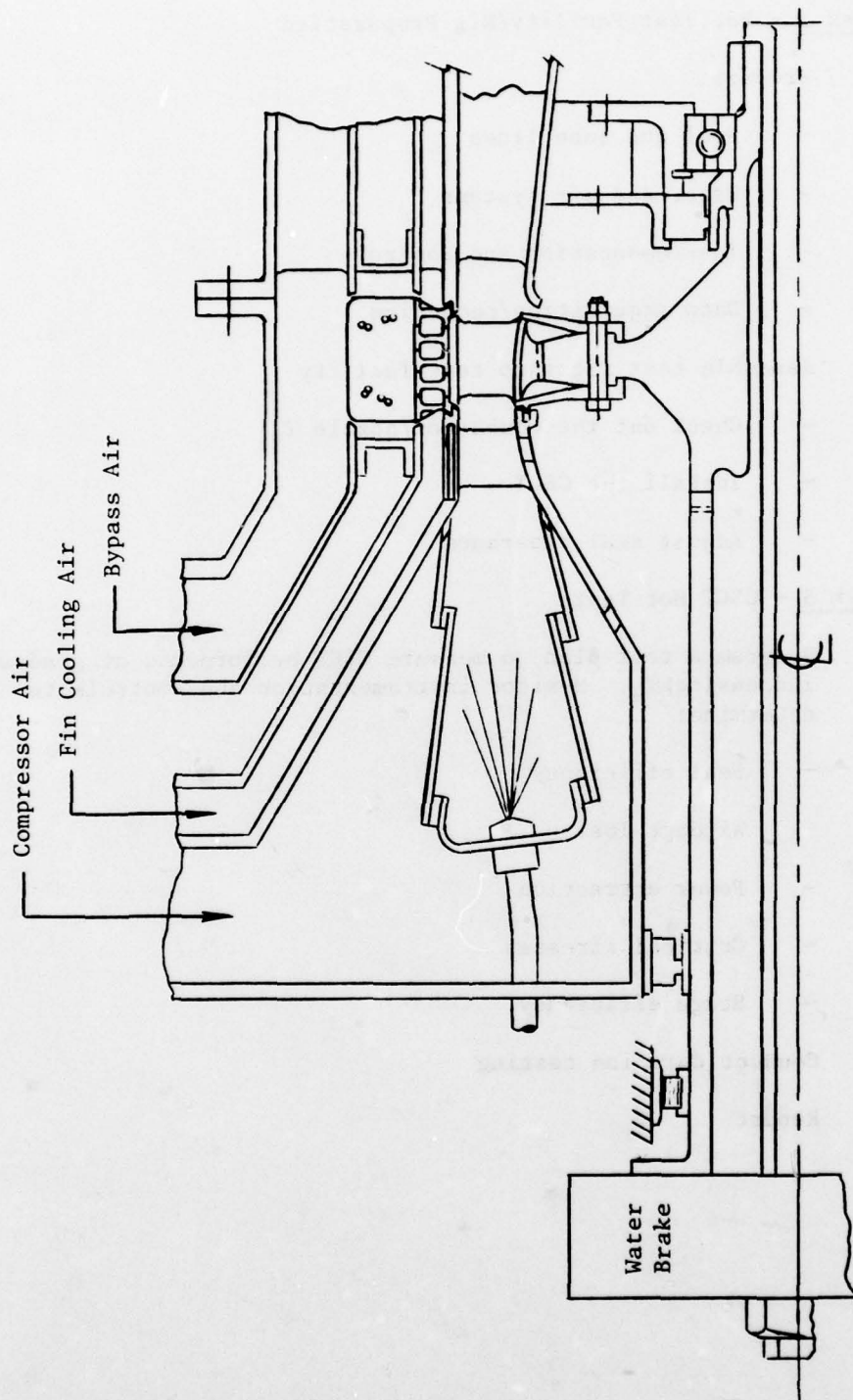


Figure 34. Hot Test Rig Facility Concept for the CSCT.



### Task 2 - Hot Test Facility/Rig Preparation

- Prepare:
  - Fuel and lube lines
  - Water and air systems
  - Instrumentation and controls
  - Data acquisition/reduction
- Assemble test rig into test facility
  - Check out the combustor/nozzle  $T_4$
  - Install the CSCT
  - Adjust seal clearance

### Task 3 - CSCT Hot Test

- Program a test plan to measure CSCT performance at gradually increasing  $T_4$ . Monitor instrumentation and controls to determine:
  - Seal efficiency
  - Windage loss
  - Power extraction
  - Critical stresses
  - Stage efficiency
- Conduct duration testing
- Report

## APPENDIX A

### HEAT TRANSFER AND WINDAGE LOSS ANALYSIS

#### 1.0 INTRODUCTION

The time-share computer program used was a modified version of a general three-dimensional cylindrical-coordinates heat transfer program developed by T.E. Russell (Reference 2). The program has been used for various sump and bearing heat transfer analysis, and most recently for the study of the aft section of AEG's C-MAPS propulsion simulator (Reference 1).

#### 2.0 MODEL

The purpose of the analysis was, basically, to estimate the temperature distribution and investigate the cooling of the graphite hoop around the compression-structured ceramic turbine.

A section of the rotor and hoop representing 1/15 of the circumferential contour (resembling a slice of pie) was considered, noting that with 30 rotor blades and 15 fins, the hoop temperatures are periodic circumferentially with an angular period of  $2\pi/15$ . Twelve sections were then taken at different radii, as shown in Figure A-1.

A nodal subdivision of each section was taken; the resulting temperature plots appear later in this section. A data file CROTDATA was formed containing the geometric data and boundary condition specifications of the model. This was used by the steady-state heat transfer program CERROTHHT to perform a heat balance calculation. This uses the successive overrelaxation numerical technique (factor = 1.5) to minimize the number of iterations required for convergence (Reference 2).

The CERROTHHT program handles several features, including mass transfer analysis, viscous heat generation, and radiation, in addition to convection and conduction (also accounting for graphite anisotropy).

#### 3.0 HEAT TRANSFER CALCULATIONS

A good approximation to the heat transfer coefficients for supersonic flow can be obtained by using the incompressible flow correlations, provided that:

- (1) In calculating the film properties, a reference temperature  $T^*$  is used, defined as (Reference 3):

$$T^* = T_f + 0.5 (T_g - T_f) + 0.22 (T_r - T_f) \quad (1)$$

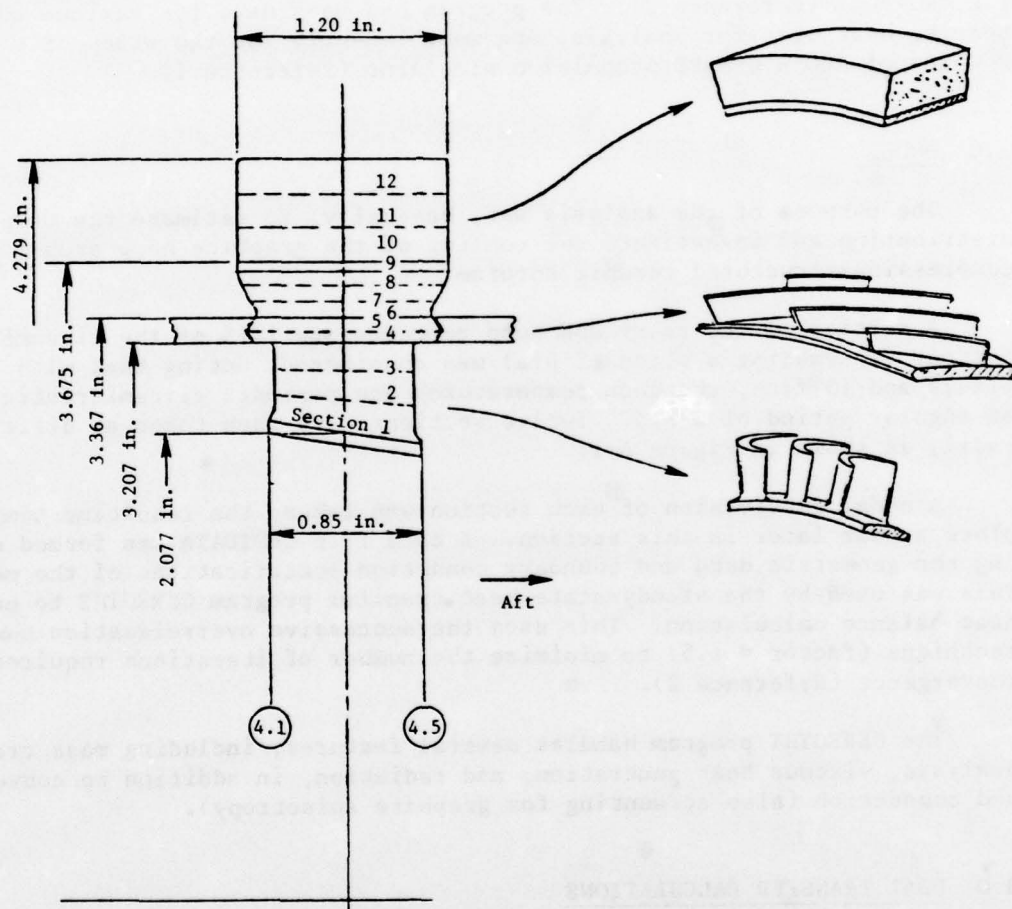


Figure A-1. Turbine, Fin, and Hoop Assembly with Nodal Volume Sections Shown.

where  $T_f$  is the static temperature of the stream,  $T_s$  is the wall surface temperature (use a guess in most cases), and  $T_t$  is the recovery temperature defined by the equation

$$\frac{T_r - T_f}{T_o - T_f} = r = \text{recovery factor} - 3 \sqrt{\text{Pr}} \text{ for turbulent flow}$$

where  $T_o$  = stream total temperature =  $T_f (1 + \frac{\gamma-1}{2} M_f^2)$ . For cooling  $T^* > T_f$  and use of  $T_f$  in the correlations gives a conservative heat transfer coefficient. Pr is the Prandtl number.

(2) The result from the correlations is interpreted as an "effective heat transfer coefficient" defined as (Reference 3)

$$h_e = \frac{\dot{q}}{A (T_w - T_{aw})} \quad (2)$$

where  $T_{aw}$  is the adiabatic wall temperature, calculated from the stream static temperature and accounting for the recovery factor.

Fin Cooling - With an inlet velocity of 600 fps, the air flows parallel to the fins, with a relative velocity of 2080 fps.

$$\text{Nu} = 0.0395 (\text{Re})^{0.75} (\text{Pr}) \quad (\text{Reference 5}) \quad (3)$$

is applied to a channel with appropriate temperatures and boundary conditions. The effect of the shock wave at the inlet is minimal.

A similar approach is taken for turbine rotor heating with an effective velocity of 1700 fps. Relative temperatures are used for boundary conditions, giving conservative temperature distribution results.

Hoop Venting - From Reference 4:

$$\text{Top of the hoop } \text{Nu} = 0.08434 \text{ Re}^{0.7} \text{ Pr}^{0.35} \text{ (rotating cylinder)} \quad (4)$$

$$\text{Sides of the hoop } \text{Re} = \frac{wr^2}{\nu}, \text{Nu} = 0.015 \text{ Re}^{0.8} \text{ (rotating disks)} \quad (5)$$

It is assumed that the hoop is well vented, with fan air flowing on top of the hoop and out from side vents to allow replenishing of air pumped by the disks.

Twenty-five boundary conditions were established, as shown in Figure A-2. The calculated heat transfer coefficients and temperatures are shown in Table A-1. Mass transfer analysis is used in the fin area to account for viscous heat generation. Note that the free-stream temperatures are used as boundary conditions, since the acceleration of the boundary layer to supersonic speeds increases its total temperature but the rise in static temperature is small (due to friction or drag heat generation).



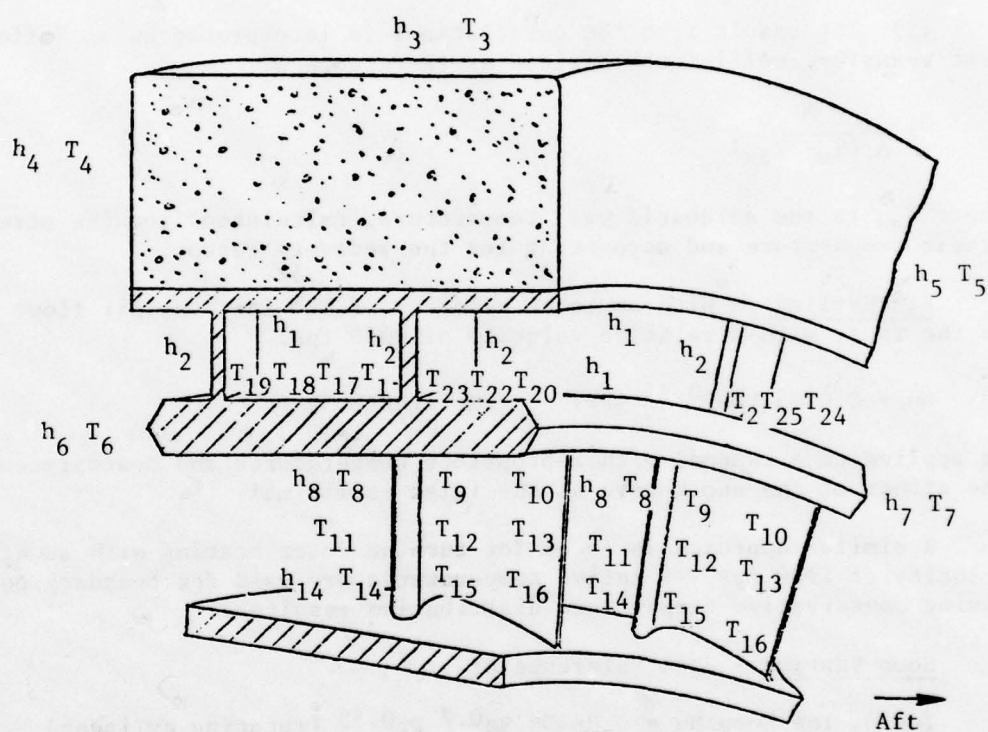


Figure A-2. Heat Transfer Coefficients and Boundary Temperature Locations.

Table A-1. Heat Transfer Coefficients and  
Temperature Boundary Conditions.

(15 fins, 0.25-inch high)

	H (° F)	T (° F)
1.	414	247
2.	828	507
3.	140	234
4.	135	259
5.	135	259
6.	1437	1950
7.	639	1600
8.	534	1950
9.	534	1775
10.	534	1600
11.	534	2225
12.	534	2001
13.	534	1776
14.	534	1895
15.	534	1744
16.	534	1592
17.		273
18.		299
19.		325
20.		351
21.		377
22.		403
23.		429
24.		455
25.		481

Good venting of the top of the hoop and wide clearances at the sides are also implied, to dissipate the friction heat generated by the rotation. (Disk pumping action at the sides of the hoop is estimated at approximately 0.67 lb/sec, and part of this has to be replenished by fan air to prevent overheating.)

Reaction bonded silicon nitride (RBSN) conductivity is taken as:

$$k_{\text{RBSN}} = 70 \text{ Btu-in./hr-ft}^2\text{-}^\circ \text{ F}^*$$

while for graphite

$$k_{\text{radial}} = 7.2 \text{ Btu-in./hr-ft}^2\text{-}^\circ \text{ F}$$

$$k_{\text{circumferential}} = 60 \text{ Btu-in./hr-ft}^2\text{-}^\circ \text{ F.}$$

Turbine-fin seal clearances were taken as 0.004 inch hot, and seal leakage was assumed negligible.

#### 4.0 DRAG CALCULATIONS

The drag coefficient on the hoop can be estimated from the solution of

$$\frac{1}{\sqrt{C_f}} = 0.6 + 4.07 \log_{10} \text{Re} \sqrt{C_f} \quad (\text{Reference 4}) \quad (6)$$

In this case  $C_f \approx 2.3 \times 10^{-3}$  for the top of the hoop,  $C_f \approx 1.7 \times 10^{-3}$  for the sides of the hoop.

For fin drag,

$$\begin{aligned} C_f &= 0.046 \text{Re}^{-0.2} \\ &= 3.5 \times 10^{-3} \end{aligned}$$

Windage or drag losses at the top and sides of the hoop are calculated as in Reference 4. The drag on the fins also represents the friction heat generation inside the fins.

---

\*The value relates to RBSN density at 2.7 grams/cc. Since the fins may be processed deliberately as light as 2.3 grams/cc, this value may be reduced to about 40.

## 5.0 RESULTS

A combined drag of approximately 91 hp is expected, with the ducted fan air temperature rising 22° F. The ceramic fin air temperature is expected to rise approximately 290° F.

A run of the heat transfer program with the boundary conditions of Table A-1 and accounting for the drag heat generation from Table A-2 gives the results plotted in Figure A-3 (for 15 fins, 0.25-inch high). Temperatures are superimposed on their respective nodes. The actual program output is shown in Table A-3.

Thirty Fins - 0.2-inch High - The above results represent the drag and temperature profiles for the 15-fin (0.25-inch high) configuration shown in Figure A-1. To consider a 30-fin (0.20 inch) model in detail would require a doubling of the effort. A good approximation to the hoop temperatures can be found, however, by simple manipulations of the program (doubling the value of H(2) and reducing the radial dimensions of nodes 61 through 93).

Figure A-4 shows a plot of the results for the hoop section. The results are shown in Table A-4. The temperature profiles for the fins and rotor are not very significant since the model has to be changed in that area.

A recalculation of the drag for this case gives a total drag of 104 hp, with fin air temperature rising 375° F. (See Figure 13.)

Radiation Effects - Hanovia Liquid Gold was suggested in the fin area to reduce radiation from the bottom to the top of the fin channels. Since a run using the radiation properties of the paint showed a temperature drop of only 2 to 3° in the profile, it is concluded that radiation is not a significant factor.

## 6.0 COOLING RECOMMENDATIONS

The results show significant heating of the fin flow due to friction drag at supersonic relative velocities. To improve cooling and decrease the fin-air temperature rise, more flow can be passed through the fins. (The increased air speed that is required alters the fin slope and effectively reduces drag area, further enhancing the cooling effect.) Figure A-5 shows the expected fin air exit temperature versus flow.

It is also essential to keep the top and sides of the hoop well vented. The downstream side of the hoop has to be sealed to prevent hot fin air from being pumped up. Wide clearances to fan air are needed for both sides of the hoop to assure against recirculation and overheating of the adjacent air.

The 15-fin model provides better cooling than the 30-fin model. (Although the heat transfer area provided is smaller, the drag heat generation is also smaller and lower temperatures result.)



Table A-2. Hoop and Fin Drag Calculations (15 Fins, 0.25-inch High).

Fin	Top of Hoop	Sides of Hoop
$Re = \frac{vD\rho}{\mu}$ $= \frac{(2080)(0.25)(0.143)(3600)}{(0.57)(12)}$ $= 3.9 \times 10^5$	$Re = \frac{\omega r^2}{\nu}$ $= \frac{(64706)(2\pi)(4.2792)}{(60)(\mu/\rho)(12^2)}$ $= 8.5 \times 10^6$	$Re = \frac{\omega r_{avg}^2}{\nu}$ $= 7.4 \times 10^6$
$C_D = 0.046 Re^{-0.2}$ $= 3.5 \times 10^{-3}$	$C_D = 2.3 \times 10^{-3}$ (Curve, Reference 5)	$C_D = 1.7 \times 10^{-3}$ (Curve, Reference 5)
$\tau = \frac{C_D \rho v^2}{2 g_c}$ $= 33.7 \text{ lb/ft}^2$	$M = \text{Frictional Torque, or Windage}$ $= c_f \pi a^4 L \rho \omega^2 / g_c$ $= 2.38 \text{ ft-lb}$	$\tau = \frac{C_D \rho v^2}{2 g_c}$ $= 19.2 \text{ lb/ft}$
$\text{Drag} = \tau A v$ $= \frac{(33.7)(0.25+0.26)(2)(3.5)(1972)}{144}$ $= 1623 \text{ (ft-lb)/sec per fin}$ $= 24790 \text{ (ft-lb)/sec total}$ $= 31.9 \text{ Btu/sec}$	$\text{Drag} = \omega M$ $= 29.4 \text{ hp}$	$A = 0.21 \text{ ft}^2$ $\text{Drag} = \tau A v$ $= 8984 \text{ (ft-lb)/sec}$ $= 16.3 \text{ hp}$
$\text{Fin Drag} = 45 \text{ hp}$ $\text{Fin Friction Heat Generated} = 47.5 \text{ hp}$ $= 34 \text{ Btu/sec}$		
$\Delta T \text{ through fins} = \frac{\dot{q}}{\dot{m} c_p}$ $= 220^\circ \text{ F}$		$\text{TOTAL DRAG} = 90.7 \text{ hp}$

<b>1</b> 246	<b>2</b> 246	<b>3</b> 247	<b>4</b> 246	<b>5</b> 246
<b>6</b> 245	<b>7</b> 245	<b>8</b> 245	<b>9</b> 245	<b>10</b> 245
<b>11</b> 247	<b>12</b> 247	<b>13</b> 247	<b>14</b> 247	<b>15</b> 247

Top Section of the Hoop  
Section 12, Top View

Aft  
↓

$R_M = 4.179$  in.  
 $t_{12} = 0.2$  in.

<b>16</b> 270	<b>17</b> 270	<b>18</b> 270	<b>19</b> 270	<b>20</b> 269
<b>21</b> 277	<b>22</b> 277	<b>23</b> 276	<b>24</b> 276	<b>25</b> 277
<b>26</b> 275	<b>27</b> 275	<b>28</b> 275	<b>29</b> 275	<b>30</b> 275

Middle Section of the Hoop  
Section 11, Top View

Aft  
↓

$R_M = 3.979$  in.  
 $t_{11} = 0.2$  in.

Figure A-3. Hoop Temperature Distribution Plot for 15-Fin  
Model (0.25-inch High).

<b>31</b> 303	<b>32</b> 305	<b>33</b> 305	<b>34</b> 304	<b>35</b> 298
<b>36</b> 332	<b>37</b> 334	<b>38</b> 334	<b>39</b> 334	<b>40</b> 333
<b>41</b> 337	<b>42</b> 334	<b>43</b> 333	<b>44</b> 336	<b>45</b> 338

Bottom Section of Hoop  
Top View, Section 10

Aft  
↓

$R_M = 3.779$  in.  
 $r = 0.2$  in.

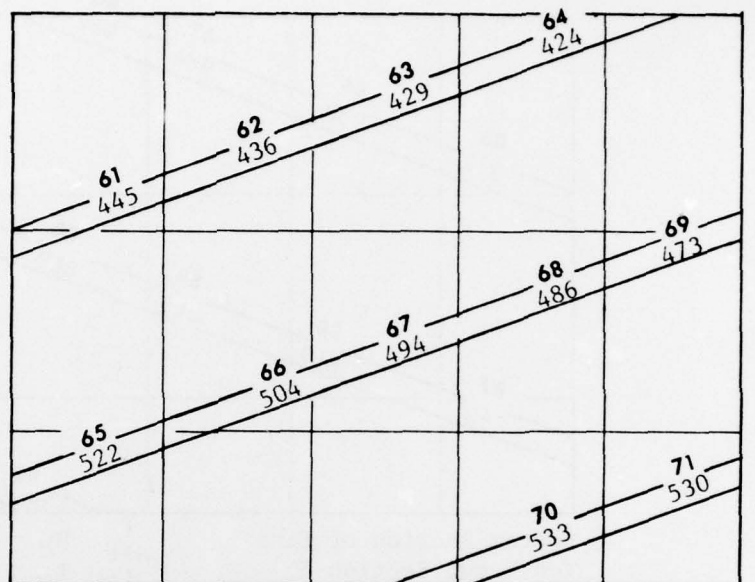
<b>46</b> 331	<b>47</b> 333	<b>48</b> 331	<b>49</b> 329	<b>50</b> 299
<b>51</b> 398	<b>52</b> 425	<b>53</b> 422	<b>54</b> 421	<b>55</b> 415
<b>56</b> 470	<b>57</b> 451	<b>58</b> 452	<b>59</b> 476	<b>60</b> 474

RBSN Section Above Fins  
Top View, Section 9

Aft  
↓

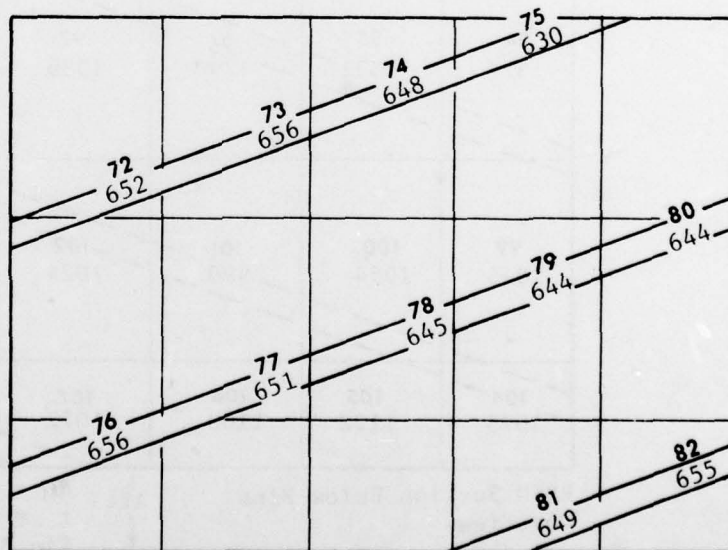
$R_M = 3.648$  in.  
 $L_4 = 0.052$  in.

Figure A-3. Hoop Temperature Distribution Plot for  
15-Fin Model (0.25-inch High).  
(Continued)



Top Section of Fins  
Top View, Section 8

Aft  
↓  
 $R_M = 3.5753$  in.  
 $t = 0.03333$  in.  
Fin Top

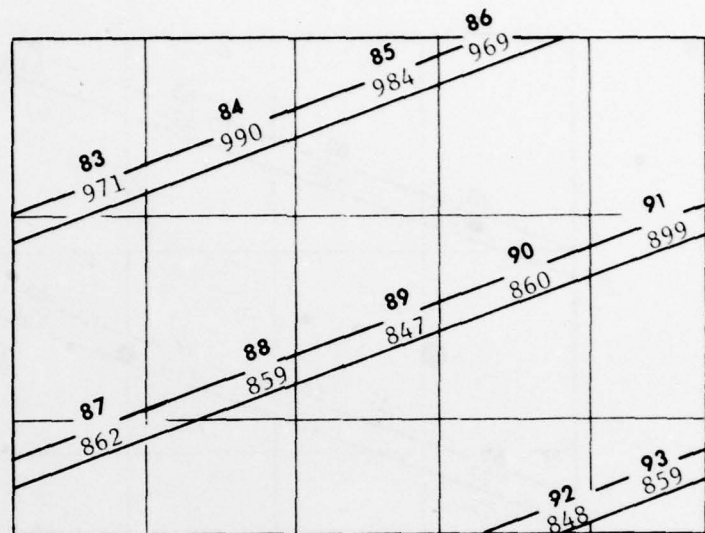


Middle Section of Fins  
Top View, Section 7

Aft  
↓  
 $R_M = 3.432$  in.  
 $t = 0.03333$  in.  
Mid Fin

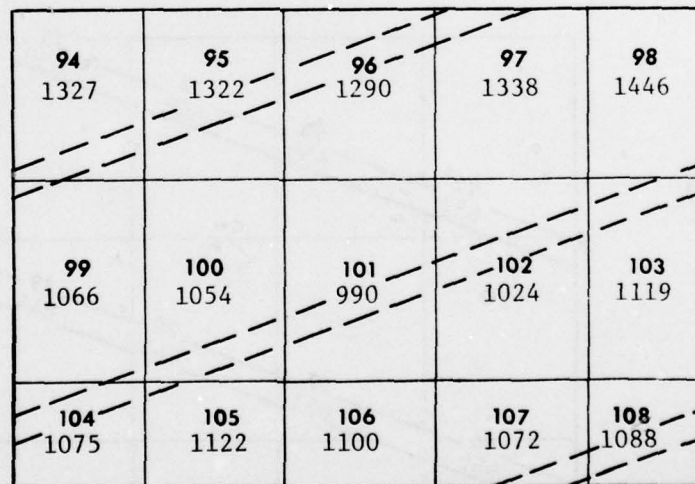
Figure A-3. Hoop Temperature Distribution Plot for  
15-Fin Model (0.25-inch High).  
(Continued)





Bottom Section of Fins  
Top View, Section 6

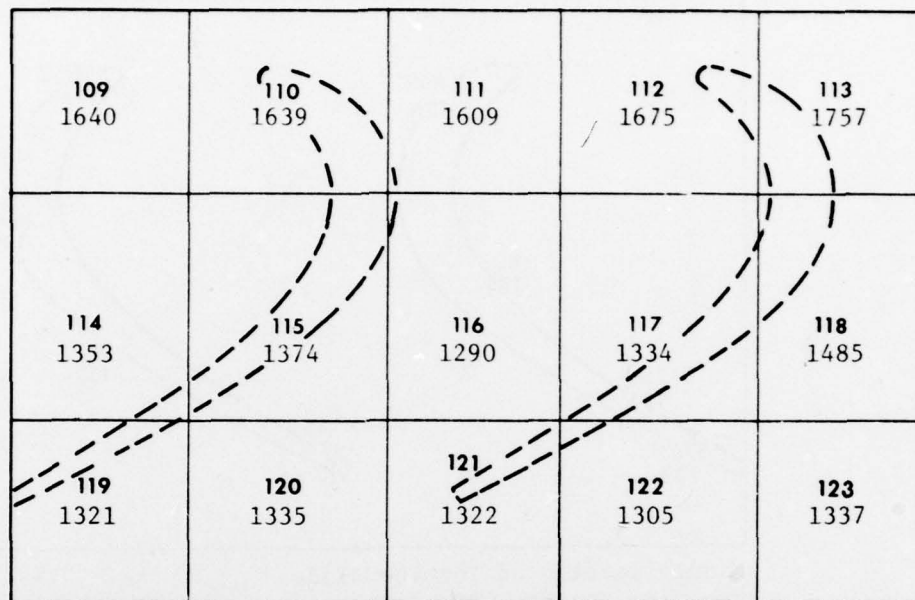
Aft  
↓  
 $R_M = 3.327$  in.  
 $t = 0.08$  in.  
Rotor-Fin Top



RBSN Section Below Fins  
Top View

Aft  
↓  
 $R_M = 3.40867$  in.  
 $t = 0.0333$  in.  
Fin Bottom

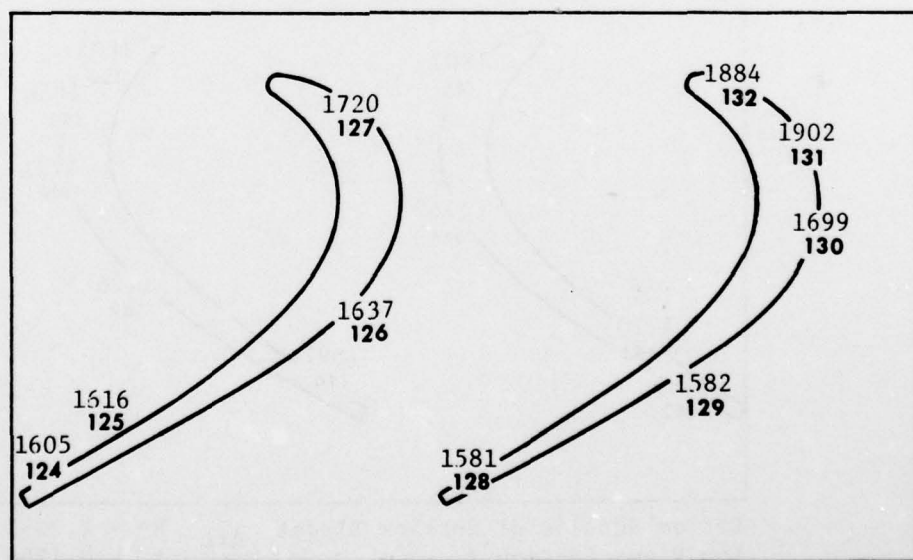
Figure A-3. Hoop Temperature Distribution Plot for  
15-Fin Model (0.25-inch High).  
(Continued)



RBSN Section Above Turbine Blades  
Top View, Section 4

Aft  
↓

$R_M = 3.247$  in.  
 $t = 0.03$  in.  
Rotor Fin-Bottom

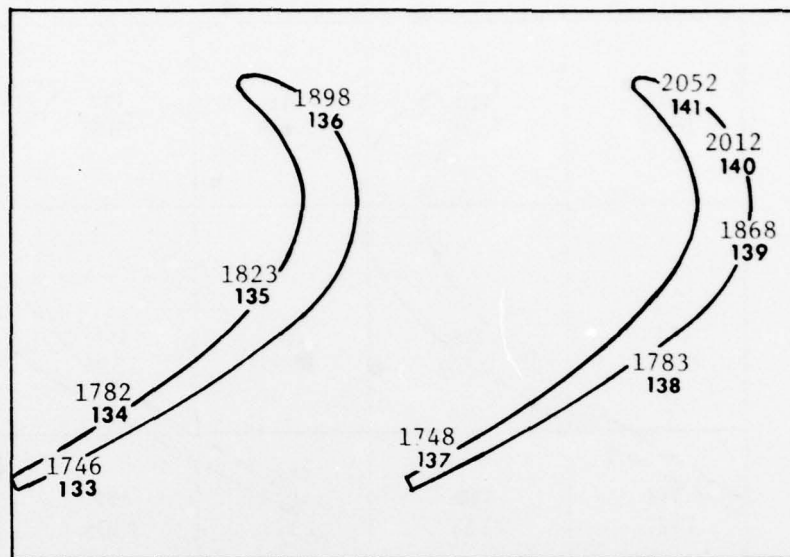


Top Section of Turbine Blades  
Top View, Section 3

Aft  
↓

$R_M = 3.11857$  in.  
 $t = 0.17666$  in.  
Rotor Top

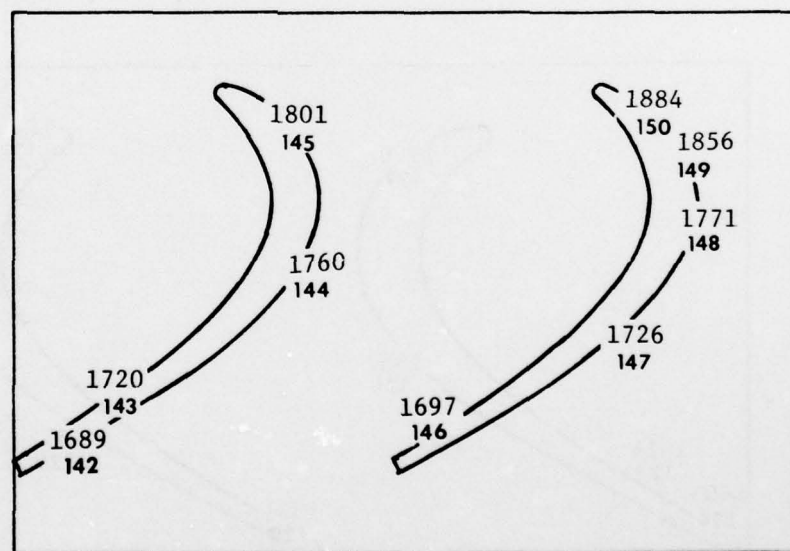
Figure A-3. Hoop Temperature Distribution Plot for  
15-Fin Model (0.25-inch High).  
(Continued)



Middle Section of Turbine Blades  
Top View, Section 2

Aft  
↓

$R_M = 2.942$  in.  
 $t = 0.17666$  in.  
Mid Rotor



Bottom Section of Turbine Blades  
Top View, Section 1

Aft  
↓

$R_M = 2.7653$  in.  
 $t = 0.17667$  in.  
Rotor Root

Figure A-3. Hoop Temperature Distribution Plot for  
15-Fin Model (0.25-inch High).  
(Concluded)

Table A-3. Temperature Distribution Results.

15-Fin (0.25-inch high) Model

Node Temperatures at Iterations = 22

1	246.09	2	246.38	3	246.72	4	246.41	5	246.02
6	244.58	7	244.83	8	245.18	9	244.86	10	244.55
11	246.62	12	246.77	13	246.99	14	246.80	15	246.61
16	270.02	17	270.46	18	270.69	19	270.26	20	269.44
21	276.73	22	276.63	23	276.43	24	276.31	25	276.56
26	275.49	27	275.04	28	274.91	29	275.07	30	275.44
31	302.59	32	304.81	33	304.82	34	303.66	35	297.84
36	331.95	37	334.27	38	333.82	39	333.78	40	332.75
41	337.05	42	333.69	43	333.28	44	336.38	45	337.57
46	331.02	47	333.15	48	330.93	49	329.19	50	299.32
51	398.07	52	424.60	53	422.41	54	421.39	55	414.94
56	470.48	57	451.47	58	451.70	59	475.66	60	473.92
61	445.25	62	436.29	63	429.13	64	423.79	65	521.74
66	504.30	67	494.21	68	486.24	69	472.67	70	533.14
71	529.82	72	652.49	73	655.99	74	647.89	75	629.77
76	655.62	77	651.49	78	645.09	79	643.50	80	643.62
81	648.97	82	654.85	83	970.99	84	990.43	85	984.46
86	969.17	87	862.15	88	859.44	89	846.81	90	860.34
91	898.82	92	847.94	93	858.52	94	1327.14	95	1321.95
96	1289.54	97	1337.75	98	1446.44	99	1065.91	100	1053.81
101	989.69	102	1023.62	103	1118.52	104	1075.27	105	1122.15
106	1099.78	107	1071.78	108	1087.57	109	1639.80	110	1639.07
111	1609.46	112	1674.68	113	1757.39	114	1352.56	115	1373.57
116	1289.59	117	1333.57	118	1484.55	119	1321.42	120	1335.49
121	1321.51	122	1305.33	123	1336.62	124	1605.45	125	1616.30
126	1636.93	127	1719.71	128	1580.97	129	1582.47	130	1699.37
131	1901.51	132	1883.61	133	1746.28	134	1782.05	135	1823.11
136	1898.43	137	1748.53	138	1783.04	139	1867.75	140	2012.42
141	2052.27	142	1689.38	143	1720.32	144	1760.43	145	1801.64
146	1697.28	147	1725.57	148	1770.91	149	1855.84	150	1883.81



<b>1</b> 247	<b>2</b> 247	<b>3</b> 247	<b>4</b> 247	<b>5</b> 247
<b>6</b> 246	<b>7</b> 246	<b>8</b> 246	<b>9</b> 246	<b>10</b> 245
<b>11</b> 247	<b>12</b> 248	<b>13</b> 248	<b>14</b> 248	<b>15</b> 247

Top Section of Hoop  
Top View, Section 12

$R_M = 4.179$  in.  
 $t_{12} = 0.2$  in.

<b>16</b> 273	<b>17</b> 274	<b>18</b> 274	<b>19</b> 273	<b>20</b> 273
<b>21</b> 282	<b>22</b> 282	<b>23</b> 282	<b>24</b> 281	<b>25</b> 282
<b>26</b> 281	<b>27</b> 280	<b>28</b> 280	<b>29</b> 280	<b>30</b> 281

Middle Section of Hoop  
Top View, Section 11

↓  
Aft

$R_M = 3.973$  in.  
 $E_{11} = 0.2$  in.  
Hoop Middle Section

Figure A-4. Hoop Temperature Plot for 30-Fin Model  
(0.20-inch High).

31 311	32 312	33 312	34 311	35 307
36 351	37 352	38 350	39 350	40 350
41 357	42 354	43 353	44 355	45 357

Bottom Section of Hoop  
Top View, Section 10

↓ Aft

$R_M = 3.779$  in.  
 $t_{10} = 0.2$  in.  
Hoop Bottom

Figure A-4. Hoop Temperature Plot for 30-Fin Model  
(0.20-inch High). (Concluded)

Table A-4. Temperature Distribution Results.

30-Fin (0.20-inch high) Model

Node Temperatures at Iterations = 22

1	246.70	2	246.97	3	247.30	4	246.98	5	246.62
6	245.52	7	245.73	8	246.02	9	245.71	10	245.46
11	247.43	12	247.56	13	247.75	14	247.56	15	247.40
16	273.44	17	273.77	18	273.90	19	273.42	20	272.82
21	282.43	22	282.06	23	281.57	24	281.39	25	282.02
26	280.75	27	280.21	28	279.90	29	279.98	30	280.55
31	310.85	32	312.48	33	311.93	34	310.60	35	306.61
36	350.72	37	351.91	38	350.48	39	349.77	40	349.60
41	357.14	42	354.22	43	353.33	44	355.45	45	356.97
46	336.80	47	336.03	48	331.94	49	329.32	50	311.27
51	441.57	52	462.79	53	458.17	54	454.51	55	446.77
56	523.69	57	512.66	58	512.92	59	530.89	60	527.44
61	429.32	62	411.39	63	397.97	64	388.66	65	553.65
66	526.72	67	508.81	68	492.79	69	470.13	70	575.29
71	567.84	72	593.77	73	585.96	74	569.27	75	545.75
76	654.84	77	641.55	78	625.31	79	612.41	80	599.09
81	662.60	82	662.28	83	903.48	84	914.02	85	900.54
86	873.48	87	847.03	88	839.73	89	820.98	90	825.08
91	846.82	92	840.36	93	847.02	94	1321.63	95	1314.11
96	1280.63	97	1332.06	98	1449.61	99	1089.20	100	1069.75
101	1006.00	102	1037.54	103	1127.82	104	1095.18	105	1150.95
106	1130.20	107	1096.66	108	1105.73	109	1637.88	110	1635.98
111	1605.68	112	1672.55	113	1758.54	114	1365.82	115	1382.43
116	1299.58	117	1341.71	118	1489.04	119	1332.56	120	1350.88
121	1337.77	122	1319.08	123	1346.28	124	1607.84	125	1619.10
126	1639.83	127	1720.90	128	1583.69	129	1585.43	130	1700.62
131	1901.81	132	1883.08	133	1746.77	134	1782.65	135	1823.83
136	1898.99	137	1748.95	138	1783.53	139	1868.12	140	2012.56
141	2052.27	142	1689.47	143	1720.42	144	1760.55	145	1801.78
146	1697.25	147	1725.51	148	1770.80	149	1855.80	150	1883.79

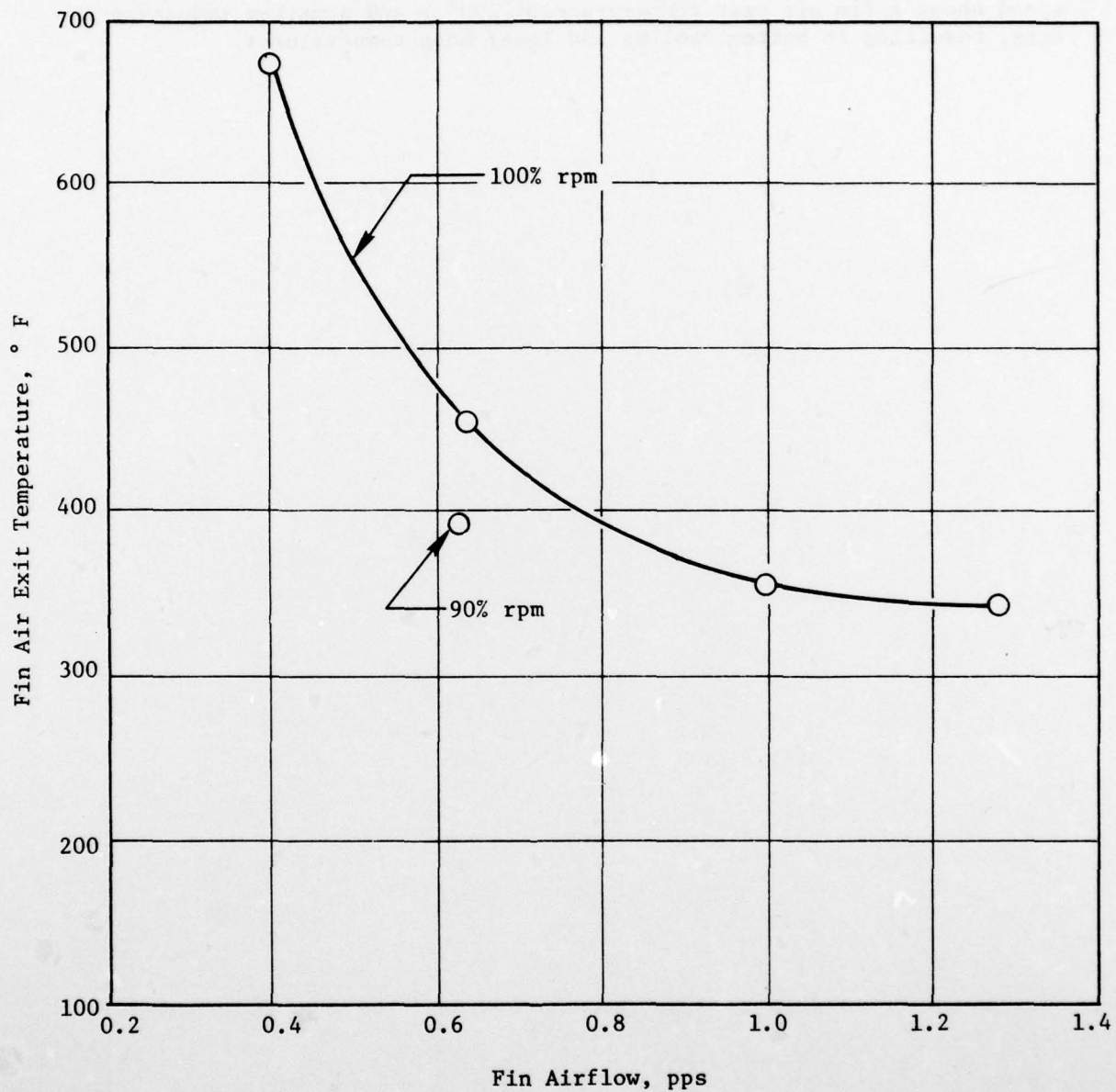


Figure A-5. Fin Air Heating Versus Flow for 15-Fin Model (0.25-inch High).



A calculation for the same airflow of 0.64 pps and a 10% reduction in speed shows a fin air exit temperature of 390° F and a marked reduction in drag, resulting in better cooling and lower hoop temperatures.



## APPENDIX B

### CONTAINMENT HOOP STRESS CALCULATIONS

The following steps are applied to calculate total hoop stress:

$$(1) \quad C_f = \frac{4\pi^2}{32.2} \times r \times N^2 \times WT$$

where -  $C_f$  = Centrifugal force per component

$r$  = Radius to C.G. of component in feet

$N$  = Revolutions of component per second

$WT$  = Weight of component in pounds

$$(2) \quad \text{psi} = \frac{\text{Total } C_f \text{ of all components}}{\text{in.}^2 \text{ of hoop I.D. area}}$$

Stress in hoop imposed by total  $C_f$ :

$$(3) \quad C_f = \text{psi} \frac{b^2 + a^2}{b^2 - a^2}$$

where -  $b$  = Radius (in.) to O.D. of hoop

$a$  = Radius (in.) to I.D. of hoop

Stress in hoop imposed by own free inertia:

$$(4) \quad \sigma_{\text{free}} = \frac{1}{4} \frac{\rho \omega^2}{386.4} \left[ (3+v) R_o^2 + (1-v) R_i^2 \right]$$

where  $\rho$  = density of hoop (lbs/in.<sup>2</sup>)

$\omega$  = radians per second  $\frac{\text{rpm}}{60} \pi$

$v$  = Poisson's ratio of hoop material

$R_o$  = outer radius of hoop

$R_i$  = inner radius of hoop

Therefore, total hoop stress:

$$(5) \quad \sigma_{\text{Total}} = \sigma_{C_f} + \sigma_{\text{free}}$$

#### REFERENCES

1. Abujawdeh, S.S. and Quam, L.A., "C-MAPS Propulsion Simulator 3-D Heat Transfer Analysis," General Electric Co., Report No. GESP-803.
2. Russell, T.E., Numerical Analysis for Engineers, GE-AEG Technical Information Series Report No. R71AEG150.
3. McAdams, W.H., Heat Transmission, McGraw Hill Co., New York, 3rd Edition, 1954.
4. GE Heat Transfer and Fluid Flow Data Books, Fluid Flow Volume, General Electric Co., Corporate Research and Development, Schenectady, New York.
5. Chapman, Alan, Heat Transfer, MacMillan Co., New York, 2nd Edition, 1967.
6. Kreith, Frank, Principles of Heat Transfer, International Textbook Co., Scranton, Pa., 2nd Edition, 1967.
7. Rosenhow and Hartnett, Handbook of Heat Transfer, McGraw Hill Co., New York, 1973.

DATE  
FILMED  
-8